



UCGE Reports  
Number 20204

Department of Geomatics Engineering

**Analysis of Integrated Sensor Orientation for Aerial  
Mapping**

(URL: <http://www.geomatics.ucalgary.ca/links/GradTheses.html>)

by

**Alan Wing Lun Ip**

**January 2005**



UNIVERSITY OF  
CALGARY

THE UNIVERSITY OF CALGARY

Analysis of Integrated Sensor Orientation for Aerial Mapping

By

Alan Wing Lun Ip

A THESIS

SUBMITTED TO THE FACULTY OF GRADUATE STUDIES

IN PARTIAL FULFILLMENT OF THE REQUIREMENTS

FOR THE DEGREE OF MASTER OF SCIENCE

DEPARTMENT OF GEOMATICS ENGINEERING

CALGARY, ALBERTA

JANUARY, 2005

© ALAN WING LUN IP 2005

## **ABSTRACT**

Integrated multi-sensor systems, with their major progress in terms of sensor resolution, data rate and operational flexibility, have become a very attractive mapping tool over the last decade. In the aerial mapping application, for example, exterior orientation parameters (EO) of the imaging sensors are required. Using the measurements from a Differential Global Positioning System (DGPS) integrated with an Inertial Measurement Unit (IMU), the direct determination of the EO parameters can be obtained. This process is referred to as Direct Georeferencing (DG). On the other hand, conventional Aerial Triangulation (AT) uses a block of images with well distributed and sufficient number of Ground Control Points (GCP) for estimating the EO parameters. The DG provides substantial benefits over AT, which include the ability to map remote and inaccessible areas and significantly reducing the cost of the overall project, especially for corridor mapping, or orthophoto generation using existing Digital Elevation Models (DEM). However, the accuracy achieved when using DG is limited by the accuracy achievable by DGPS, IMU and any remaining residual camera/boresight/datum calibration errors. Typically these errors can be as large as 10 cm RMS, which is not sufficient for some large scale mapping applications. However, by combining the direct EO data in a traditional block adjustment, these errors can be minimized. This technique is known as Integrated Sensor Orientation (ISO) which has been promoted for a few years now. ISO has several advantages over traditional AT, primarily since; the stable geometry provided by direct EO can reduce the number of required GCP and tie-point to a minimum. At the same time, ISO provides excellent means

to control the quality of the estimated EO parameters from a DG system. Furthermore, while ISO can be used to improve direct EO performance, it provides an opportunity to use less accurate IMU/DGPS navigation systems for projects that have a well structured block of imagery.

## ACKNOWLEDGEMENTS

I would like to thank my supervisor Dr. Naser El-Sheimy for his guidance, support and encouragement throughout my research work, and especially for giving me the opportunity to study at Department of Geomatics Engineering, The University of Calgary.

I would also like to thank Dr. Mohamed M.R. Mostafa, Mr. Joe Hutton, Mr. Greg Lipa and Dr. Bruno Scherzinger from Applanix Corporation for allowing me to perform the research in such an advanced industrial environment and for their guidance, comments and for providing a number of navigation and photogrammetry software packages and datasets for my research. Dr. Michael A. Chapman is thanked for introducing me to the world of Geomatics Engineering, giving me a strong motivation to continue my education.

Applanix Corporation, Z/I Imaging Corporation, Leica Geosystems, and BAE Systems are acknowledged for providing their software license and support which are used for the work presented here. I would like to acknowledge the following for providing different datasets:

- PhotoScience Inc. for providing the PhotoScience UofK flight data
- PASCO Corporation for providing the PASCO 310 flight data
- Z/Imaging Corporation (Dr. Mostafa Madani) for DMC Alaska and DMC F-Block flight data
- 3001 Inc. for the flight crew time, and logistics of the DMC F-Block flight data

- Airborne Sensing Corporation for the flight crew time, and logistics of the Southern Ontario flight data acquisition

Financial support from my supervisor and the National Science and Engineering Research Canada (NSERC), University of Calgary and Applanix Corporation are greatly acknowledged.

Mr. Ng, Mr. Hutton and Dr. Mostafa are thanked for reviewing my thesis draft. The examination committee members (Dr. El-Sheimy, Dr. A. Habib, Dr. Mostafa and Dr. Ronsky) are thanked for taking the time to evaluate my thesis draft and for their valuable comments.

Last but not least, I am very grateful to my parents' and friends' support. Teresa's support for 8 continuous years throughout my University Studies will always be remembered.

Remembrance to my Grandmother

(1912 – 2004)

# TABLE OF CONTENTS

ABSTRACT .....	iii
ACKNOWLEDGEMENTS .....	v
LIST OF FIGURES .....	xii
LIST OF TABLES .....	xiv
LIST OF SYMBOLS, ABBREVIATIONS, NOMEMCLATURE .....	xvii
CHAPTER ONE: INTRODUCTION .....	1
1.1. Background and Objective.....	1
1.2. Thesis Outline .....	3
CHAPTER TWO: IMAGE GEOREFERENCING FOR AIRBORNE APPLICATIONS .....	5
2.1. Background.....	5
2.2. Direct Georeferencing, Indirect Georeferencing and Integrated Sensor Orientation .....	6
2.2.1. Direct vs. Indirect Georeferencing.....	7
2.2.2. Integrated Sensor Orientation .....	9
2.3. Error Sources in Image Georeferencing .....	11
2.3.1. Sensor Errors.....	18
<i>Imaging Sensor</i> .....	18
<i>Global Positioning System (GPS)</i> .....	21
<i>Inertial Navigation System (IMU)</i> .....	23
2.3.2. Integration Errors .....	26
<i>Sensor Placement</i> .....	26
<i>Synchronization</i> .....	27
<i>Filtering Technique</i> .....	28
2.3.3. Calibration Errors .....	30

<i>Sensor Errors</i> .....	30
<i>Lever Arm Offset</i> .....	34
<i>Boresight Mis-Alignment</i> .....	36
<i>Sensor Synchronization</i> .....	37
<i>IMU Initial Alignment</i> .....	38
2.3.4. Time-Dependent vs. Time Independent Errors .....	39
<i>Time-Dependent Errors</i> .....	39
<i>Time-Independent Errors</i> .....	45
CHAPTER THREE: QUALITY CONTROL OF DIRECT GEOREFERENCING DATA ..	
.....	52
3.1. The Need for Quality Control .....	52
3.2. Methods used for Quality Control .....	53
3.2.1. Quality Control Requirements .....	55
3.2.2. Optimizing the Quality Control Process .....	56
3.2.3. Integration with Photogrammetry Softcopy .....	62
CHAPTER FOUR: DATA DESCRIPTION .....	66
4.1. Imaging Data .....	66
4.2. Simulating a Less Accurate Direct Georeferencing Data .....	67
4.2.1. Data Simulation using Monte Carlo Analysis .....	69
4.3. Film Camera Flights .....	76
4.3.1. PhotoScience University of Kentucky Flight .....	77
4.3.2. PASCO Toyonaka City Flight Using a POS AV 310 .....	80
4.4. Large Format Digital Camera Flights .....	84
4.4.1. DMC Alaska Flight .....	85
4.4.2. DMC F-Block New Mexico Flight .....	88
4.5. Medium Format Digital Camera Flight .....	89
4.5.1. DSS Ajax Flight .....	90

CHAPTER FIVE: DATA RESULTS AND ANALYSIS.....	94
5.1. Typical DG Performance .....	95
5.1.1. DG System Error Budget Analysis.....	95
5.1.2. DG Performance of Simulated POS AV 310 Data.....	100
<i>PhotoScience UofK (1:6000)</i> .....	102
<i>DMC Alaska (1:6000 / 0.15m GSD)</i> .....	103
<i>DSS Ajax (1:20000 / 0.18 GSD)</i> .....	104
5.2. Quality Controlled DG vs. ISO.....	105
5.2.1. Film Camera Flights .....	107
<i>PhotoScience UofK Flight</i> .....	107
<i>PASCO Toyonaka City Flight</i> .....	113
5.2.2. Large Format Digital Camera Flights.....	116
<i>DMC Alaska Flight</i> .....	116
<i>DMC F-Block Flight</i> .....	121
5.2.3. Medium Format Digital Camera Flights.....	124
<i>DSS Ajax Flight</i> .....	124
5.3. Performance of Less Accurate GPS/IMU Data, Simulation vs. Real Data .....	130
5.4. Calibration Error and ISO.....	132
 CHAPTER SIX: IMPACT OF DIRECT GEOREFERENCING ON MAPPING PRODUCT.....	 140
6.1. Fast DEM Generation and Orthophoto Production .....	141
6.2. Near Real-time Data for Rapid Response.....	145
 CHAPTER SEVEN: CONCLUSIONS AND RECOMMENDATIONS .....	 147
7.1. Conclusions.....	147
7.2. Recommendations.....	150
7.2.1. Direct Georeferencing.....	150
7.2.2. Quality Control and Integrated Sensor Orientation .....	151

7.3. Recommendation on Future Research .....	152
REFERENCES .....	154
APPENDIX A: DATASET INFORMATION .....	168
A-1. PhotoScience UofK Flight .....	168
A-2. PASCO Toyonaka City Flight .....	169
A-3. DMC Alaska Flight.....	170
A-4. DMC F-Block Flight.....	171
A-5. DSS Ajax Flight.....	172
A-6. DSS Japan Data .....	173
APPENDIX B: SYSTEM SPECIFICATIONS .....	175
B-1. Applanix POS AV Specification .....	175
B-2. Leica Geosystems ADS40 Specification .....	176
B-3. ZI/Imaging DMC Specification .....	176
B-4. Vexcel UltraCam Specification .....	177
B-5. Applanix DSS Specification .....	177
APPENDIX C: DERIVATION OF EQUATIONS .....	178
C-1. Equations for DG System Error Budget Analysis .....	178

## LIST OF FIGURES

Figure 2-1:	Illustration of the Relationship between Image and Mapping Fame .....	6
Figure 2-2:	An Airborne Mapping System.....	13
Figure 2-3:	Concept of Direct Georeferencing Model .....	15
Figure 2-4:	Aerial Digital Camera Systems.....	20
Figure 2-5:	De-Centralized Loosely Coupled GPS/IMU Integration Mechanism using Kalman Filtering Technique .....	30
Figure 2-6:	Terrestrial Calibration Cage (left – special setting for signalized target, right – standard setting for airborne environment).....	33
Figure 2-7:	Illustration of Terrestrial Calibration’s Camera Locations.....	33
Figure 2-8:	GPS/IMU Lever Arm computed by Kalman Filtering .....	35
Figure 2-9:	Imaging Sensor / IMU Boresight.....	37
Figure 2-10:	Navigation error due to 1 millisecond Synchronization Error.....	41
Figure 2-11:	Heading Error Improvement after maneuvers .....	45
Figure 2-12:	Navigation Position Error due to 10 centimetre Lever Arm Error in flight direction .....	47
Figure 2-13:	Illustration of Boresight Error on Ground Position .....	49
Figure 3-1:	Difference in workflow between the QC and ISO approaches.....	55
Figure 3-2:	Tie Point distribution when the number of Points per Von Gruber Section is 7 (illustration only) .....	57
Figure 3-3:	Difference in boresight value using 4 strips of flight data.....	58
Figure 3-4:	Difference in boresight value using 3 strips of flight data.....	59
Figure 3-5:	Difference in boresight value using 2 strips of flight data.....	60
Figure 3-6:	Image Block Footprint of a DSS mission using Direct EO Data.....	63
Figure 3-7:	GPS/IMU QC/QA function in ISAT Automatic Tie Point Collection Module .....	64
Figure 3-8:	Collected tie point distribution using ISAT QC/QA on a DSS data.....	65
Figure 4-1:	RMS Difference of a Film Camera DG data Simulation Trial .....	73
Figure 5-1:	Error Budget Analysis of 153mm Film Camera System .....	96
Figure 5-2:	Error Budget Analysis of Digital Mapping Camera (DMC) .....	98
Figure 5-3:	Error Budget Analysis of Digital Sensor System (DSS) .....	99
Figure 5-4:	EO Analysis on PhotoScience UofK POS AV 310 Simulated Data .....	102
Figure 5-5:	EO Analysis of DMC Alaska POS AV 310 Simulation.....	103
Figure 5-6:	EO Analysis on DSS Ajax POS AV 310 Simulated Data .....	104
Figure 5-7:	ISO Results of the PhotoScience UofK Simulated POS AV 310 Data (Control Free) .....	108
Figure 5-8:	ISO Result of PhotoScience UofK POS AV 510 Flight (Control Free).....	111
Figure 5-9:	ISO Results of the PASCO 310 Flight (Control Free).....	115
Figure 5-10:	.....ISO Results of the DMC Alaska Simulated POS AV 310 Data (Control Free).....	117

Figure 5-11:	ISO Results of the DMC Alaska POS AV 510 Data (Control Free) .....	120
Figure 5-12:	ISO Results of the DMC F-Block Flight (Control Free) .....	123
Figure 5-13:	ISO Results of the DSS Ajax Simulated POS AV 310 Data .....	126
Figure 5-14:	ISO Results of the DSS Ajax POS AV 410 Data (Control Free) .....	129
Figure 6-1:	Illustration of Aerial Mapping Workflow using Traditional Technique and Latest Technology.....	140
Figure 6-2:	Extracted DEM and Fast Orthophoto from the DSS Ajax Flight .....	142
Figure A-1:	Flight Trajectory of PhotoScience UofK Data .....	168
Figure A-2:	Block Configuration of PhotoScience UofK Flight.....	168
Figure A-3:	Flight Trajectory of PASCO 310 Data .....	169
Figure A-4:	Block Configuration of PASCO 310 Flight.....	169
Figure A-5:	Flight Trajectory of DMC Alaska Data .....	170
Figure A-6:	Block Configuration of DMC Alaska Flight .....	170
Figure A-7:	Flight Trajectory of DMC Alaska Data .....	171
Figure A-8:	Block Configuration of DMC Alaska Flight .....	171
Figure A-9:	Flight Trajectory of DSS Ajax Data .....	172
Figure A-10:	Block Configuration of DSS Ajax Flight .....	172
Figure A-11:	Flight Trajectory of DSS Japan Data.....	173
Figure A-12:	Block Configuration of DSS Japan Flight .....	173
Figure A-13:	Flight Dynamics of DSS Japan Data .....	174

## LIST OF TABLES

Table 2-1:	Characteristics of different Image Georeferencing approaches.....	11
Table 2-2:	General difference between GPS and IMU .....	14
Table 2-3:	Terms in the Direct Georeferencing Equation.....	16
Table 2-4:	Terms in the Collinearity Equation.....	17
Table 2-5:	Information on Airborne Digital Camera Systems .....	20
Table 2-6:	GPS Error Source in Single Point Positioning using Single Frequency .....	22
Table 2-7:	Error Sources in Differential Dual Frequency GPS (DDFGPS).....	22
Table 2-8:	Characteristics of IMUs .....	23
Table 2-9:	Statistics of Synchronization Error Influence on Navigation Position and Attitude in Post-Processing, 1 millisecond simulation .....	42
Table 2-10:	Statistics of Synchronization Error Influence on Navigation Position and Attitude in Post-Processing, 2 millisecond simulations.....	43
Table 2-11:	Statistics of Lever Arm Error Influence on Navigation Position in Post-Processing, 10 centimetre simulation in flight direction (x-axis).....	47
Table 2-12:	Statistics of Boresight Error Influence on Check Point Coordinate Computational Accuracy by Direct Georeferencing .....	51
Table 4-1:	Summary of the configuration of Datasets used for ISO analysis.....	66
Table 4-2:	POS AV Post-Processed Accuracy.....	67
Table 4-3:	RMS Difference in performance between POS AV 510 and 310 .....	71
Table 4-4:	Statistical report of the Simulation Trial.....	74
Table 4-5:	Simulated parameters using different numbers of Monte Carlo trials.....	75
Table 4-6:	Configuration of the PhotoScience UofK Flight .....	76
Table 4-7:	Configuration of the PASCO Toyonaka City Flight .....	77
Table 4-8:	Boresight Values and RMS Residuals of the PhotoScience UofK QC .....	77
Table 4-9:	RMS of Navigation Error estimated by the Kalman Filter of the PhotoScience UofK Flight.....	78
Table 4-10:	Statistical report of Monte Carlo Trials on the PhotoScience UofK POS AV 310 Simulation.....	79
Table 4-11:	Ensemble RMS difference and RSS of the PhotoScience UofK POS AV 310 Simulation.....	80
Table 4-12:	QC Block Combinations of the PASCO 310 Flight .....	82
Table 4-13:	Boresight Values and RMS Residuals of the PASCO 310 QC using different Block Combinations .....	82
Table 4-14:	RMS of Navigation Error estimated by the Kalman Filter of the PASCO 310 Flight.....	83
Table 4-15:	Configuration of the DMC Alaska Flight .....	84
Table 4-16:	Configuration of the DMC F-Block Flight.....	85
Table 4-17:	Boresight Values and RMS Residuals of the DMC Alaska QC .....	86

Table 4-18:	RMS of Navigation Errors estimated by the Kalman Filter of the DMC Alaska Flight.....	86
Table 4-19:	Statistical report of Monte Carlo Trials on the DMC Alaska POS AV 310 Simulation.....	87
Table 4-20:	Ensemble RMS and RSS of the DMC Alaska POS AV 310 Simulation .....	87
Table 4-21:	Boresight Values and RMS Residuals of the DMC F-Block QC .....	88
Table 4-22:	RMS of Navigation Error estimated by the Kalman Filter of the DMC F-Block Flight .....	89
Table 4-23:	Configuration of the DSS Ajax Flight .....	90
Table 4-24:	Boresight Values and RMS Residuals of the DSS Ajax QC .....	91
Table 4-25:	RMS of Navigation Error estimated by the Kalman Filter of the DSS Ajax Flight.....	91
Table 4-26:	Statistical report of Monte Carlo Trials on the DSS Ajax POS AV 310 Simulation.....	92
Table 4-27:	Ensemble RMS and RSS of the DSS Ajax POS AV 310 Simulation .....	93
Table 5-1:	Statistical Report of EO Analysis on the PhotoScience UofK POS AV 310 Simulation.....	102
Table 5-2:	Statistical report of EO Analysis on the DMC Alaska POS AV 310 Simulation.....	103
Table 5-3:	Statistical report of EO Analysis on DSS Ajax POS AV 310 Simulated Data .....	104
Table 5-4:	PhotoScience UofK Flight – POS AV 510 (after QC) vs. Simulated POS AV 310 (after ISO), Control Free.....	107
Table 5-5:	PhotoScience UofK Flight – POS AV 510 (after QC) vs. Simulated POS AV 310 (after ISO), 1 Center GCP.....	109
Table 5-6:	ISO Results of the PhotoScience UofK POS AV 510 data, Control Free vs. 1 Center GCP .....	110
Table 5-7:	Block Combinations for the PASCO 310 ISO Test.....	113
Table 5-8:	EO Analysis Results of the PASCO 310 Flight (after QC), Control Free vs. 1 Center GCP .....	113
Table 5-9:	ISO Results of the PASCO 310 Flight, Control Free vs. 1 Center GCP....	114
Table 5-10:	DMC Alaska Flight – POS AV 510 (after QC) vs. Simulated POS AV 310 (after ISO), Control Free.....	117
Table 5-11:	DMC Alaska Flight – POS AV 510 (after QC) vs. Simulated POS AV 310 (after ISO), 1 Center GCP.....	118
Table 5-12:	ISO Results of the DMC Alaska POS AV 510 data, Control Free vs. 1 Center GCP .....	119
Table 5-13:	EO Analysis Results of the DMC F-Block Flight (after QC), Control Free .....	121
Table 5-14:	ISO Results of the DMC F-Block Flight, Control Free vs. 1 Center GCP.	122
Table 5-15:	DSS Ajax Flight – POS AV 510 (after QC) vs. Simulated POS AV 310 (after ISO), Control Free.....	125

Table 5-16:	DSS Ajax Flight – POS AV 510 (after QC) vs. Simulated POS AV 310 (after ISO), 1 Center GCP.....	128
Table 5-17:	ISO Results of the DSS Ajax POS AV 410 data, Control Free vs. 1 Center GCP Solution .....	128
Table 5-18:	Boresight RMS Residual of Less Accurate GPS/IMU Data.....	131
Table 5-19:	Combinations of Calibration Error applied to the PASCO 310 EO Parameters.....	134
Table 5-20:	PASCO 310 Block 1 EO Analysis result after Calibration Error applied ..	134
Table 5-21:	PASCO 310 Block 2 EO Analysis result after Calibration Error applied ..	135
Table 5-22:	PASCO 310 Block 3 EO Analysis result after Calibration Error applied ..	135
Table 5-23:	ISO result of PASCO 310 Block 1 (Calibration Error Inserted) .....	137
Table 5-24:	ISO result of PASCO 310 Block 2 (Calibration Error Inserted) .....	137
Table 5-25:	ISO result of PASCO 310 Block 3 (Calibration Error Inserted) .....	138
Table 6-1:	Approximate Processing Time for Fast DEM Generation and Orthophoto Production.....	141
Table 6-2:	Hardware and Software Specification .....	142
Table 6-3:	Orthophoto Check Point Residuals.....	144
Table 6-4:	USGS. Orthophoto Horizontal Accuracy Requirement.....	144
Table B-1:	Detail Specification of the POS AV Systems .....	175
Table B-2:	Detail Specification of the ADS 40 .....	176
Table B-3:	Detail Specification of the DMC .....	176
Table B-4:	Detail Specification of the UltraCAM.....	177
Table B-5:	Detail Specification of the DSS .....	177

## LIST OF SYMBOLS, ABBREVIATIONS, NOMEMCLATURE

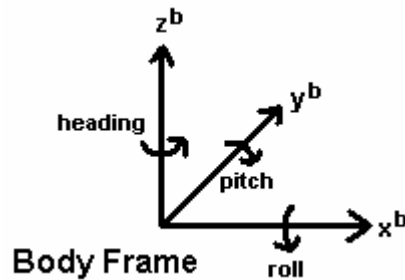
### 1. Conventions

- a. Matrices are in upper case and bold letter
- b. Vectors are in lower case and bold letter
- c. Rotation matrix  $\mathbf{R}$  is specified by two indices denoting the two coordinate systems, e.g.  $\mathbf{R}_b^m$  indicates a transformation from the body frame (b) to the mapping frame (m)

### 2. Coordinate Frames

#### a. body frame (b-frame)

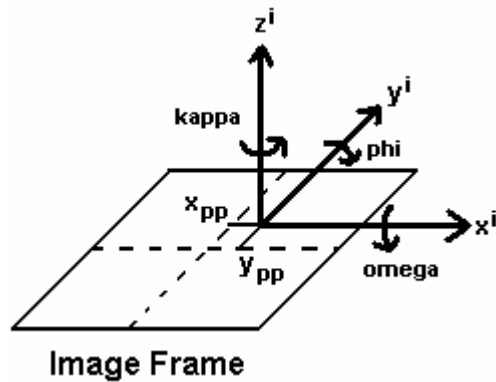
origin: centre of rotation of the sensor unit  
x-axis: forward  
y-axis: right hand side when looking forward  
z-axis: upward and completes the right-handed system



#### b. image frame (i-frame)

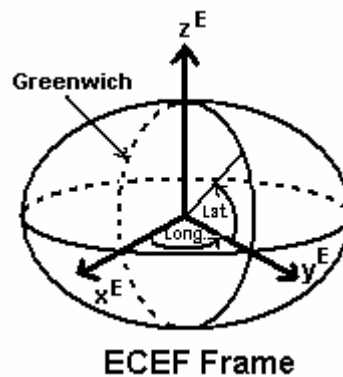
origin: principal point of perspective center  
x-axis: forward

y-axis: right hand side when looking forward  
 z-axis: upward and completes the right-handed system  
 $x_{pp}$ : principal point offset in x-axis  
 $y_{pp}$ : principal point offset in y-axis



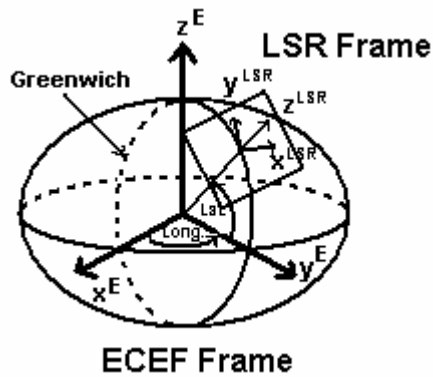
c. Earth Center Earth Fixed frame (ECEF-frame), WGS 84

origin: centre of mass of the Earth  
 x-axis: orthogonal to z-axis, in mean Greenwich meridian plane  
 y-axis: completes right-handed system  
 z-axis: direction of mean spin axis of the Earth



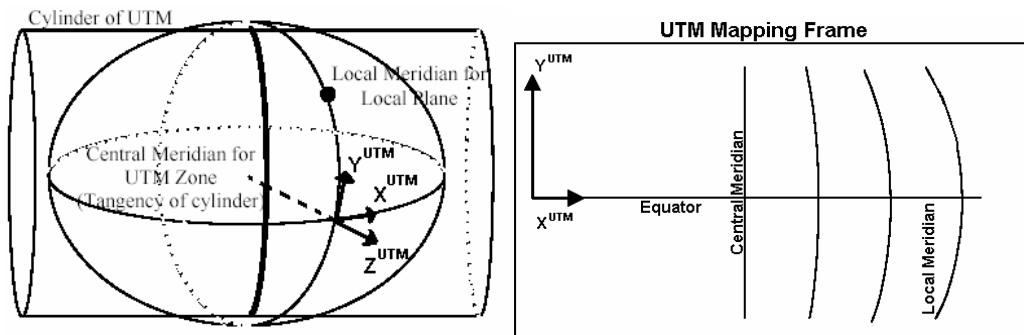
d. Local Space Rectangle frame (LSR-frame)

- origin: centre point of interest
- x-axis: ellipsoidal east
- y-axis: ellipsoidal north
- z-axis: upward along the ellipsoidal normal



e. Universal Transverse Mercator (UTM)

- origin: intersection between equator and local meridian
- x-axis: equatorial east
- y-axis: equatorial north
- z-axis: upward along the equatorial normal



[Courtesy of PCI Geomatics]

### 3. Acronyms

2-D	Two Dimensional
3-D	Three Dimensional
ADS	Airborne Digital Sensor
AT	Aerial Triangulation
CCD	Charge Couple Device
CORS	Continuously Operating Reference Stations
COTS	Commercial Off-The-Self
CPU	Central Processing Unit
DDGPS	Differential Dual Frequency Global Positioning System
DEM	Digital Elevation Model
DGPS	Differential Global Position System
DMC	Digital Mapping Camera
DSS	Digital Sensor System
DTG	Dry Tuned Gyro
DTM	Digital Terrain Model
EO	Exterior Orientation
EOP	Exterior Orientation Parameters
FOG	Fibre Optic Gyro
GPS	Global Positioning System
INS	Inertial Navigation System
IMU	Inertial Measurement Unit
I/O	Input/Output
ISO	Integrated Sensor Orientation
ISAT	Image Station Aerial Triangulation
LIDAR	Light Detection and Ranging
LPS	Leica Photogrammetry Suite
LSR	Local Space Rectangular

MEMS	Micro ElectroMechanical Sensors
MMS	Mobile Mapping System
OEEPE	European Organization for Experimental Photogrammetric Research
POS	Position & Orientation System
POSCAL	Position & Orientation System Calibration
POSEO	Position & Orientation System Exterior Orientation
POSPac	Position & Orientation System Post-Processing Package
PPVG	Point Per Von Gruber
QC	Quality Control
RAM	Random Access Memory
RLG	Ring Laser Gyro
RMS	Root Mean Square
RSS	Root Sum Square
SAR	Synthetic Aperture Radar
SPP	Single Point Positioning
UKF	Unscented Kalman Filter
USGS	United States Geological Survey
UTM	Universal Transverse Mercator
WADGPS	Wide Area Differential Global Position System

## **CHAPTER ONE: INTRODUCTION**

### **1.1. Background and Objective**

During the recent years in aerial mapping, two major components have undergone major research and development. **First**, the use of digital imaging sensors, large format digital frame and line scanning cameras as alternatives to the traditional film-based cameras. As well, there is a plethora of new imaging sensors appearing on the market: medium format digital cameras, multi and hyperspectral imagers, Light Detection and Ranging (LIDAR), and Synthetic Aperture Radar (SAR). **Second**, the direct determination of exterior orientation parameters (EOP). This allowed the mapping industry to move from traditional aerial triangulation (AT) techniques to integrated multi-sensor systems using Differential Global Positioning System (DGPS) and Inertial Measurement Units (IMU). The first component focuses on the data acquisition format in which the digital mapping environment has played an important role. Using IMU instead of the conventional image positives, direct digital sensors provide imagery ready to map, saving on film development and scanning cost. The second component provides a major change in aerial mapping applications by providing direct measurements of the EOP regardless of the type of imaging sensor being used. This is very important especially for new sensors such as line scanners, SAR and LIDAR where the EOP cannot be obtained using the traditional AT techniques. Therefore, the use of integrated DGPS/IMU systems allows the estimation of the EOP directly from the output of the integrated navigation systems. This is known as

Direct Georeferencing and provides a total solution for the problem. Such integrated solutions are also known as Mobile Mapping Systems (MMS).

In traditional large area mapping projects, there always exists a block of images with side and end-laps. Having such blocks of images, make it possible to combine the advantages of both direct georeferencing systems and aerial triangulation by using Integrated Sensor Orientation (ISO). The ISO concept has been discussed widely in the last few years, most extensively by the OEEPE test in 2001 [Jacobsen and Wegmann (2001), Heipke et al (2001a)]. This thesis investigates the use of ISO for processing blocks of images, collected by different imaging sensors namely; Film camera, Large and Medium format digital camera. The investigation looks into the performance of ISO when applied on different quality of GPS/IMU data from a DG System and analyses the ways to optimize the processing procedure. Further, the impact of DG technology on map production (particularly on fast orthophoto generation) is addressed. The major objectives of the thesis are summarized as following:

- Investigating the error sources of image Georeferencing
- Discussing the concept of ISO and its extended use in Quality Control
- Analyzing the performances of ISO using different frame camera systems integrated with high end GPS/IMU systems
- Analyzing the possibility of using less accurate GPS/IMU system in conjunction with ISO to achieve similar performance as high end GPS/IMU systems
- Demonstrating the impact of direct georeferencing on map production

## **1.2. Thesis Outline**

In Chapter 2, airborne image georeferencing is introduced, focusing on the determination and acquisition of EOP. Two major approaches are presented and compared. For the use of both approaches, error sources in image georeferencing are reviewed. Error models are formulated based on time-dependent and time-independent variables, and finally some examples are presented.

In Chapter 3, the need for quality control for direct georeferencing is discussed. This is an important step and is closely related to ISO. Some current methods on how quality control is being used are discussed. In addition, the optimization and integration of quality control process are demonstrated.

In Chapter 4, the GPS/IMU dataset to be used in Chapter 5 is described. An algorithm towards less accurate GPS/IMU data simulation is formulated and some examples are presented. For each dataset, project information, imaging sensor type and system performance are discussed

In Chapter 5, the ISO analysis in comparison with direct Georeferencing is described. The relationship between GPS/IMU data quality and ISO performance is discussed through examples. Also, analysis is carried out to optimize the ISO workflow.

In Chapter 6, methods by which direct georeferencing can be used for fast Digital Elevation Model (DEM) extraction and fast orthophoto generation are demonstrated. Then, an on-going development of near real-time data for rapid response is discussed.

In Chapter 7, the research results and recommendations for future work are presented and summarized.

## CHAPTER TWO: IMAGE GEOREFERENCING FOR AIRBORNE APPLICATIONS

### 2.1. Background

Typically image georeferencing is defined as the transformation of the 3D coordinate vector  $\mathbf{r}^i$  of a point, with respect to the image frame (i-frame), to its corresponding 3D ground coordinate vector  $\mathbf{r}^m$  with respect to the mapping frame (m-frame). This requires two quantities to be known – the coordinates of the camera's lens perspective centres in the m-frame,  $\mathbf{r}_{pc}^m(t)$  and the rotation matrix between the i-frame and the m-frame,  $\mathbf{R}_i^m(t)$ . The 3D ground coordinate vector of any point ( $p$ ) in the m-frame,  $\mathbf{r}_p^m$ , can be written as [El-Sheimy (1996b)]

$$\mathbf{r}_p^m = \mathbf{r}_{pc}^m(t) + s\mathbf{R}_i^m(t)\mathbf{r}_p^i \quad (2.1)$$

Where ( $t$ ) is the time of exposure and ( $s$ ) is the scale factor

$\mathbf{r}_{pc}^m(t)$  and  $\mathbf{R}_i^m(t)$  are usually called the exterior orientation parameters. These three translations and three rotations essentially describe a rigid-body motion in space. Figure 2-1 illustrates the relationship between the camera and the mapping frame. For details, see [El-Sheimy (1996b), Mostafa et al (1997) and Schwarz et al (1993)].

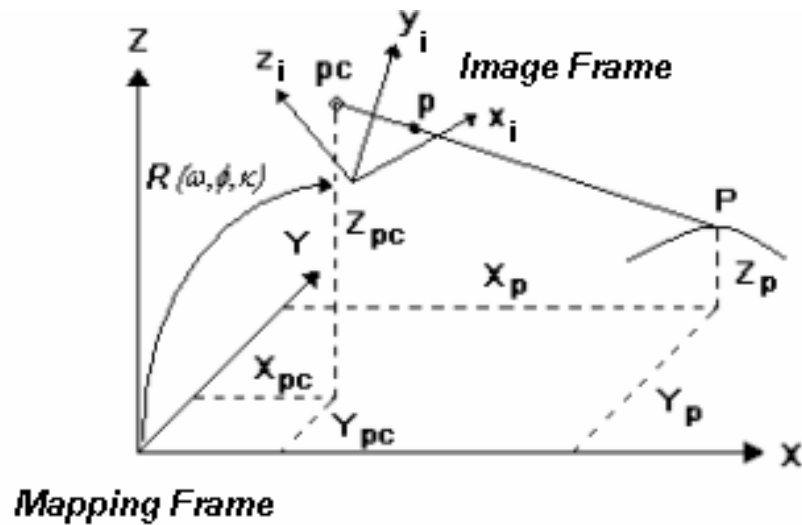


Figure 2-1: Illustration of the Relationship between Image and Mapping Frame

## 2.2. Direct Georeferencing, Indirect Georeferencing and Integrated Sensor Orientation

There are three basic approaches for computing the EOP of an imaging sensor, they can be described as:

- Determining the EOP *directly* using suitable positioning and orientation sensors. This approach is referred to here as DG, also known as Direct Sensor Orientation
- Determining the EOP *indirectly* by extracting them from a block of images using a sufficient number of well-distributed known ground control points and Aerial Triangulation

- Determining the EOP using a combination of a block of images, positioning and orientation sensors' measurements, and , when necessary, ground control points (GCPs) This approach is referred to as ISO.

### 2.2.1. Direct vs. Indirect Georeferencing

The **DG** approach is most commonly achieved using an integrated DGPS/IMU. Such approaches have been introduced by [Schwarz et al (1984), Schwarz et al (1993)] where the mathematical model and proposed applications were presented Later on, studies on the implementation of DG in many applications [see for example, Abdullah (1997), El-Sheimy (1996a,b), Mostafa et al (1997), Schwarz (1995), Skaloud et al (1996) and Toth and Grejner-Brezinska (1998)] and in commercial products [see for example, Bossler et al (1996), El-Sheimy and Lavigne (1998), Reid et al (1998), Mostafa et al (2001a,b), Mostafa and Hutton (2001), Toth (1997)].

The **Indirect Georeferencing** approach uses AT, which relies on adjusting a network of tie points in a block of images with a sufficient number of well distributed known GCPs.

When the availability of ground control points is in question, such as within forests, snow-covered grounds, desert, or along a coastline, the ability to resolve the EOP indirectly is limited. Often these areas are also very important when emergency response application is required, such as in the case of a forest fires, flooding and hurricanes. Such an application requires fast orthophoto generation, and there is insufficient time and resources to extract

the EOP using traditional AT. In addition, some projects only require a single strip or single photo orientation. For instance, in the case where there is an existing DEM, the use of traditional AT to determine the EOP is unpractical because it requires excessive GCPs and additional overlapping photos. Hence in many applications direct georeferencing is either the only practical solution, or the most cost effective solution [Schwarz and El-Sheimy (2004)].

The ground accuracy of objects coordinates, when using a direct georeferencing system, is dependent upon the GPS accuracy for position and the IMU accuracy for orientation. The orientation error produces a position error on the ground as a function of the flying height (or photo scale). At best, GPS provides about 5 - 10 cm RMS when using dual frequency differential processing with highly accurate GPS basestation data. For a high end direct georeferencing system using ring-laser gyros (RLG), fibre optic gyros (FOG) or dry-tuned gyros (DTG), the orientation accuracy is typically about 0.005 deg RMS for roll and pitch, and about 0.008 deg RMS for the heading. For traditional large scale mapping projects that are flown relatively low above the ground, the ground accuracy becomes dominated by the DGPS position error [Mostafa et al (2001b)]. Therefore, for large scale mapping ( $> 1:1000$ ) projects requiring centimetre accuracy, direct EO usage from DG system is marginal for film camera system [Dardanelli et al (2004)]. To improve the GPS positioning accuracy, further research has to be done [Bruton et al (2001)]. However, using AT to improve the photo centre positioning accuracy has long been considered by researchers as an acceptable

solution, and has been introduced in OEEPE tests as the Integrated Sensor Orientation (ISO) [Jacobsen and Wegmann (2001), Heipke et al (2001a)].

### **2.2.2. Integrated Sensor Orientation**

GPS/IMU assisted AT or ISO combines benefits from both DG and traditional AT, when the imagery is flown in a block configuration with sufficient overlap. By using the EOP from DG systems as an initial approximation for AT, only a limited number of tie points in the overlapping area are needed. GCPs are only required to check for datum shifts and correct for systematic residual errors in the DGPS. Furthermore, using the direct EOP in the tie-point matching process reduces the computational time and number of blunders, making the entire process truly automatic. While the DG system allows direct determination of exterior orientation parameters with high accuracy and reliability, there exist some projects which require higher accuracy. Such projects will require the directly estimated EOP to be refined before they can be used in these mapping projects, since they are limited in accuracy to the accuracy of the DGPS. In this case, ISO can be performed to refine the accuracy of the EOP in order to improve both absolute and relative accuracy [Heipke et al (2001b), Cramer et al (2001a,b), Jacobsen et al (2001), Honkavaara et al (2002), Casella et al (2004), Casella (2004) and Henskin et al (2002)]. In terms of the ISO mathematical model it is based on the well known collinearity equations. But, instead of solving for the EOP as unknowns, initial approximate with proper standard deviation are provided. More information about the mathematical model is presented in section 2.3.

Except for large scale engineering projects which are limited by the accuracy of DGPS, a high end DG system is sufficiently accurate to perform all types of projects such as: corridor mapping, single photo orientation, mapping in remote areas, or large area mapping. This total solution provides the flexibility of being able to do any project without the limitation of needing to fly in a block configuration. However, it is useful to investigate if a lower accuracy DG system, hence lower cost, can achieve similar accuracy of a high end system when ISO is used.

One may argue that the collection of tie points in a block of images is a time consuming process, and hence this limits any benefits that ISO with a lower cost/lower accuracy DG system might achieve. However, the seeded EOP given by the less accurate DGPS/IMU system provides an important piece of information for the automatic tie point collection process. The search areas for potential tie point locations can be narrowed down, and therefore both performance and accuracy is significantly improved. In addition, if the number of tie point required to perform ISO can be optimized hence processing time can also be minimized.

Table 2-1 lists the advantages and disadvantages of the three approaches; DG, Indirect Georeferencing and ISO,

**Table 2-1: Characteristics of different Image Georeferencing approaches**

<b>Approach</b>	<b>Advantages</b>	<b>Disadvantages</b>
<b>Direct Georeferencing</b>	<ul style="list-style-type: none"> <li>• Aerial Triangulation is not required (except for system calibration)</li> <li>• Control free environment (except for quality control)</li> <li>• Corridor, remote area mapping, and single photo orientation</li> </ul>	<ul style="list-style-type: none"> <li>• Position accuracy is limited by GPS solution</li> <li>• High accuracy GPS/IMU is recommended</li> <li>• Increase system cost</li> <li>• Precise system calibration parameters are required</li> </ul>
<b>Indirect Georeferencing</b>	<ul style="list-style-type: none"> <li>• Redundant solution using additional GCP</li> <li>• Robust solution against error in interior orientation parameters</li> </ul>	<ul style="list-style-type: none"> <li>• Well distributed GCP is always required</li> <li>• Block of imagery is always required</li> <li>• High operation cost</li> </ul>
<b>ISO</b>	<ul style="list-style-type: none"> <li>• Combine all advantages from both approaches</li> <li>• Potential possibility of using less accurate GPS/IMU system</li> </ul>	<ul style="list-style-type: none"> <li>• Block of imagery is always required</li> <li>• Unpractical for projects where orthophoto is generated using existing DEM</li> </ul>

### **2.3. Error Sources in Image Georeferencing**

After introducing the different techniques for estimating the EOP and the way to improve it, this section discusses why a perfect system is not possible, and what parameters are critical for the operation of a Mobile Mapping System (MMS) [Grejner-Brezinska (2001), Ip et al (2004b), Ellum et al (2003) and Yastikli (2004)]. An airborne MMS consists of two

major components; an imaging component and a georeferencing component, in addition to a flight management system and an on-board controlling unit. The imaging component may be a film or digital camera, a multi-spectral pushbroom scanner, an interferometric radar system, or a scanning laser system. If a digital camera is used as the imaging component and fixed to the same rigid body as an IMU and a GPS antenna (i.e. to the aircraft), then the EOP can simply be determined by interpolating the translation and rotation vectors at the moment of exposure. These parameters can be stamped on each digital image. In this way, the complex time-dependent positioning problem is transformed into a spatial problem from which time has been eliminated as a variable. This obviously requires very accurate time synchronization in the millisecond level (one millisecond is equivalent to 3.33 cm position error at a velocity of 120 km/h) between the different sensors [Grejner-Brezezinska (2000)]. The resulting georeferenced digital images obtained in this way become the building blocks for the digital mapping program. It should be noted that a multi-sensor system defined in this way is completely self-sufficient, i.e. only data collected in the platform is needed to solve the georeferencing problem. It is independent of GCPs because GPS, by linking into a system of Earth orbiting satellites, will output all its results in an Earth-fixed Earth-centered coordinate frame – the WGS 84 [Titterton (1997)] (see Figure 2-2 for an example of the concept of airborne-based MMS). MMS thus provides an integrated problem solution, rapid data acquisition, fully digital data storage, and great flexibility in post-mission data processing.

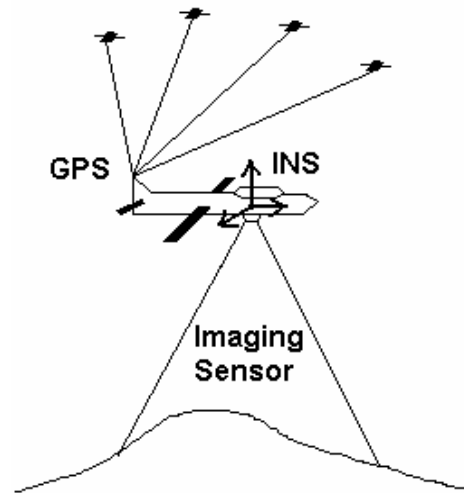


**Figure 2-2: An Airborne Mapping System**

[Mostafa and Schwarz, 2001]

The main components of a DG system for mobile mapping applications are composed of different technologies. GPS uses range measurements from satellites, and IMU uses gyros and accelerometers to measure angular velocity and specific force. Table 2-2 lists the characteristics of a stand-alone GPS, a stand-alone IMU and an integrated GPS/IMU.

**Table 2-2: General difference between GPS and IMU**

[Schwarz et al, 1994 ;El-Sheimy, 1996b]

	<b>Advantage</b>	<b>Disadvantages</b>
<b>IMU</b>	<ul style="list-style-type: none"> <li>• Self contained and independent system</li> <li>• Continuous data acquisition</li> <li>• Three positioning and three attitude components</li> <li>• High data sampling rate (up to 600 Hz)</li> </ul>	<ul style="list-style-type: none"> <li>• Sensor errors grows with time causing positioning error divergence</li> </ul>
<b>DGPS</b>	<ul style="list-style-type: none"> <li>• High accuracy of position and velocity estimation</li> <li>• Time-independent error model</li> </ul>	<ul style="list-style-type: none"> <li>• Losses of lock causing gaps in the trajectory</li> <li>• Low data sampling rate (1-20 Hz)</li> <li>• Slow ambiguity resolution time over long baseline and/or in presence of higher ambient noise</li> </ul>
<b>IMU / DGPS</b>	<ul style="list-style-type: none"> <li>• Combine all advantages of both systems</li> <li>• Redundant and complementary data (both systems' errors are separately observable)</li> <li>• Navigation through GPS outages</li> <li>• GPS fixes allow IMU error estimation</li> </ul>	<ul style="list-style-type: none"> <li>• No significant limitations</li> <li>• Precise time synchronization needed</li> </ul>

As depicted in Table 2-2, the low noise and high bias of the IMU, and the high noise and low bias GPS are complementary systems. Their integration, therefore, reduces or eliminates their limitations. The DG mathematical model has been used for numerous applications in land, airborne and marine applications [Schwarz et al (1993) El-Sheimy (1996a) and Mostafa (2003)]. Several forms of the mathematical model have been previously presented to accommodate certain applications. In this section, the basic unified

formula is re-visited. As shown in Figure 2-3, the georeferencing basic model can be expressed by Equation (2.2), (2.3) and (2.4). Different terms being used in the equations are explained in Table 2-3:

$$\mathbf{r}_p^m = \mathbf{r}_{INS}^m(t) + \mathbf{R}_b^m(t)(s\mathbf{R}_i^b r_p^i - \mathbf{a}_1^b) \quad (2.2)$$

where,  $\mathbf{r}_{INS}^m(t) = \mathbf{r}_{GPS}^m(t) - \mathbf{R}_b^m(t)\mathbf{a}_2^b$  (2.3)

therefore  $\mathbf{r}_p^m = \mathbf{r}_{GPS/INS}^m(t) + \mathbf{R}_b^m(t)(s\mathbf{R}_i^b r_p^i - \mathbf{a}_1^b - \mathbf{a}_2^b)$  (2.4)

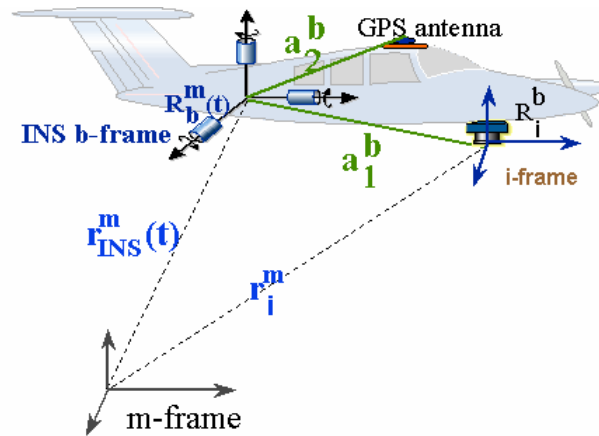


**Figure 2-3: Concept of Direct Georeferencing Model**

[El-Sheimy, 1996b]

**Table 2-3: Terms in the Direct Georeferencing Equation**

Variable	Description
$r_p^m$	Position of the point of interest represented in the mapping frame
$r_{GPS}^m(t)$	GPS antenna position represented in the mapping frame
$r_{GPS/INS}^m(t)$	GPS antenna position presented in mapping frame after GPS/IMU data post-processing and interpolation
$R_b^m(t)$	Rotation matrix between the IMU body frame and the mapping frame
$s$	Scale factor between the image space and the object space
$R_i^b$	Rotation matrix between the image frame and the IMU body frame
$r_p^i$	Location of the point of interest represented in the image frame
$a_1^b$	Lever arm offset between the IMU body frame and the image frame
$a_2^b$	Lever arm offset between the IMU body frame and the GPS antenna

While the DG model is based on the determination of EOP using positioning and orientation sensors, the ISO is to improve the EOP using image measurement collected from stereopairs. Therefore, the well known collinearity equation is required; see Equations (2.5) and (2.6):

$$x = -f \frac{r_{11}(X - X_0) + r_{21}(Y - Y_0) + r_{31}(Z - Z_0)}{r_{13}(X - X_0) + r_{23}(Y - Y_0) + r_{33}(Z - Z_0)} \quad (2.5)$$

$$y = -f \frac{r_{12}(X - X_0) + r_{22}(Y - Y_0) + r_{32}(Z - Z_0)}{r_{13}(X - X_0) + r_{23}(Y - Y_0) + r_{33}(Z - Z_0)} \quad (2.6)$$

**Table 2-4: Terms in the Collinearity Equation**

Variables	Description
$x, y$	Image coordinate of the measured tie points or GCPs
$f$	Calibrated focal length
$X, Y, Z$	Tie point coordinates ( $r_p^m$ ) in the mapping frame
$X_0, Y_0, Z_0$	Position of the camera perspective centre ( $r_i^m$ ) in the mapping frame
$r_{ij}$	Elements of the rotation matrix $R_i^m(\omega, \phi, \kappa)$ between the image frame and the mapping frame

Since initial approximates are provided for both  $r_i^m$  and  $R_i^m(\omega, \phi, \kappa)$  using the EOP from the DG system, image measurements from GCPs are no longer a mandatory requirement in the GPS/IMU assisted bundle adjustment. However, the use of proper standard deviation over the initial EOP is very important, and such information should be available from the Kalman Filter after GPS/IMU data post-processing. More discussion on the use of proper standard deviation is discussed in Chapter 4. Although one of the conditions about the use of ISO is the sensor calibration should be pre-determined, under operational conditional system self calibration can also be performed [Wegmann (2002)]. This will be further discussed in Chapter 3.

For a MMS, a number of parameters play a role when the system performance, accuracy, and reliability are concerned. These parameters can be classified into the following categories: sensor error, integration error and calibration error.

### **2.3.1. Sensor Errors**

Three major sensors are used in airborne mobile mapping systems: Imaging sensor, GPS and IMU. All these sensors contain different error sources which will be discussed separately.

#### ***Imaging Sensor***

Current frame-based imaging sensors can be categorized into three types: analog film camera, large format digital camera and medium format digital camera. Analog film camera has been used for decades, such as the Leica RC series and the Z/I Imaging LMK&RMK series. These cameras usually have two types of lens cones: 153 mm (6") wide angle and 305 mm (12") normal angle. Their large coverage and geometry stability have made them standard imaging sensors in large area aerial mapping projects. Since film cameras use film negatives for image acquisition, the film must be developed first before they can be used either in analog or analytical photogrammetric plotters or even scanned into digital format for use in digital photogrammetric workstations. Scanning resolution usually ranges from 7 to 28 microns depending on the scanning devices and the application. After the transformation into digital format, interior orientation must be performed using fiducial marks to relate the image coordinate system to the pixel coordinate system. This transformation is known as the 2-D transformation which consists of 2, 4, 6, or 8 parameters. The performance of the interior orientation process is based on the

measurement accuracy of the fiducial marks. Most commercial tie points matching modules support automatic fiducial marks collection after the user input a template of measurements.

Large format digital cameras are especially developed as a replacement for analog film cameras. Using arrays of Charge Couple Device (CCD), images can be directly acquired in digital form, saving numerous costs in film development and scanning process. In addition, these sensors are capable of collecting multispectral data which enhances the applications for these sensors. Large format digital cameras include the Leica Geosystems's Airborne Digital Sensor (ADS), the Z/I Imaging's Digital Mapping Camera (DMC) and the Vexcel's UltraCam. In addition to large format digital frame camera, medium format digital camera is also available for different applications. Using Commercial Off-The-Shelf (COTS) components, these types of cameras are especially designed for mobilization, allowing fast orthophoto generation for emergency applications. The Applanix's Digital Sensor System (DSS) is an example of these types of cameras. Figure 2-4 shows different airborne digital camera systems and Table 2-5 lists some information about these cameras. Appendix B-1 provides detailed information about these cameras.

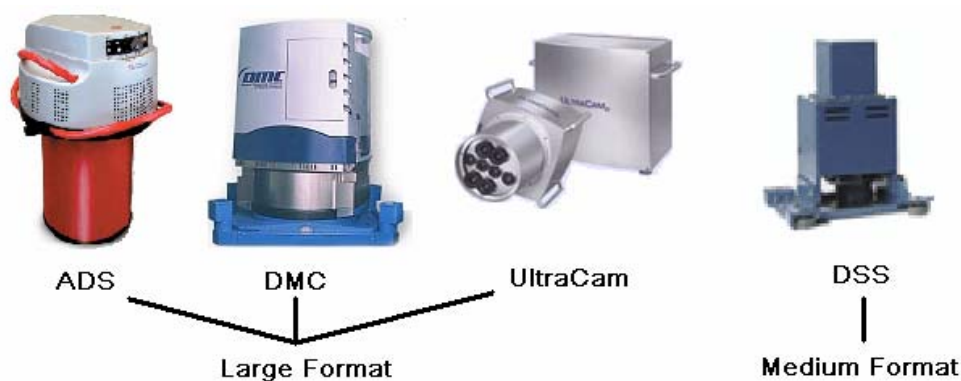


**Figure 2-4: Aerial Digital Camera Systems**

[Courtesy of Leica Geosystems, ZI/Imaging, Vexcel and Applanix, respectively]

**Table 2-5: Information on Airborne Digital Camera Systems**

Imaging Sensor	Focal Length	Image Size	Pixel Size	Sensor Type
Airborne Digital Sensor (ADS)	62.5 mm	2k x 12k	6.5 $\mu\text{m}$	3-Line Scanner
Digital Mapping Camera (DMC)	120 mm	14k x 8k	12 $\mu\text{m}$	Multiple Frame
UltraCam	100 mm	11.5k x 7.5k	9 $\mu\text{m}$	Multiple Frame
Digital Sensor System (DSS)	35, 55 mm	4k x 4k	9 $\mu\text{m}$	Single Frame

When images are collected in digital form, the fixed CCD size and location allow the same pixel coordinate system on each acquired image, with respect to the camera's perspective center; i.e. the 2D-affine transformation is no longer required to create the relationship between image and pixel coordinate system. However, no camera is built without errors, calibration reports are usually available to compensate for some of these errors, e.g. principle point offset and lens distortion. While the large format digital camera combines

several CCDs to deliver the large ground coverage, the calibration becomes more complicated than single CCD camera systems (e.g. the DSS system). Therefore, camera calibration is very important as it is highly correlated with image measurement accuracy. More information about camera calibration is discussed in section 2.3.3. Since all these digital camera systems are designed for aerial mapping, their rigid mounting provides stable camera parameters. In addition, these sensors are compatible to use with the DG system and therefore the IMU is mounted inside or onto the camera's frame.

### ***Global Positioning System (GPS)***

The GPS is deployed by the United States Department of Defense. It provides accurate position, velocity and time anywhere on or near the Earth. This is achieved by the measurement of range between the satellites and the receiver on the mapping platform, using continuously broadcast signals on two L-band carrier frequencies. The first is L1 frequency of 1575.42 MHz and the other is the L2 frequency of 1227.60 MHz. At any location on the Earth's surface, four or more satellites are always visible through the 24 (full constellation) operational GPS satellites at an altitude of about 20,200km above the Earth's surface. Upon the removal of Selective Availability in May 2000, GPS accuracy has been improved by ~70%. However, for single point positioning (SPP) using single frequency data, GPS cannot provide sub-metre accuracy due to the effect of satellite orbit and clock errors as well as atmospheric attenuation and receiver errors. Table 2-6 summarizes the contribution of these factors on the achievable accuracy of GPS SPP.

**Table 2-6: GPS Error Source in Single Point Positioning using Single Frequency**

[Olynik et al, 2002]

Error Source	Approximate Magnitude
Satellite Orbit and Clock	~ 2.3 m
Atmospheric (Ionosphere and Troposphere)	~ 2.7 m
Receiver (Multipath and Noise)	0.01 – 10 m
Total Error	~ 5 m – 15 m

To overcome these limitations, dual frequency GPS receivers in Differential GPS (DGPS) processing mode are typically used. The additional frequency (L2) data can be used to model the ionosphere effect which significantly improves the position accuracy. In addition, the differencing between two receivers allows the removal of both satellite and receiver clock errors. Table 2-7 summarizes the approximate magnitude of different errors sources for the DGPS mode of operation.

**Table 2-7: Error Sources in Differential Dual Frequency GPS (DDFGPS)**

[Olynik et al, 2002]

Error Source	Approximate Magnitude
Satellite and Receiver Clock	Differenced Out
Atmospheric	~ 0.4 ppm
Orbital	~ 0.5 ppm
Noise	~ 2 mm
Multipath	~ 3 mm
Total Error	~ 0.5 mm + 0.9 ppm

Based on the approximate total error for DDFGPS, an airborne mapping project usually has a baseline separation between 50 km – 100 km. Therefore, 5 cm – 10 cm root-mean-square (RMS) position accuracy can be achieved. Notice that this requires highly accurate base

station data with well known coordinates. In remote area where GPS base station cannot be setup, Continuously Operating Reference Stations (CORS) can be used [see Bruton et al (2001), Soler et al (2003) and Snay et al (2002) for more details on CORS]. However, data rate and quality of CORS data may not be suitable for aerial mapping applications, especially when baseline separation is >50km. Since GPS base station data is very important for DGPS solution, integration with the Wide Area Differential Global Position System (WADGPS) is currently under research to improve long baseline solutions. Examples of such services are the OmniSTAR and the NavCom's Starfire [Cannon et al (2002)].

### *Inertial Navigation Systems (INS)*

While INS are self-contained and independent systems, performance of INS are categorized by its Inertial Measurement Unit's (IMU) gyro drift rate and accelerometer bias. Table 2-8 lists the characteristics of three types of IMUs commonly used in the market: navigation, tactical and Micro-Electro-Mechanical-Sensors (MEMS).

**Table 2-8: Characteristics of IMUs**

[El-Sheimy, 2000]

IMU Type	Navigation	Tactical	MEMS
Gyro Drift Rate (deg/hr)	0.005 – 0.015	1 – 3	100 – 300
Accelerometer Bias ( $\mu\text{g}$ )	50 – 100	100 – 1000	1 - 10
Cost (USD)	70 – 100 k	10 – 20 k	0.8 – 3 k

Navigation grade IMU has very low gyro drift rate such that in the case of GPS outage or jamming, the position error can remain at a very low level. Less expensive commercial type navigation grade IMUs are currently being used in commercial aircraft for accurate attitude determination. Furthermore, they are used in land based MMS as a bridging system to maintain high level of position accuracy when GPS position is affected by blockage or multipath [Lithopoulos et al (1996) and Reid et al (1998)]. Most DG applications use tactical grade IMU. Although its performance is lower than the navigation grade IMU, through the integration with GPS, both position and attitude determination can remain at high accuracy [Mostafa and Hutton (2001), Grejner-Brezezinska (2000) and El-Sheimy (1996a,b)]. In addition, the target application is in an environment in which GPS blockage and multipath influence is minimal (e.g. airborne and land-based rural mapping). MEMS IMU is the new generation which provides small (chip size) and low cost alternative. However, stability for such sensors sometimes is in question, especially in the scale factor. Research of MEMS is still in progress to continuously improve the performance [Abdel-Hamid et al, (2004)]. Such sensors have been used in several applications such as vehicle and personal navigation.

The performance characteristics of inertial sensors can be summarized by four categories: Sensor Bias, Sensor Scale Factor, Axes Misalignment and Noise [Titterton (1997) and El-Sheimy (1996b)]. First, sensor bias consists of two parts – deterministic and stochastic. The deterministic part is a constant offset which can be determined by calibration. While the

stochastic part is a drift such that sensor error accumulates over time; this error is random in nature and should be modeled as a stochastic process. Through proper modeling the error is left with the angular random walk over the random bias of the sensor. Second, scale factor is the relationship between the output signal of the sensor and the physical quantity being measured. Since scale factor error is deterministic in nature, it therefore can be determined by calibration. Third, the imperfection of sensor mounting may result in a non-orthogonality of the axes defining the IMU body-frame. Such imperfection will affect each axis by the measurements of the other two axes. Generally speaking, axes misalignment can be calibrated or modeled in the IMU error equation. Finally, the sensor noise includes noise from the sensor itself or other electronic equipment. While noise is non-systematic, it can only be modeled by a stochastic process. Fourth, as a property of white noise, the noise level is proportional to the square root of the measurement bandwidth. As there is an inverse relationship between the bandwidth and measurement time, noise decreases with the square root of the measurement time. This is an important relationship which applies to a process called initial alignment to minimize system noise through Kalman Filtering. More information about initial alignment is discussed in Section 2.3.4.

### **2.3.2. Integration Errors**

In order to combine measurements from multiple sensors, three parameters must be considered: sensor placement, synchronization and filtering technique [Skaloud (1999) and Grejner-Brezezinska (2001)].

#### ***Sensor Placement***

Due to the operating condition between sensors, they are placed in different locations on the airborne MMS platform. First, the imaging sensor is placed at the bottom of the aerial photography aircraft to allow maximum visibility for image acquisition. Also, with the help of a gimbal system, maximum possibility of acquiring true vertical imagery can be achieved, in which tilting of imagery can be minimized. Second, to allow continuous GPS signal reception at all times, the GPS antenna is placed outside of the platform. It is always preferable to mount the GPS antenna directly above the centre of the imaging sensor to improve the calibration efficiency. But, the aircraft wings must be taken into consideration, as GPS blockage might happen during large banking angles. Practically, pilots will have to take wider turns ( $<20$  deg) to minimize banking angles. Third, as the IMU is a self contained instrument, it does not have specific installation requirements except for being rigidly mounted to the imaging sensor. Rigid mounting of the IMU is a key factor to maintain the constant rotation matrix between the IMU body frame and the camera frame, as defined by the Direct Georeferencing formula in Equation (2.4) [Skaloud (1999)].

Therefore, it established a calibration parameter called boresight mis-alignment (the angular misalignment between the IMU and camera frames). Boresight calibration is periodically done at system installation and is a quality control check for the entire system. On the other hand, the spatial offset between sensors after installation is referred to as the lever arm. This includes the lever arm between the GPS antenna and the IMU and the lever arm between Imaging Sensor and the IMU. The IMU is rigidly mounted on the imaging sensor and therefore the lever arm offset can be calibrated easily. Information about boresight and GPS/IMU lever arm calibration is discussed in section 2.3.3.

### ***Synchronization***

For high accuracy position and orientation determination by MMS, precise synchronization of the different data streams is very important. The three sensors: GPS, IMU and imaging sensor operate at their own time frame and frequency. The synchronization of all different components is an essential assumption in the direct georeferencing case. In principle, GPS provides the best time reference with GPS time. IMU comes with an integrated timing module, but is rarely to be directly synchronized with the GPS. On the other hand, imaging sensors do not come with any timing module, and the acquisition of imagery does not occur at a fixed time interval. To resolve this timing problem, newer imaging sensors provide a linkage to the data logging computer or GPS receiver, in order to time-tag the imagery exposure time and synchronize with the Pulse Per Second (PPS) signal from the GPS receiver. For example, to determine the imaging sensor time tag in GPS time frame

$(T_{\text{ImagingSensor}}^{GPS})$  when it is connected to the data logging computer, three pieces of information is required; computer time when the logging computer responds to the PPS ( $T_{PPS}^c$ ), GPS position record time tagged in GPS time frame ( $T_{PPS}^{GPS}$ ) and the imaging sensor time tag in the computer frame ( $T_{\text{ImagingSensor}}^c$ ). Once the offset between the GPS time frame and the computer time frame ( $T_{PPS}^{GPS} - T_{PPS}^c$ ) is known, ( $T_{\text{ImagingSensor}}^{GPS}$ ) can be determined using Equation 2.7 [El-Sheimy (1996b)].

$$T_{\text{ImagingSensor}}^{GPS} = T_{\text{ImagingSensor}}^c + (T_{PPS}^{GPS} - T_{PPS}^c) \quad (2.7)$$

Whether it is real-time or post-processing integration, interpolation is used to synchronize all the measurements from different sensors. Since all measurements are collected by the controlling computer system, data transmission delays must be considered. Such delays can result from cable length, computer clock error or Analog to Digital (A/D) conversion. For precise system design, these delays can be determined easily and calibrated [Skaloud (1999)].

### ***Filtering Technique***

Filtering is the heart of the GPS/IMU integration which handles both GPS and IMU data streams and provides the necessary error estimation and correction. In GPS/IMU Integration, Kalman Filtering (KF) is the most popular technique due to its recursive form

and prediction capability [Titterton (1997), Britting (1997) and Scherzinger (1997)]. In addition to KF, Neural Network and Unscented Kalman Filter (UKF) Data Fusion are considered by some researchers as alternative to improve both performance and accuracy [Chian et al (2004), Eun-Hwan and El-Sheimy (2004), and Reda et al (2003)]. For Kalman Filtering, there are a few integration mechanisms such as loosely, tightly and deeply coupled. The use of design architecture is based on the application and the operation environment. For example, in the deeply coupled integration the structure is more complex and requires more computational power. Overloading the system might lead to data gap and possible performance degradation might occur. Therefore, in airborne application with little GPS blockage and multipath, loosely coupled (GPS aided) is commonly used with a closed loop feedback for cycle slip detection. With this de-centralized approach, the IMU Kalman Filter gives systematic error modeling of the IMU measurements and provides feedback to the navigator, which continuously improves the accuracy of the system. However, the performance of error modeling is based on the number of states included in the Kalman Filter state vector. The minimum number of states that the KF requires is 6 states which define the change in velocity and acceleration along the three axes. But, if additional states are included such as gyros drift, accelerometers bias and gyros/ accelerometers scale factors, the estimation is more accurate and the performance of the system will be better. Some Kalman Filter designs may include up to 32 states of error estimation, but high computational power is required. Figure 2-5 illustrates the de-centralized loosely coupled

Kalman Filter design architecture [Wei et al (1990), Titterton (1997) and El-Sheimy (1996b)].

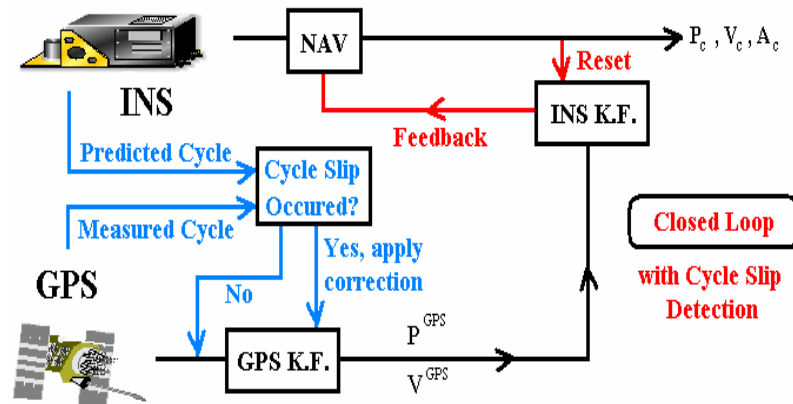


**Figure 2-5: De-Centralized Loosely Coupled GPS/IMU Integration Mechanism using Kalman Filtering Technique**

[El-Sheimy, 1996b]

### 2.3.3. Calibration Errors

Through the earlier discussion on the use of sensors, there are a number of parameters which need to be calibrated to complete the system design and maintain certain system accuracy. This includes sensor errors, lever arm offset, boresight mis-alignment, synchronization and initial alignment.

#### *Sensor Errors*

Sensor errors such as GPS and IMU can be calibrated using proper modeling of the deterministic part through Kalman Filtering. Furthermore, the GPS receiver and IMU

manufacturers provide accurate information about the deterministic parameters. But, the stochastic part such as noise and random walk are difficult to model, this requires long term stability testing to build up a proper model [Titterton (1997), Britting (1997) and Scherzinger (1997)].

On the other hand, frame-based imaging sensor calibration contains two categories: film-based and digital-based calibration. As mentioned in Section 2.3.1, both type of sensors contain interior orientation parameters, which are typically chosen as focal length, principal point offset and lens distortion parameters. The only exception is the fiducial coordinates which are only available in film-based cameras. The calibrations of film-based cameras are usually controlled by government agencies such as U.S. Geological Survey (USGS) and have relatively high accuracy with long term stability. While the digital camera format has not been standardized, the calibration relies on the manufacturer, this requires terrestrial, airborne or both Large format digital frame cameras have similar camera body designs as the film camera, and therefore the camera stability is better than the small and medium format digital cameras when COTS components are used. Evaluation of the digital camera's stability is based on repeating calibration and therefore new calibration algorithms are developed to calibrate digital cameras efficiently. Also, some researches have been carried out to analyze the correlation between the accuracy of camera parameters and the performance of direct georeferencing [Habib et al (2004), Habib et al (2002), Fraser (1997)]. For frame cameras, terrestrial calibration is better because of the calibration site setup and the ability to determine lens distortion parameters. By measuring targets on a

calibration cage from different angles, change of scale is available to allow de-correlation between the camera focal length, principal point offset and lens distortion parameters [Mostafa (2001)]. An example of a calibration cage is shown in Figure 2-6, and an illustration of camera positions for parameter de-correlation is shown in Figure 2-7. Providing similar de-correlation of parameters as in airborne calibration, imagery from at least three flying heights are required and therefore it is not a cost-effective procedure. However, differences in temperature, pressure and refraction may render calibration parameters that are not valid from terrestrial calibration. Therefore airborne calibration is usually carried out afterwards to refine camera parameters when necessary (excluding lens distortion parameters because the lack of scale variation). But, not every imaging sensor can be calibrated terrestrially. In the case of digital line scanners, airborne calibration must be carried because post-processed GPS/IMU data is required to calibrate the system, which can only be collected in airborne environment [Henskin et al (2002)]. After camera calibration, user-side quality control on calibration parameter might need to be monitored every once in a while (for example every few missions) to ensure system stability.

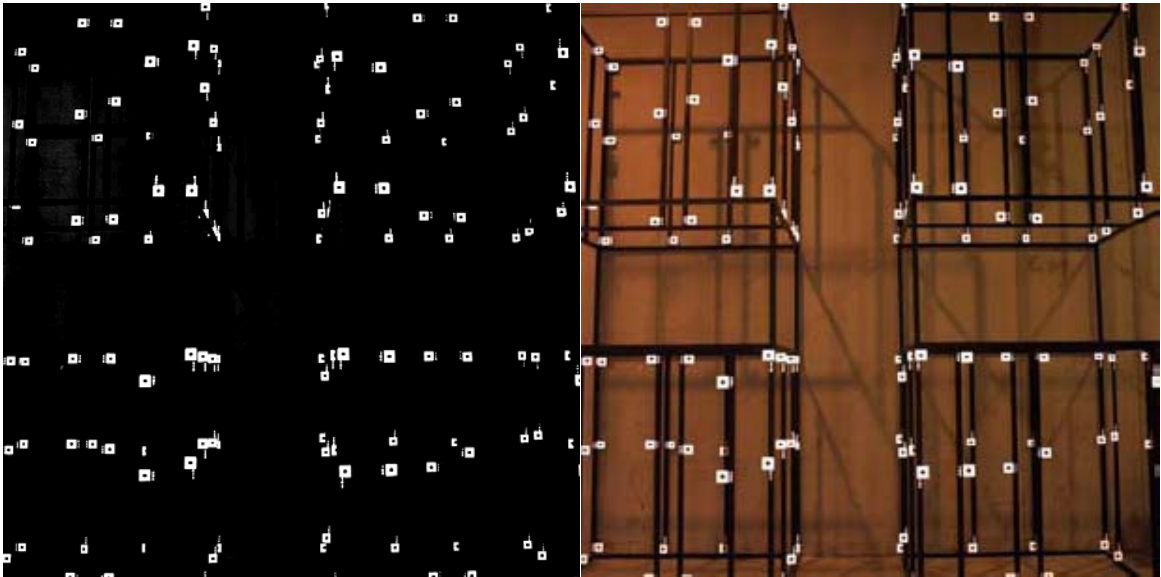


**Figure 2-6: Terrestrial Calibration Cage (left – special setting for signaled target, right – standard setting for airborne environment)**

(Courtesy of Applanix)

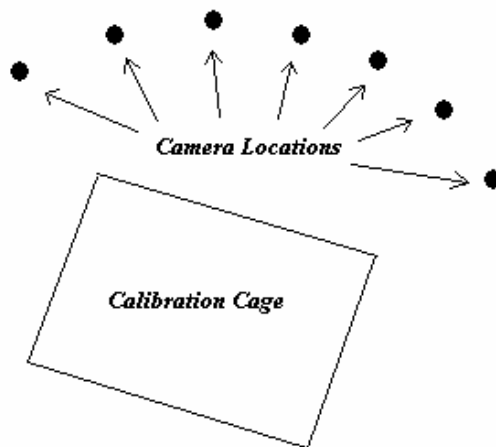


**Figure 2-7: Illustration of Terrestrial Calibration's Camera Locations**

### *Lever Arm Offset*

While the IMU is usually mounted rigidly to the Imaging Sensor, the exact dimensions of the IMU/Imaging Sensor lever arm should be well known through installation, and therefore the error of this component is negligible. For the GPS/IMU lever, only an estimated value can be obtained through installation or the use of total station because the exact location of the GPS phase centre and imaging sensor's perspective centre must be considered. To determine this parameter, two methods are available [Skaloud (1999)]. First, indirectly computing the lever arm using the photogrammetric bundle adjustment. In this method, the lever arm components are modelled as unknown parameters. It, however, increases the complexity of the bundle adjustment algorithm and might introduce correlation with the GPS-derived antenna position [Ackermann (1992)]. Therefore, such an approach is not entirely favourable from the photogrammetric stand point. The second method is indirectly computing the lever arms using the GPS and IMU measurements during data collection. Kalman filter is used for that purpose in either real-time or more accurately in post-mission. Practically speaking, initial values are fed into Kalman filter because the calibration requires direction and elevation changes of the platform, and providing initial values will shorten the calibration time. Therefore, adjacent strips are recommended to be flown in opposite directions to allow better determination of the lever arm offset, in order to separate the correlation with attitude error; and elevation changes are already available after takeoff and before landing. Figure 2-8 shows the values of the GPS/IMU lever arm as estimated by Kalman Filtering in GPS/IMU data post-processing

using the dataset described in Appendix A-6. In this experiment, initial lever arm values for all axes are set to zero to illustrate the efficiency of Kalman Filtering. Lever arms in both x and y axis converge to a relatively constant value after about 15 minutes of data collection while the z-lever arm takes at least 40 minutes to become relatively stable. Explaining this requires the understanding of two factors: first, the magnitude of z-lever is much greater than x and y-lever arm. In real missions, initial values of lever arms are roughly determined (by tape measurements with sub-meter accuracy) and provided to data real-time or post-processing software. Therefore, lever arm calibration is much faster. Second, image acquisition starts approximately 15 minutes after takeoff. Without initial value of the z-lever arm, the flight dynamics in vertical direction makes the z-lever arm even harder to resolve.

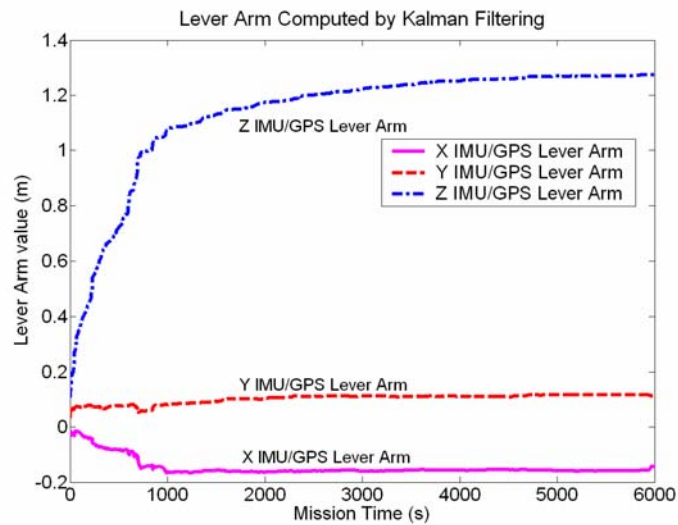


**Figure 2-8: GPS/IMU Lever Arm computed by Kalman Filtering**  
(Ip et al, 2004b)

### ***Boresight Mis-Alignment***

Boresight mis-alignment is due to the imperfect alignment between the imaging sensor and the IMU during hardware integration, as shown in Figure 2-9. From Equation (2.4), the boresight value is constant over time and is one of the key definitions in Direct Georeferencing. While the boresight angle cannot be determined directly, two determination methods are available:

- Comparing the GPS/IMU-derived angles with those independently computed using Aerial Triangulation [Skaloud (1999)]. The constant difference between the two sets of angles is extracted as the three components of the boresight angles
- Computing the boresight angles as additional unknown parameters in the GPS/IMU-assisted Bundle Adjustment [Mostafa (2001)].

When comparing the two methods, the first method has been used as a standard process in the 1990s, where AT-derived EO is compared to the GPS/IMU directly measured EO. On the other hand, the second method is more flexible and efficient because the assisted GPS/IMU bundle adjustment can be performed in the absence of ground control point. To perform either type of boresight calibration method, a block of aerial imagery is collected for a calibration area in which GPS or land survey ground control points are evenly distributed. Although only relative accuracy is mainly concerned in boresight calibration, an absolute accuracy check using ground control points allows a redundant check on

camera parameters. If necessary, camera parameters can be self-calibrated depending on the airborne calibration block configuration.

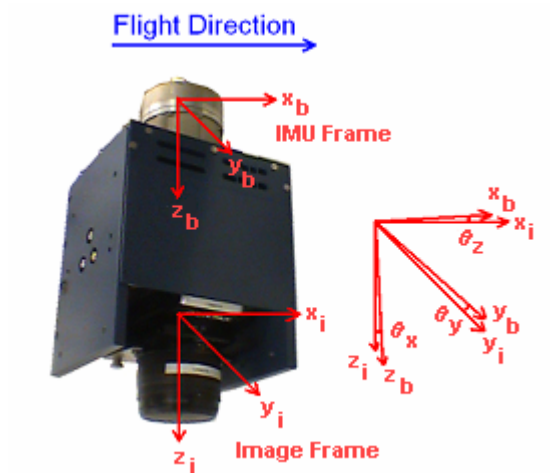


**Figure 2-9: Imaging Sensor / IMU Boresight**

### *Sensor Synchronization*

Sensor Synchronization is typically carried in static condition to minimize noise and systematic error. Alternatively, synchronization can also be calibrated in-flight using opposite flight lines. However, the strong correlation with the GPS/IMU lever arm makes it unpractical. Therefore, calibrating in static mode is usually recommended with a highly accurate Input/Output (IO) timing board [El-Sheimy (1996b)].

### ***IMU Initial Alignment***

Finally, IMU initial alignment is a very important procedure to calibrate the system into certain level of attitude accuracy before using it for typical image acquisition. Initial alignment is accomplished by two steps; levelling and gyro-compassing. Levelling refers to obtaining the roll and pitch of the IMU using the accelerometer outputs and gyro-compassing refers to obtaining the heading information using the gyroscope outputs. In the IMU alone system, the initial alignment accuracy is dependent on alignment time, especially on the Heading angle (H) due to angler random walk of the inertial gyroscopes, [Titterton (1997) and El-Sheimy (1996b)]. Equation (2.8) expresses the relationship between alignment error in Heading angle ( $\delta H$ ) with Angular Random Walk (ARW) in the z-gyro, the alignment time ( $T_a$ ), the latitude ( $\phi$ ) at location of initial alignment and the earth rotation ( $\omega_e$ ).

$$\delta H = \frac{ARW}{\omega_e \cos \phi \sqrt{T_a}} \quad (2.8)$$

Such relationship requires static data to be collected to allow enough alignment time to minimize the heading error, usually between 10 min to 15 min. But, this only applies to the IMU-alone environment where no aiding sensor is available. Such environments include terrestrial calibration because the camera position is at a fixed location during image acquisition and no GPS measurement is required. Also, terrestrial calibration is performed in-door, in which the GPS signal is usually unavailable. However, in the airborne

environment, the GPS aiding provides a procedure, which allows in-flight alignment. Levelling and gyro-compass are performed in kinematic mode because such processes are intended to provide coarse levelling (few degrees) and heading alignment (<10 degrees) only. Since heading error causes the acceleration of the IMU to be misresolved in the navigation, such error will be integrated into very large position and velocity errors that are observable against the GPS measurements. Thus, Kalman filter can estimate the heading error to fractions of a degree [Mostafa and Hutton (2001)].

#### **2.3.4. Time-Dependent vs. Time Independent Errors**

All the above errors influence the direct georeferencing results obtained from Equation (2.4). It is also important to understand that these errors can be separated into two categories: Time-Dependent and Time Independent Errors.

##### ***Time-Dependent Errors***

Although the errors mentioned in previous sections involve the time variable (t), not all of them are considered as time-dependent error. The navigation error, for example, will change with time and flight dynamics and therefore can be classified as a time-dependent error. Synchronization error is also time-dependent because the magnitude of error is directly proportional to the velocity of the aircraft. Environmental condition varies with the aircraft speed and therefore synchronization error changes throughout the mission [Skaloud

(1999)]. Based on Equation (2.4), the error model of synchronization error ( $\delta t$ ) is presented in Equation (2.9) [Ellum et al (2003)]:

$$\delta r_p^m = \delta t [v(t) + R_b^m(t)(sR_i^b r_p^i - a_1^b - a_2^b)] \quad (2.9)$$

Where  $v(t)$  is the flying speed

To illustrate this, a 1 millisecond synchronization error is introduced in the DSS flight described in Appendix A-6 (flight trajectory and dynamics). The corresponding position and attitude errors are shown in Figure 2-10 and the statistical report is listed in Table 2-9.

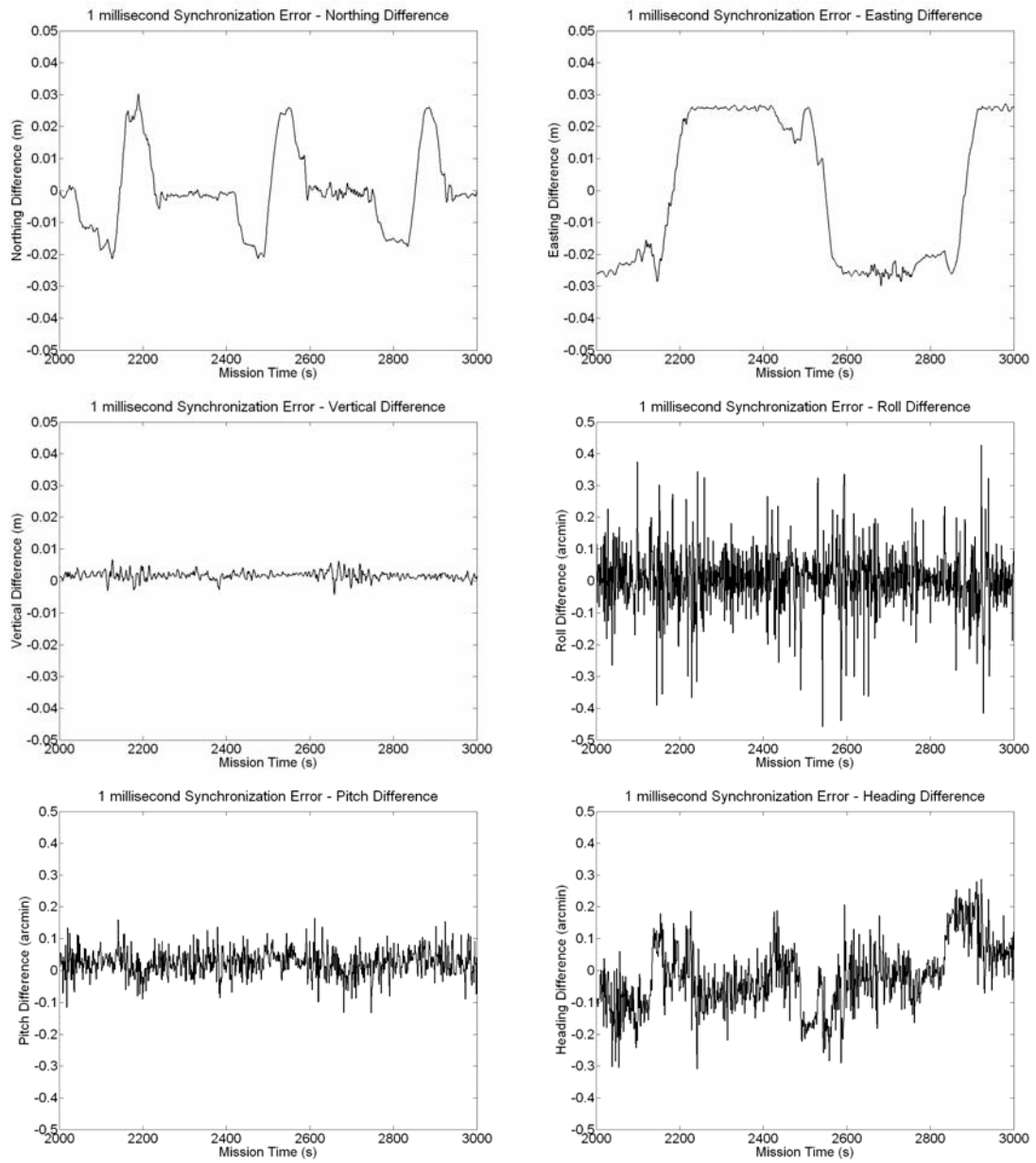


**Figure 2-10: Navigation error due to 1 millisecond Synchronization Error**

[Ip et al, 2004b]

**Table 2-9: Statistics of Synchronization Error Influence on Navigation Position and Attitude in Post-Processing, 1 millisecond simulation**

Navigation error	Min	Max	Mean	RMS
Northing (m)	-0.02	0.03	0.00	0.01
Easting (m)	-0.03	0.03	0.00	0.02
Vertical (m)	-0.00	0.01	0.00	0.00
Roll (amin)	-0.84	0.70	0.00	0.14
Pitch (amin)	-0.28	0.32	0.02	0.06
Heading (amin)	-0.39	0.34	-0.02	0.11

Notice that Table 2-9 reflects the absolute value of the simulation results. Although the original data was available at 200Hz data rate, Figure 2-10 was plotted using a 1 Hz data rate to avoid large quantity of data presenting in a single plot, which allow the trend of changes to be observed clearly. 1 millisecond is chosen to be used in the simulation because it is a small quantity when compared to a typical 1 MHz of the data logging computer. This value is far less than the actual IMU data rate reported (typically 600-1000 Hz). This would also result in centimetre level errors in position which is adequate for the presentation shown here. Although the results and statistics shown in Figure 2-10 and Table 2-9 are insignificant in comparison to map production standards, these only reflect a simulation where synchronization error is small in the system. Due to the nature of electronic systems, some CCDs require up to several seconds for a single image acquisition; in this case synchronization error is relatively large. In addition, these errors will be projected to the ground which is directly related to the system dynamic and project scale. Therefore synchronization error is very important especially on small scale projects with high flying attitude and/or flights with high dynamics. For example, in the DSS camera,

there is a known delay (through calibration) in the CCD chip of about 2 milliseconds. When this delay is inserted in Equation (2.9) with the same simulation data, a 2 millisecond synchronization error should introduce twice of the error as in the 1 millisecond simulation. The result of the 2 milliseconds simulation is presented in Table 2-10.

**Table 2-10: Statistics of Synchronization Error Influence on Navigation Position and Attitude in Post-Processing, 2 millisecond simulations**

Navigation error	Min	Max	Mean	RMS
Northing (m)	<b>-0.04</b>	<b>0.06</b>	0.00	0.03
Easting (m)	<b>-0.06</b>	<b>0.06</b>	0.00	0.05
Vertical (m)	-0.01	0.01	0.00	0.00
Roll (amin)	-1.69	1.40	0.00	0.28
Pitch (amin)	-0.51	0.61	0.05	0.12
Heading (amin)	-0.74	0.63	0.00	0.20

From Table 2-10, expected results are achieved with twice the navigation error experienced under 1 milliseconds synchronization error. Both Table 2-9 and Table 2-10 clearly indicate that the mean values in navigation error are close to zero. This is a result of opposite flight lines where the errors are cancelled by each other. This shows that synchronization error is flight direction related and therefore change in flight direction helps to capture synchronization error in flight environment. In the existence of synchronization error, error in navigation presents a opposite sign when flight line direction changes by 180 degrees. However, when the project is flown in the same direction on each flight line, synchronization error cannot be captured directly as it is correlated with the local datum shift and/or GPS base station coordinate error [Skaloud (1999) and Grejner-Brezekinska

(1998)]. Therefore, calibration of synchronization error is usually carried out in lab environments where static mode can be achieved. Using accurate timing equipment, synchronization error can be captured in static mode without the influence from system dynamics.

Another component that is categorized into time-dependent error is alignment error. Initial alignment accuracy of the Heading angle (H), Equation (2.8) is dependent on the inverse of the square-root of the alignment time. Therefore, with longer alignment time, attitude accuracy will continue to improve by observing the gravity signal in each accelerometer and the earth rotation from the gyro measurement, until the estimation reaches the noise and residual bias level of the sensors. But, such residual error will continue to introduce attitude error and therefore IMU orientation should be changed once in a while to update the measurement. This can be easily achieved when the camera position changes during terrestrial calibration.

In airborne in-flight alignment, the condition is similar because attitude errors will grow at a rate defined by the noise and residual bias from the IMU. Through the aid of GPS, an error reset will occur when a significant acceleration is experienced. During straight-and-level flight, there is little or no acceleration information and therefore attitude errors continue to grow without limit until flight manoeuvre. Therefore, periodical flight manoeuvres are recommended every 10 to 30 minutes, depending on the quality of the IMU to allow Kalman Filter smoothing in the GPS/IMU data post-processing. Figure 2-11

illustrates the heading error improvement after manoeuvres in both the forward and smoothed solutions. In an aerial survey mission with a block of imagery, this is typically not a problem. However, in strip/corridor mission that focuses on straight-and-level flight, the manoeuvre interval will be longer and therefore a higher quality of IMU is recommended [Mostafa and Hutton (2001)]. In either case, error in initial alignment is treated as attitude error throughout the mission, and the error model is expressed in Equation (2.10).

$$\delta r_p^m = \delta R_b^m(t)(sR_i^b r^i) \quad (2.10)$$

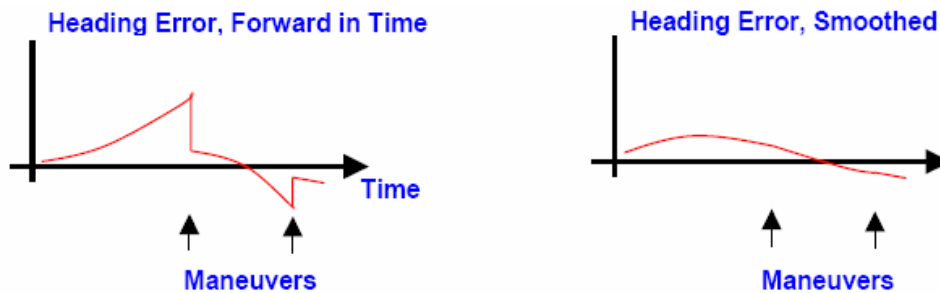


**Figure 2-11: Heading Error Improvement after maneuvers**

[Mostafa and Hutton, 2001]

### ***Time-Independent Errors***

To be considered as time-independent errors, the navigation errors being generated from these components will be constant throughout the mission. Lever arm error and boresight error are constant position offset and angular mis-alignment, and therefore, they are considered in this category. As mentioned in Section 2.3.2, two types of lever arm exist

(section 2.3.2) in the aerial MMS platform: the IMU/Imaging Sensor lever arm and the GPS/IMU lever arm. However, lever arm error usually refers to the GPS/IMU lever arm because it cannot be directly measured like the IMU/Imaging Sensor. Instead, it is estimated by Kalman Filtering and therefore residual error exists. Even though the error might be a small magnitude using an advanced Kalman Filtering technique, such error should not be ignored. The error model of lever arm error is presented in Equation (2.11), based on Equation (2.4). Demonstrating the effect of lever arm error in navigation, the same dataset in Appendix A-6 is used to perform a simulation. A 10 centimetre x-axis (flight direction) lever arm offset is introduced in GPS/IMU data post-processing, and the resulting navigation error is shown in Figure 2-12, with respect to the imaging sensor. Corresponding statistical report of the lever arm error simulation is listed in Table 2-11. A similar test has also been performed on phase residual error [Grejner-Brezezinska (2001)].

$$\delta \mathbf{r}_p^m = \mathbf{R}_b^m(t)(\delta \mathbf{a}_1^b - \delta \mathbf{a}_2^b) \quad (2.11)$$

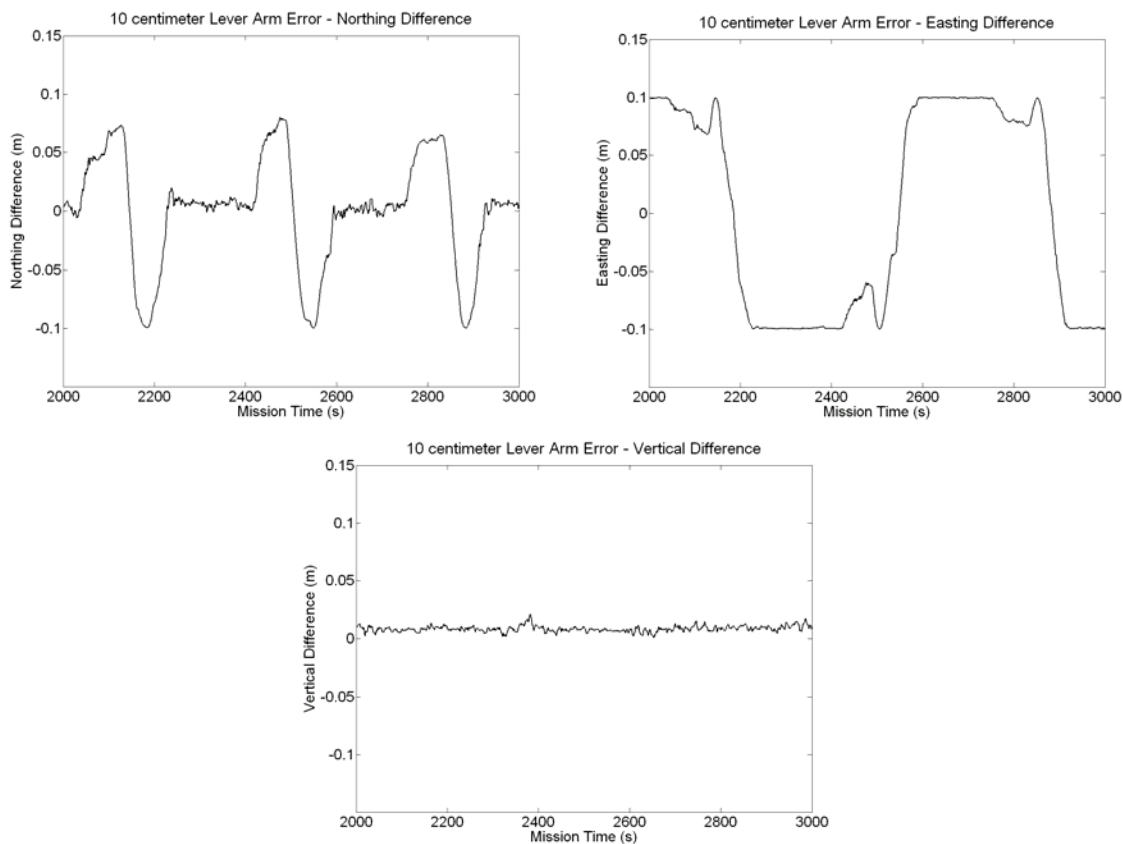


**Figure 2-12: Navigation Position Error due to 10 centimetre Lever Arm Error in flight direction**

[After Ip et al, 2004b]

**Table 2-11: Statistics of Lever Arm Error Influence on Navigation Position in Post-Processing, 10 centimetre simulation in flight direction (x-axis)**

Navigation error	Min	Max	Mean	RMS
Northing (m)	<b>-0.11</b>	<b>0.08</b>	0.00	0.05
Easting (m)	<b>-0.10</b>	<b>0.10</b>	0.00	0.01
Vertical (m)	0.00	0.00	0.01	0.01

Although the lever arm usually has a magnitude from centimetre to sub-metre level, especially in the z axis, this simulated result can describe the relative influence of lever arm error. From Figure 2-12, lever arm error appears in maximum magnitude in the Northing component during the banking of the aircraft, and to the Easting component when the flight direction is parallel to x-axis. Further, the aircraft pitches occasionally in this DSS flight, thus the vertical position component has also been influenced but with insignificant magnitude. Therefore, lever arm error can be projected in any direction depending on the dynamics of the flight. Similar to synchronization error, lever arm error is flight direction dependent and therefore it can be captured through opposite flight lines.

When all sensors are mounted rigidly on the platforms, the 3-D position offset in the lever arm is constant over time. The only exception is when a gimbal system is installed with the camera. Through the motion compensation, the tilting of the imaging sensor is minimized, providing nearly vertical imagery all the time. However, the rotation of the gimbal system makes the IMU/GPS lever arm offset change over time, creating a time-dependent variable. To compensate for the change of lever arm offset, the gimbal motion is recorded and applied as correction during the GPS/IMU post-processing.

Boresight error results from residual error after boresight calibration as the calibration procedure is based on indirect determination using Aerial Triangulation or the GPS/IMU assisted bundle adjustment (section 2.3.3). Especially in GPS/IMU assisted bundle

adjustment, the accuracy of calibrated boresight is correlated with the accuracy of the GPS/IMU data being used. However, for high end DGPS/IMU systems having arc minute attitude accuracy, boresight residual error is relatively small in magnitude. For example, when a system provides an accuracy of  $\sim 0.005$  degree in roll and pitch and  $\sim 0.008$  degree in heading, the corresponding boresight is less than 1 arc minute which is nearly negligible. Although boresight mis-alignment error is time-independent with the error level being constant in the navigation frame, it has similar behaviour as attitude error. When the error is projected to mapping frame, higher the flying height ( $h$ ), more error will be introduced. Formulating from Equation (2.4), boresight error can be expressed by Equation (2.12) [Ellum et al (2003)] and illustration of the error is shown in Figure 2-13.

$$\delta r_p^m = R_b^m(t)(s \delta R_i^b r^i) \quad (2.12)$$

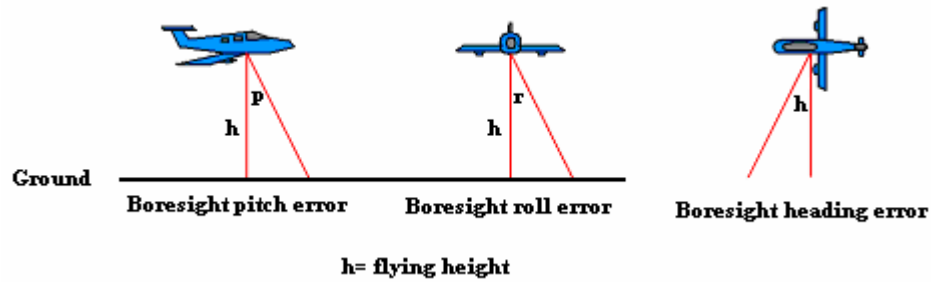


**Figure 2-13: Illustration of Boresight Error on Ground Position**

[Ip et al, 2004b]

To demonstrate the effect of boresight error on the navigation results, a simulation is performed using the dataset described in Appendix A-6. A 10 arc-minute boresight error is introduced on each IMU axis independently. This value is chosen because the typical

magnitude of boresight residual is insignificant and therefore the corresponding error behaviour cannot be presented clearly. Instead this value is based on the typical boresight angle found on a Direct Georeferencing Systems. Therefore, this simulation generates a condition that the boresight calibration has been mistakenly forgotten by operator when generating EO parameters from the GPS/IMU data. The resulting parameters are then used to perform space intersections for 7 ground control points within the project area shown in Figure A-12. Table 2-12 lists the RMS of the checkpoint residuals computed as the difference between the check point coordinates computed by space intersection (using the EO Analysis function in ISAT) and their values measured by land surveying techniques. The first entry of the table which is labelled “no error” shows the RMS of check point residuals of the 7 points without any intentional boresight error. The second entry labelled “x-axis” shows the RMS when an error of 10 arc-minutes in the boresight x-component is introduced. Note that the Northing component has increased about twenty times due to the intentionally introduced boresight error. Similarly, the introduction of a boresight error of 10 arc-minutes on the y-component of the boresight results in increasing the Easting error about 16 times and increasing the error in the vertical component by twice as much. This is due to the fact that the intentional boresight error is projected on the mapping frame and it affected all coordinate components. In the third entry, labelled “z-axis”, an intentional boresight error of 10 arc-minutes has been introduced to the z-component of the boresight angle and it resulted in degrading the Easting and Northing components 2-3 times. Through

this simulation, the importance of the boresight calibration is very important toward the use of Direct Georeferencing.

**Table 2-12: Statistics of Boresight Error Influence on Check Point Coordinate Computational Accuracy by Direct Georeferencing**

Boresight error on	Check Point RMS		
	Easting (m)	Northing (m)	Vertical (m)
no error	0.15	0.15	0.66
x-axis	0.14	<b>2.89</b>	0.74
y-axis	<b>2.46</b>	0.19	<b>1.20</b>
z-axis	0.49	0.40	0.76

Through the above sections, the theory of Image Georeferencing was reviewed and the use of GPS/IMU technology in conjunction of latest imaging sensor was discussed. In addition, the limitations of each sensor in the Mobile Mapping System Platform were illustrated and these systematic errors lead to the overall accuracy of the system. In addition to systematic errors, random noise and operational errors such as local datum shift and incorrect base station coordinates also exist in the data. They must be minimized to provide maximum accuracy of the system. This brings an important step in post-mission data processing which is the Quality Control of Direct Georeferencing Data.

## **CHAPTER THREE: QUALITY CONTROL OF DIRECT GEOREFERENCING DATA**

### **3.1. The Need for Quality Control**

One of the key assumptions in the use of Direct Georeferencing is that the calibrated system parameters are constant over the mission. These system parameters include a GPS/IMU and IMU/Imaging Sensor lever arm offset, a boresight mis-alignment, camera internal geometry and a local datum shift. The calibration of all these parameters has been discussed, especially the lever arm offsets and boresight. As for the camera's internal geometry, film and digital cameras usually have very stable residual errors as they are designed for aerial usage. Only the focal length of the film cameras might change slightly over time as a function of temperature and pressure. In contrast, the geometric stability of the calibrated parameters of some small and medium format digital cameras need to be monitored on a regular basis because COTS components are used (section 2.3.3).

Although one could run a terrestrial and flight calibration (section 2.3.3) [Ellum et al (2003), Hinsken et al (2002), Mostafa (2002), Greening (2000) and Fryer (1996)] before every direct georeferencing mission to check both the boresight and camera parameters, this is not cost-effective. Instead, a cost effective Quality Control (QC) procedure can be performed using actual images or additional imagery flown for strip/corridor projects. The following summarizes the benefits of such QC procedures:

- Minimizing mission specific residual errors from the DG System: including boresight and camera parameters
- Redundant check on DG system performance through check point and boresight residuals
- Detecting calibration error: including values for IMU/Imaging Sensor lever arm and sensor synchronization
- Detecting the following errors when ground control points (GCPs) are available in the QC block;
  - Incorrect basestation coordinates
  - Local datum shift

### **3.2. Methods used for Quality Control**

Based on the benefits of QC, it can be understood that the concept comes from the airborne calibration, or the GPS/IMU assisted/controlled bundle adjustment (section 2.3.3). Instead of flying on a calibration range, the imagery being used in the GPS/IMU assisted bundle adjustments is taken directly from part of the mission [Mostafa et al (2001a)]. In airborne calibration, relative accuracy is the most important because the calibration parameters to be concerned are the boresight mis-alignment and the camera parameters only. Other system parameters like the IMU/Imaging sensor lever arm and sensor synchronization have been calibrated precisely. Also, ground control point coordinates and base station coordinates are

under strict controlled. However, anything can happen in a real mission and therefore QC allows blunder detection on both system and mission specific parameters [Madani and Mostafa (2001)]. In some Geodetic and Control Surveys, the control points are not surveyed by GPS, therefore Local Space Rectangular (LSR) frame may be used. In such cases the ground control point coordinates may disagree with the mapping frame used in the exterior orientation parameters such as Universal Transverse Mercator (UTM) or State Plane. This is mainly due to the inconsistency between the two mapping frames in which scale factor is considered during the transformation from latitude/longitude/height to Easting/Northing/Height (Ellipsoid or Orthometric), while LSR is not. The position bias introduced by this inconsistency is known as local datum shift. The QC procedure, is different from GPS/IMU assisted Aerial Triangulation, or Integrated Sensor Orientation because the ISO, , exterior orientation parameters are refined directly without considering the GPS/IMU integrated system parameters. Instead, QC focuses on refining the boresight and/or camera parameters (excluding lens distortion parameters because of the insufficient observability). Similar to ISO, the good geometry from the initial EO parameters collected by GPS/IMU makes GCP is not a mandatory requirement in the GPS/IMU assisted bundle adjustment. However, when possible local datum shift exists in the data, one or more GCPs must be used to determine the position bias. After QC, the refined system and mission specific parameters are used to compute a new set of EO parameters for the whole project. The mathematic model of the QC is similar to airborne calibration [Mostafa (2002),

Greening (2000) and Ellum et al (2003)] and Figure 3-2 presents how final solution of EO parameters is determined through the QC approach and is compared with the ISO approach.

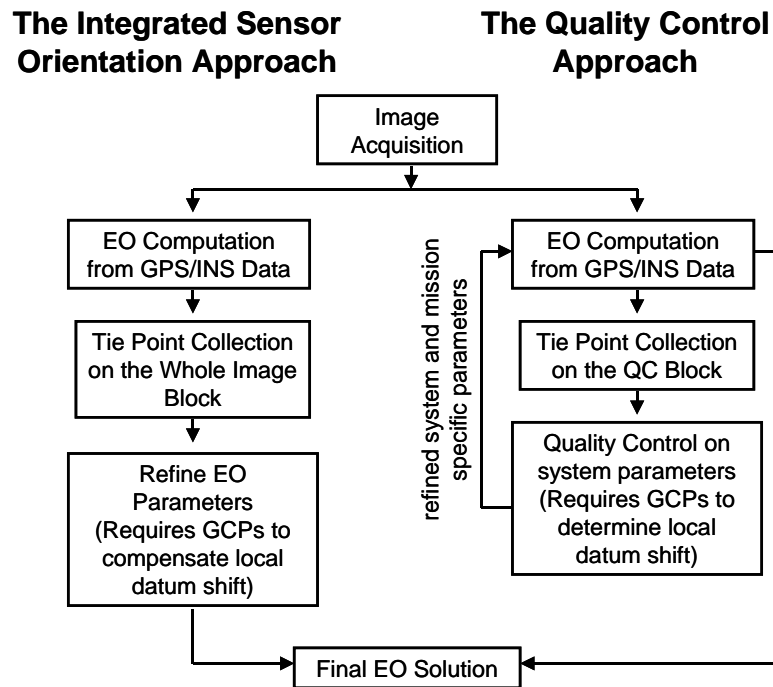


Figure 3-1: Difference in workflow between the QC and ISO approaches

### 3.2.1. Quality Control Requirements

Although the size of a QC block does not have a specific requirement, Good geometry is necessary. This is the reason why single strip data is not recommended to be used for QC because of the lack of side overlap which can lead to an unstable determination of the boresight angle, especially about the axis in the flight direction. In addition to block geometry, image measurement is also an important factor towards the importance of QC.

Ground feature availability has strong correlation with image measurement accuracy. If the QC block area covers area with little ground features, such as rural area with vegetation, forest, desert or mountains, some measured points might fall into shadows, tree tops or even rocks. This happens quite often when using the automatic tie point collection software. Although advanced searching strategies are available to avoid or filter suspect measurement, such algorithms mainly rely on edge detection and quality of measured points after space intersection. Therefore, manual editing might be necessary which requires more time. Thus, the selection of the QC block is very important, and the inclusion of some ground features, residential or commercial areas is highly recommended. In such a case the automatic tie point software can collect accurate image measurement with minimum user interaction.

### **3.2.2. Optimizing the Quality Control Process**

In addition to the QC block size, another factor that affects the cost efficiency of QC is the number of image measurements required per image. Illustrating how to optimize the QC process, a film camera dataset is used and image measurements are collected through using different patterns of tie points and a QC block size. The data consists of a 4x8 block (detailed description is available in Appendix A-1). When the full block is used, it represents a similar condition to an airborne calibration. By using a dense pattern of a tie point collection, the calibrated boresight is treated as a reference. Then, the block size and number of tie points are decreases to determine the optimal combination. To control the pattern of the tie point collection, ImageStation Aerial Triangulation (ISAT) is used which

allows the user to control the approximate number of tie points recorded using the point matching process. By dividing the photo into 9 von Gruber (grid) regions, Points Per Von Gruber (PPVG) value can limit the number of matched points created in each region. Figure 3-2 illustrates the result when PPVG value is seven.

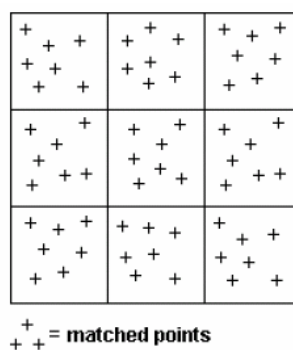


**Figure 3-2: Tie Point distribution when the number of Points per Von Gruber Section is 7 (illustration only)**

[Courtesy of Z/I Imaging]

After the QC blocks are processed in ISAT with different PPVG values, the collected tie points in each trial are exported into POSCAL<sup>TM</sup> (Applanix's Calibration and Quality Control Softcopy) to calibrate the boresight mis-alignment between IMU and Imaging Sensor (Tx, Ty and Tz along x, y and z axis, respectively). Figure 3-3, Figure 3-4 and Figure 3-5 represent the difference in boresight value (dTx, dTy and dTz) with the reference value (from 4x8 Block with PPVG = 9) using 4, 3 and 2 strips of data, respectively.

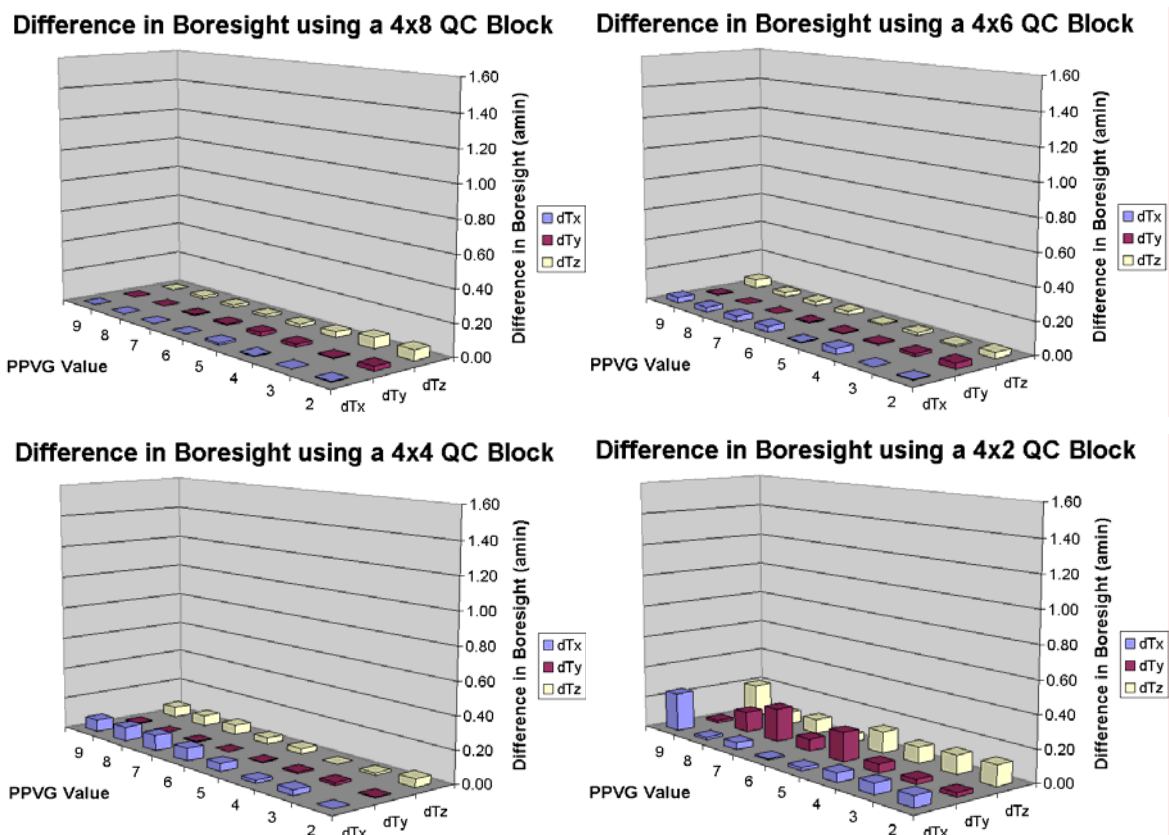


**Figure 3-3: Difference in boresight value using 4 strips of flight data**  
(see Appendix A-1)

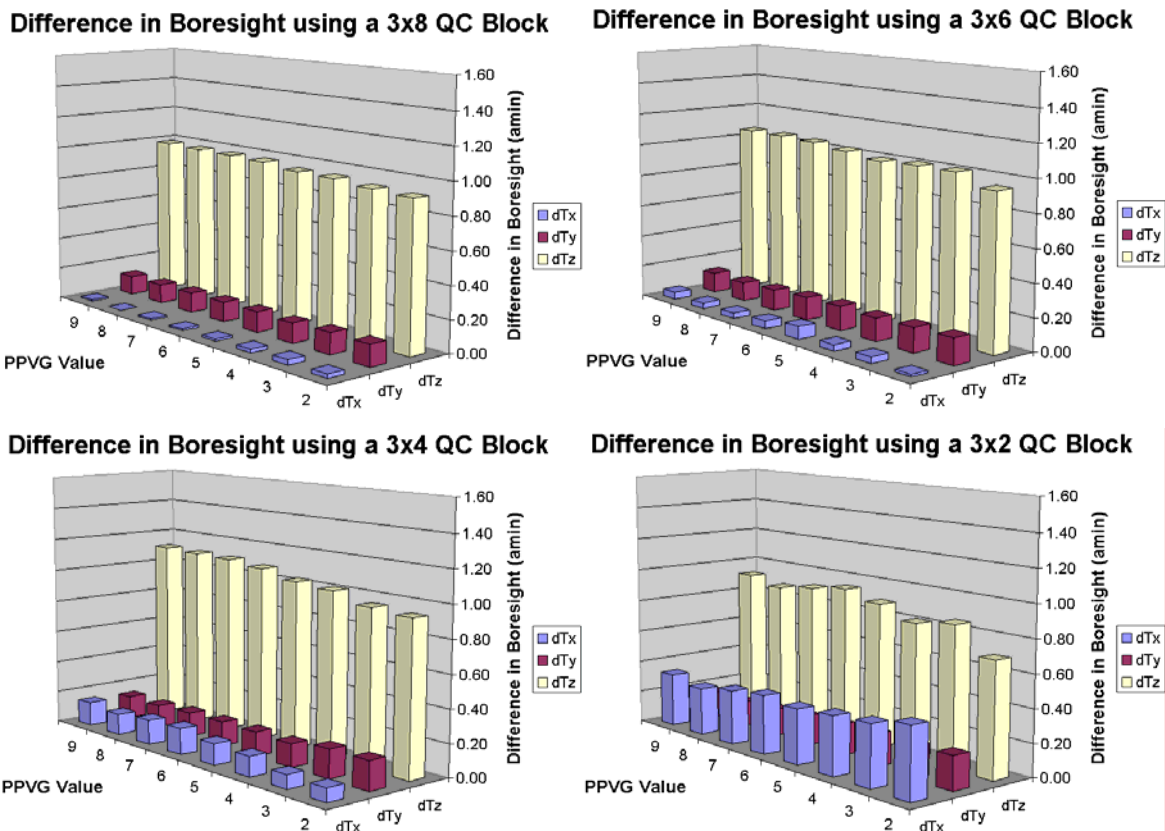


**Figure 3-4: Difference in boresight value using 3 strips of flight data**  
(see Appendix A-1)

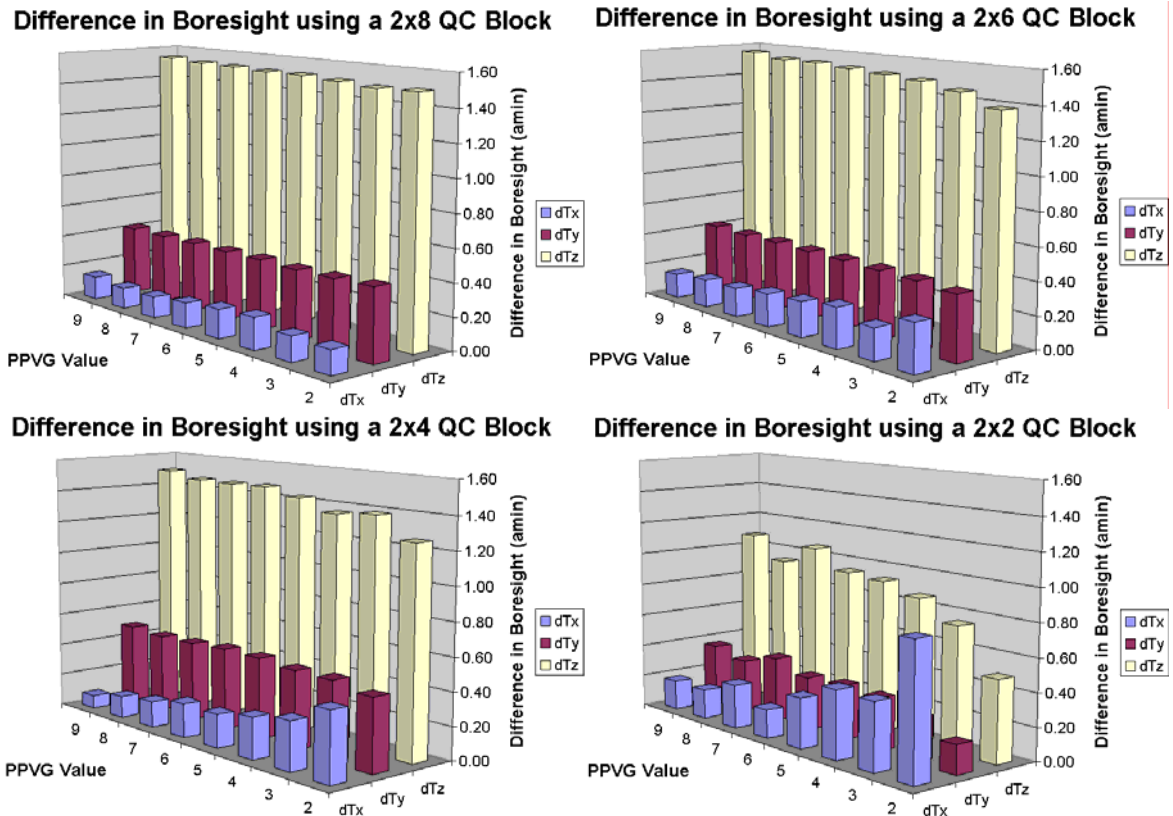


**Figure 3-5: Difference in boresight value using 2 strips of flight data**

(see Appendix A-1)

From the above figures, it is clear that regardless of the numbers of strips used in the QC block, having 2 or 4 images per strip cannot provide a stable boresight value, especially in the determination of Tx. Resolving this requires a high PPVG value which becomes unpractical. In addition, when only 2 strips are used, the boresight value is again unstable. No matter how many images are used per strip or how many tie points are collected, Tz is unable to reach arc-minute performance. The above test does not consider single strip imagery because of its poor geometry. But, the result can be easily predicted through the

observation of the result from 2 strips of flight data – which will be even worse.. Therefore, to allow arc-minute accuracy in the boresight angle in all three axes, the most cost effective combination is the **3x8** block, because boresight residual between sub-second and arc-minute level is nearly negligible. Such combination gives the minimum number of strips for QC, and the 8 images per strips provide redundancy towards ground feature availability for tie point collection. Still, it is less expensive to collect more images on the same strip than acquiring an addition strip. Currently the determined QC block size from the above test is recommended by Applanix Corporation for the Quality Control process using GPS/IMU data collected by their system.

Considering the tie point requirement, it is left up to the user's choice, as the automatic tie point software is getting more advanced and sub-pixel accuracy can be easily achieved. In addition, Central Processing Unit (CPU) and Random Access Memory's (RAM) efficiency are constantly improving, therefore handling a **3x8** QC block with any tie point pattern does not make a lot of difference in processing time. The only exception is for film camera images if scanned in a very high resolution, for example on the order of 15 micron. Such image files are over 500 Mb each and more processing time will be needed. In such a case less PPVG value may be considered to maintain the high efficiency of Quality Control.

### **3.2.3. Integration with Photogrammetry Softcopy**

Photogrammetric softcopy vendors have been working to fully integrate the DG technology in their softcopies. The availability of the EO parameters allows proper handling of image position and orientation, and such information can be used to automatically define the image block. Therefore image footprint and stereo viewing can be achieved without EO initialization through absolute or relative orientation with manually collected tie points. For Quality Controlled DG data, the EO parameter can be used directly for Digital Terrain Model (DTM) or Digital Elevation Model (DEM) extraction and Orthophoto Production. Figure 3-6 presents a sample of image block footprint for a DSS project in ISAT, using quality controlled DG data. Notice that the displayed image is automatically orientated to the north-up direction. This characteristic is very useful for feature identification with existing maps for GIS and remote sensing application.

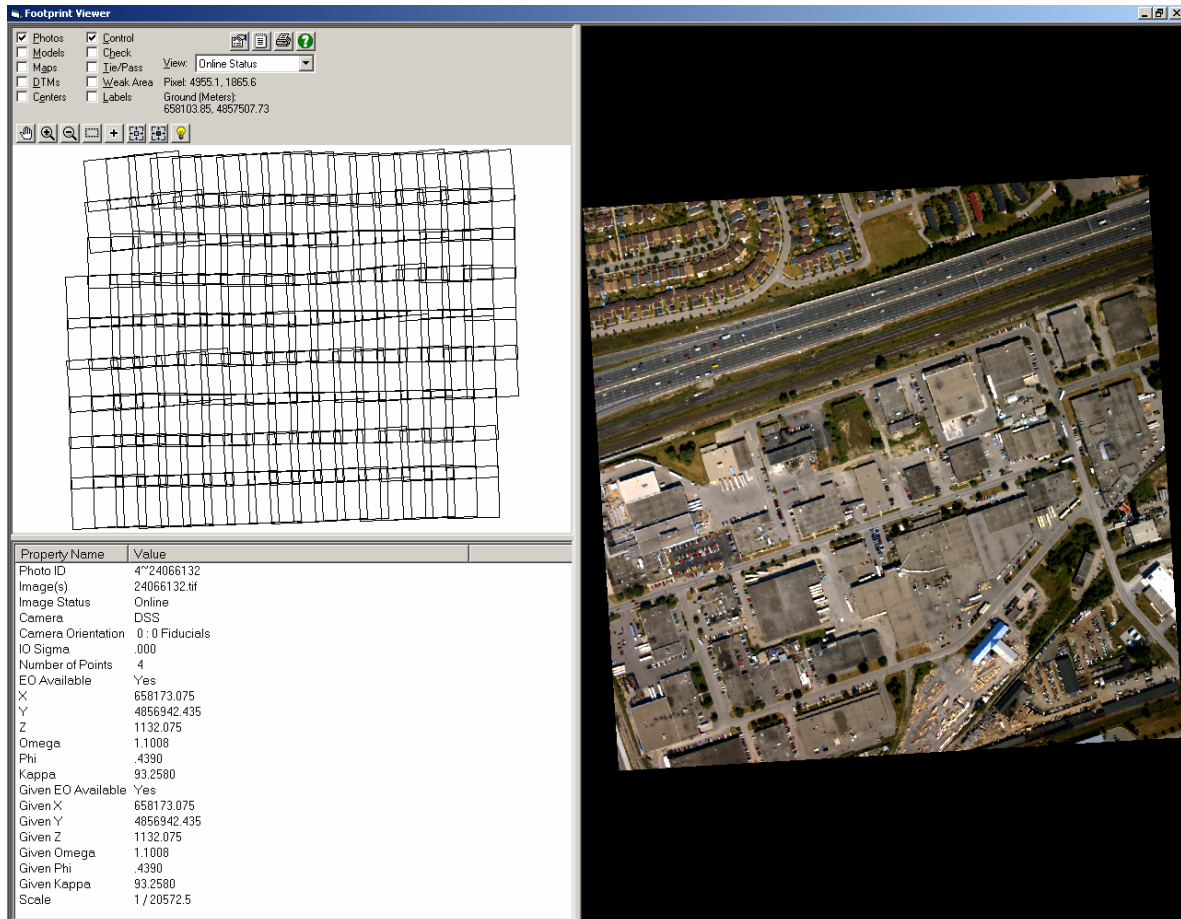


**Figure 3-6: Image Block Footprint of a DSS mission using Direct EO Data**  
 [ISAT software, courtesy of Z/I Imaging]

For automatic tie point collection, users will have the option to use the EO parameters from DG systems to improve the match point searching strategy. Once a potential target is located, any adjacent images that contain the point can be determined and windowed through the EO parameters. Such enhancement is better than the window by window searching strategy throughout each adjacent image when Direct EO data is not available. Thus, processing time is significantly decreased and less blunder match points are produced.

On the other hand, algorithms have been developed to integrate the QC concept into automatic tie point collection in some softcopy software. Understanding that only a few number of tie points are required for the procedure, the softcopy software helps users to choose the proper point collection pattern. By focusing on the overlapping areas only, a minimum number of tie points are collected without spending time on unnecessary area. Figure 3-7 shows the GPS/IMU QC/QA (Quality Control and Quality Assurance) function available in ISAT, and Figure 3-8 shows the collected tie points distribution using ISAT QC/QA strategy [Madani and Mostafa (2001)].

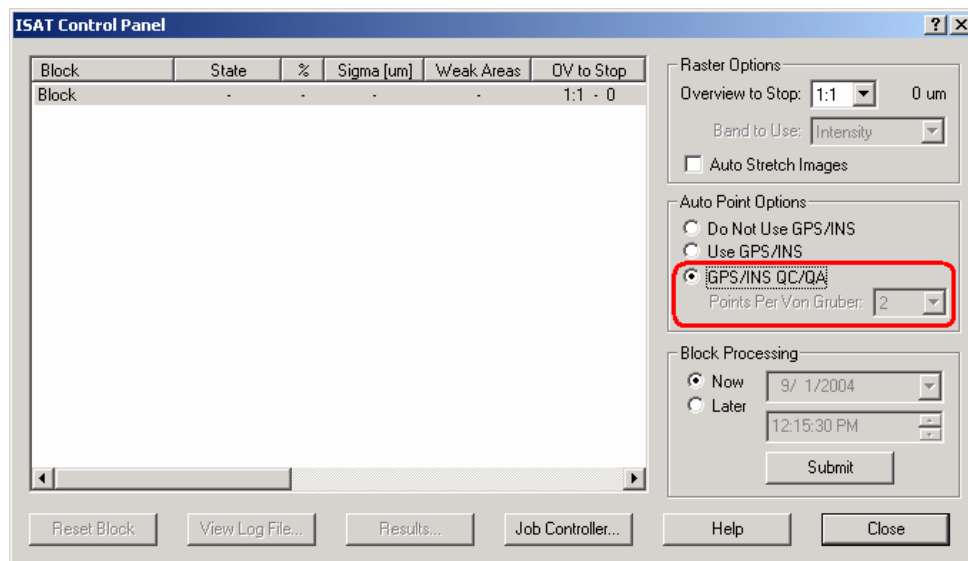


**Figure 3-7: GPS/IMU QC/QA function in ISAT Automatic Tie Point Collection Module**

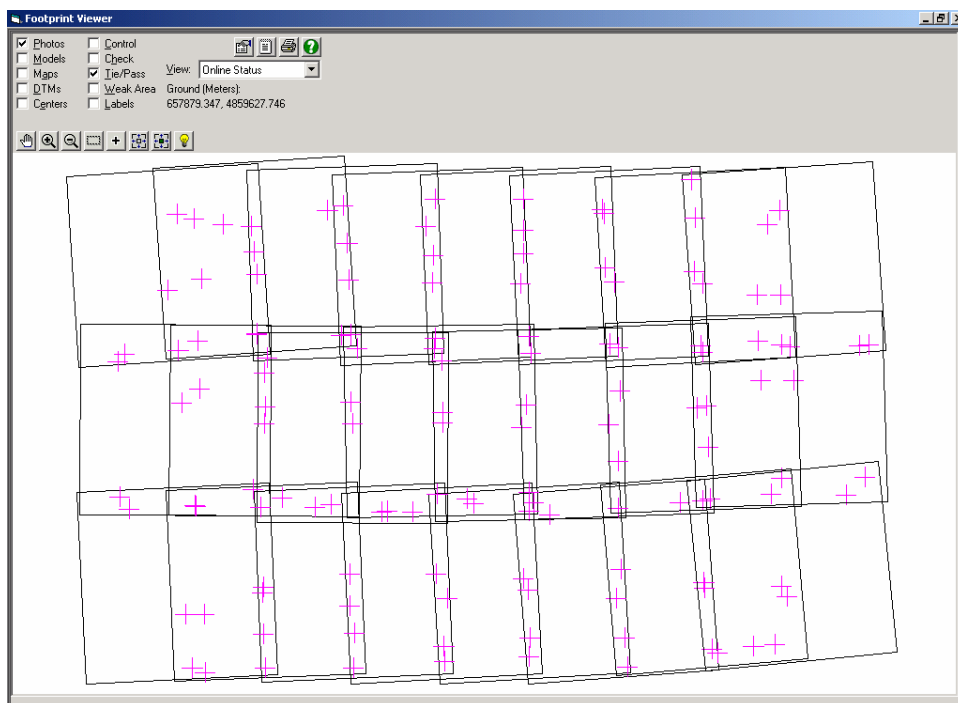


**Figure 3-8: Collected tie point distribution using ISAT QC/QA on a DSS data  
(PPVG = 2)**

## CHAPTER FOUR: DATA DESCRIPTION

### 4.1. Imaging Data

Several types of datasets are used in Chapter 5 to investigate the performance of the Integrated Sensor Orientation (ISO). These datasets are collected by different companies, imaging sensors, direct georeferencing systems and at different locations. A quick summary of the datasets is given in Table 4-1.

**Table 4-1: Summary of the configuration of Datasets used for ISO analysis**

Location	Imaging Sensor	DG System	Collected by	Collected on
University of Kentucky, United States	Analogue Film	POS AV 510	PhotoScience Inc.	Feb., 2001
Toyonaka City, Japan	Analogue Film	POS AV 310	PASCO Corporation	Feb., 2004
Alaska, United States	Large Format Digital (DMC)	POS AV 510	ZI/Imaging Corporation	April, 2003
Northern New Mexico, United States	Large Format Digital (DMC)	POS AV 510	3001 Inc.	Aug., 2003
Ajax, Ontario, Canada	Medium Format Digital (DSS)	POS AV 410	Airborne Sensing Corporation	Aug., 2003

The datasets being used cover a wide range of sensor types from film camera to large and medium format digital cameras. All GPS/IMU data collected for Direct Georeferencing were collected by the POS AV Systems and the corresponding post-processing accuracy of

each DG system type is presented in Table 4-2. Detailed specification is given in Appendix B-1. Basically, POS AV 510 and 410 represent high accuracy DG system and POS AV 310 represents a less accurate DG system.

**Table 4-2: POS AV Post-Processed Accuracy**

[Courtesy of Applanix Corporation]

Post-Processed Accuracy	POS AV 510	POS AV410	POS AV 310
Position (m)	0.05 – 0.3	0.05 – 0.3	0.05 – 0.3
Roll and Pitch (deg) / (amin)	0.005 / 0.30	0.008 / 0.48	0.013 / 0.78
True Heading (deg) / (amin)	0.008 / 0.48	0.015 / 0.90	0.035 / 2.10

## 4.2. Simulating a Less Accurate Direct Georeferencing Data

One of the objectives of this research is conducting a performance analysis of Integrated Sensor Orientation using less accurate GPS/IMU data. The benefits of high accurate systems have been realized by the mapping society, especially for the use of strip/corridor and single photo orientation projects. Also, the high accurate systems can be integrated to any kind of imaging sensor; therefore, less accurate GPS/IMU systems are not commonly used in the industry even though they are less expensive (up to 50% less on price). A limited amount of actual flight data using a less accurate system is available in the mapping industry. But, PASCO Corporation in Japan is interested in the ISO application and therefore a dataset using a film camera / POS AV 310 combination collected in early 2004 is used in this thesis. However, to test a single dataset is not sufficient to define the actual

performance of a less accurate GPS/IMU system, especially when different types of imaging sensors are used. In addition, another difficulty with analyzing the less accurate GPS/IMU performance is the need for reference data – high accuracy GPS/IMU data. The ideal environment is to collect both qualities of data in the same mission. This can be achieved by mounting both high and less accurate IMU onto the imaging sensor as a single configuration. Therefore, both types of IMU data collected are based on the same block configuration, flight conditions, trajectories and dynamics. However, the limited funding of this research does not allow such configuration to be achieved. Thus, data simulation is used as an alternative to acquire both high and less accurate GPS/IMU data under the same conditions, by simulating one of them, while using the other one as a reference..

In a GPS/IMU system, the most expensive component is the IMU. Therefore, when a less accurate IMU is used, a low cost GPS/IMU is resulted. This strategy is currently used by the inertial-navigation industry. While GPS measurements are very accurate in airborne environment with minimum influence from multi-path effect, loss of satellite lock and ambiguity resolution, both high and less accurate GPS/IMU systems have very similar post-processed position accuracy but different attitude performance (see Appendix B-1). This is the result of GPS/IMU post-processing using different quality of IMU data with the same quality of GPS data [Mostafa and Hutton (2001), Mostafa et al (2001a)]. Therefore, one can degrade any high accuracy GPS/IMU data into a less accurate one by adding additional noise, bias, drift and axis mis-alignment into the raw IMU data (based on the knowledge of

difference in IMU performance), and leaving the GPS data untouched. When the simulated IMU data is post-processed with the untouched GPS data, the corresponding performance should behave similar to a less accurate GPS/IMU system (in comparison to the expected accuracy being simulated).

#### **4.2.1. Data Simulation using Monte Carlo Analysis**

In theory, to develop a proper model to degrade a high accuracy GPS/IMU data into certain accuracy, an infinite number of data samples are required such that the simulation results will represent the nature of the system, especially the randomized parameters such as noise and random walk. Unfortunately, to collect an infinite number of data samples is nearly impossible, especially in airborne environment. Therefore, to statistically evaluate the simulation, the **Monte Carlo Analysis** approach has been used. Monte Carlo Analysis or Monte Carlo Simulation is a famous methodology for simulation (imitate a real-life system) which randomly generates values for uncertain variables over and over to simulate a model. [Efron (1982)]

During simulation, the objective is to simulate a model with parameters that contains different noises, which is assumed to be random and distributed with a Gaussian normal distribution about the mean. However, this requires a large number of samples (~10,000 times) over the same system and becomes nearly impossible in many cases, such as an airborne mapping project. As a result, instead of repeating the experiment numerous times,

Monte Carlo analysis can be used in which the random number generator will generate different distributions of noises for each trial which have the same properties, i.e. is random, and has a Gaussian distribution with the same standard deviation. The simulated data will therefore behave similar to a system that has been run infinite number of times [Koopman (2002)].

Simulating a less accurate GPS/IMU system data for this research, Monte Carlo analysis is performed using the Applanix Inertial Data Simulator [Scherzinger (1997)] to generate 10 sets of random numbers for the 10 trials of simulation. In the last section, the POS AV 310 is considered as a less accurate GPS/IMU system in the commercial market. Therefore, such specification is considered to be the post-processed accuracy to be achieved in the simulation. But, it is very difficult to directly analyze the relative post-processed accuracy of each simulation and evaluate whether it achieves the target accuracy. Thus, an alternative approach is formulated.

Notice that the objective of the simulation is to degrade the IMU data only. When both original and simulated data are under the flight condition and dynamics, the integration and calibration errors between the two datasets should be consistent. Therefore, the relative difference between the two datasets can be used to analyze the magnitude of degradation achieved by the Monte Carlo Analysis. In this simulation, the *relative* difference is more important than *absolute* because there is no real definition of the performance of the *less accurate GPS/IMU system*, except based on some commercial systems such as the POS AV

310. So, for example, to degrade a POS AV 510 data into a POS AV 310 data, the first step is to look at the Root-Mean-Square (RMS) difference in performance between the two systems. Table 4-3 represents the specifications of POS AV 510 and 310 systems and their relative RMS differences.

**Table 4-3: RMS Difference in performance between POS AV 510 and 310**

Post-Processed Accuracy	POS AV 510	POS AV 310	RMS Difference
Position (m)	0.05 – 0.3	0.05 – 0.3	0
Roll and Pitch (deg)	0.005	0.013	0.012
True Heading (deg)	0.008	0.035	0.034

From Table 4-3, the relative RMS Difference ( $RMS_{diff}$ ) represents the magnitude of degradation to be achieved on the POS AV 510 data in order to simulate the POS AV 310 data. Since 10 sets of trials exist in the Monte Carlo Analysis, each trial produces one set of RMS difference ( $RMS_{diff_i}$ ). Then, an ensemble RMS difference ( $RMS_{diff_e}$ ) can be computed based on the result from each trial. Finally, the RMS error of the simulated POS AV 310 data is estimated as the Root-Sum-Square ( $RSS_{Simulated\ 310}$ ) of the ensemble and the RMS performance of POS AV 510 system. Such  $RSS$  values should represent the post-processing accuracy of the desired Simulated GPS/IMU data. The following equations formulate the algorithms.

$$RMS_{diff} = \sqrt{RMS_{510}^2 - RMS_{310}^2} \quad (4.1)$$

$$RMS_{diff_e} = \sqrt{(\sum_{i=1}^{10} RMS_{diff_i}^2) / 10} \quad (4.2)$$

$$RSS_{Simulated310} = \sqrt{RMS_{510}^2 + RMS_{diff_e}^2} \quad (4.3)$$

In addition to the RSS value, the pattern of the RMS difference is also very important to ensure the randomness of the simulation. Figure 4-1 presents the RMS difference from one Monte Carlo trial of simulation to degrade a film camera GPS/IMU data from POS AV 510 to POS AV 310 performance. Table 4-4 presents the corresponding statistical report on navigation parameters of this trial.

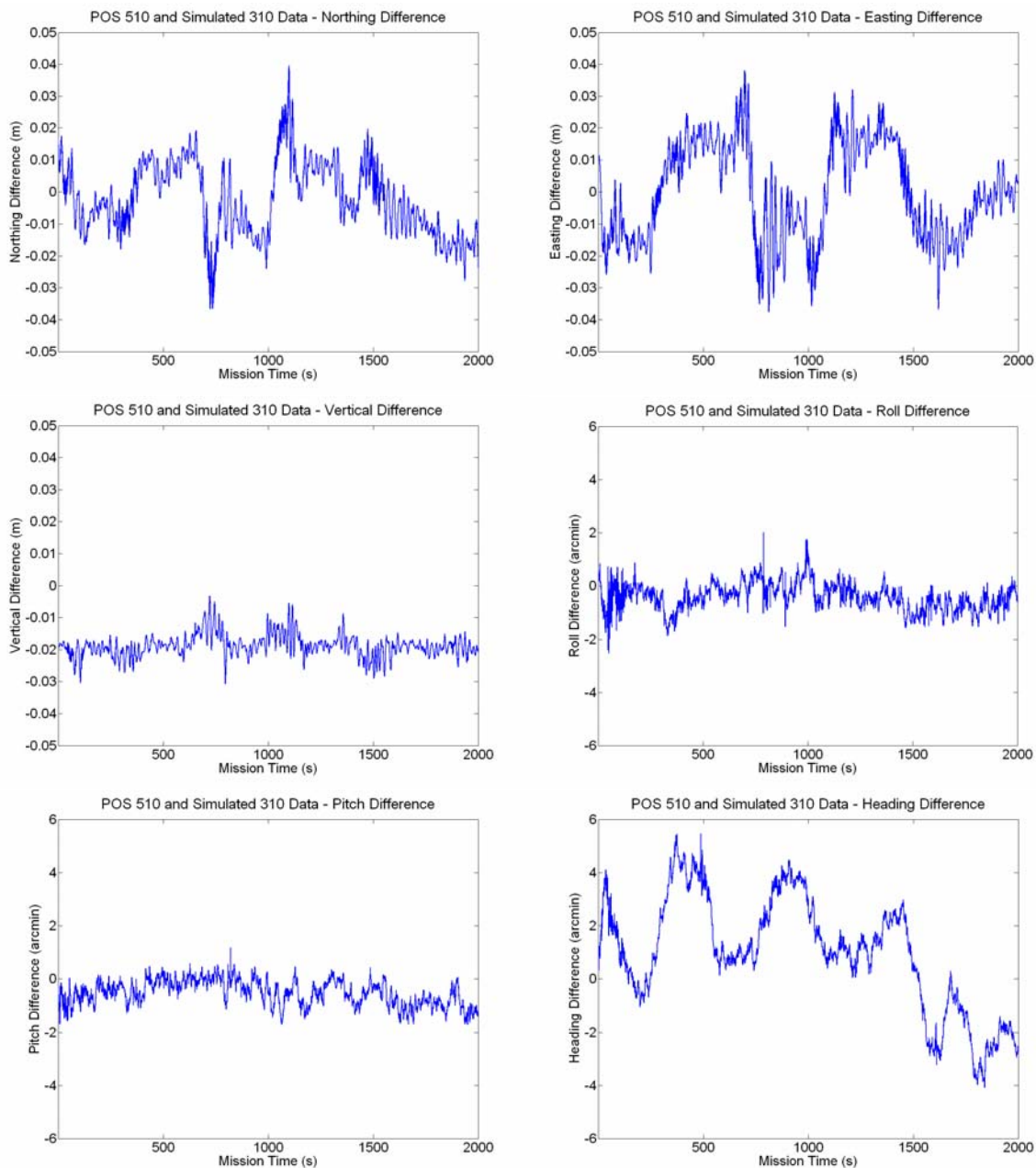


**Figure 4-1: RMS Difference of a Film Camera DG data Simulation Trial**

**Table 4-4: Statistical report of the Simulation Trial**

Navigation Parameters	Theoretical RMS Difference	RMS Difference of a Monte Carlo Trial
Northing (m)	0	0.01
Easting (m)	0	0.01
Vertical (m)	0	0.02
Roll (arc minute)	0.72	0.64
Pitch (arc minute)	0.72	0.71
Heading (arc minute)	2.10	2.35

From Figure 4-1 and Table 4-4, it is clear that the randomness of the simulation can be observed and the position difference is in the centimetre level only. While position difference is insignificantly influenced in post-processing, the degraded IMU data with untouched GPS data, proves the theory that only the IMU data is degraded. Although the RMS difference in Roll is slightly lower than the theoretical value, the above result only represents a single trial of the Monte Carlo Analysis. In the datasets to be described, more simulations have been performed (10 Monte Carlo trials) with a full statistical report, especially the *RSS* from the ensemble RMS difference are presented.

Through the derivation of the simulation, the number of Monte Carlo trials was selected as 10 trials. First, it is the maximum number of random numbers that can be generated by the simulator. Although there aren't any guidelines on the number of trials required to statistical evaluate a simulation, a rule of thumb is usually followed and states that the accuracy should increase with the square-root of the number of trials [Koopman (2002)]. Secondly, when the simulator only accepts up to 10 Monte Carlo trials, the difference in

accuracy becomes insignificant in comparison to other numbers of trials (e.g. a trial number of 5). To evaluate this a test is performed using the simulated data presented in Table 4-4, the simulated parameters are determined using Monte Carlo trial numbers of 1, 3, 5 and 10, the results are presented in Table 4-5.

**Table 4-5: Simulated parameters using different numbers of Monte Carlo trials**

Simulated Parameters	Number of Monte Carlo trials used			
	1	3	5	10
Northing (m)	0.03	0.03	0.03	0.04
Easting (m)	0.05	0.04	0.04	0.05
Vertical (m)	0.03	0.03	0.03	0.03
Roll (arc minute)	0.64	0.70	0.70	0.70
Pitch (arc minute)	0.81	0.78	0.78	0.71
Heading (arc minute)	2.03	2.11	2.15	2.12

From Table 4-5, it can be seen that the number of Monte Carlo trial has insignificant influence on the simulated parameters ( $\pm 1$  cm in position and  $\pm 0.07$  arc-minute in orientation). Therefore, the less accurate GPS/IMU simulation can be performed using less Monte Carlo trials. However, to ensure maximum accuracy of the simulation, 10 trials are used because additional processing time is insignificant when comparing with less number of trials.

### 4.3. Film Camera Flights

The two film camera datasets used in Chapter 5 were collected at the University of Kentucky Campus, United States and Toyonaka City, Japan, using POS AV 510 and a POS AV 310 DG Systems, respectively. We will refer to these simply as the PhotoScience UofK and PASCO 310 data. Both datasets were collected using a 230 x 230 mm (9 x 9 inch) film and 153 mm (6 inch) lens cone. Table 4-6 and Table 4-7 list the properties of the two datasets, detailed information such as flight trajectory and block configuration are referenced in Appendix A-1 and A-2, respectively.

**Table 4-6: Configuration of the PhotoScience UofK Flight**

Dataset	PhotoScience UofK
Location	University of Kentucky, United States
Camera	Leica RC 20
Scale	1 : 6000
# of Strips	4
# Photo / Strip	8
Flying Height, AGL (m)	900
Photo Scan Resolution ( $\mu\text{m}$ )	15
Forward /Side Overlap (%)	60 / 25
# of Check Points	18
Mapping Projection	StatePlane Zone 1601
Datum	WGS84
Height	Orthometric
DGPS/IMU System	Applanix POS AV 510

**Table 4-7: Configuration of the PASCO Toyonaka City Flight**

Dataset	PASCO 310		
Location	Toyonaka City, Japan		
Camera	Leica RC 30		
Scale	1 : 4000	1 : 8000	1 : 20000
# Strips (forward / cross)	10 / 2	5	4
# Images / Strip	17 / 19	9	5
Flying Height, AGL (m)	600	1200	3000
Scan Resolution ( $\mu\text{m}$ )	20		
Forward / Side Overlap (%)	60 / 30		
Mapping Projection	Japanese Projection Zone 6		
Datum	WGS84		
Height	Orthometric		
# of Check Points	272	218	14
DGPS/IMU System	Applanix POS AV 310		

#### 4.3.1. PhotoScience University of Kentucky Flight

PhotoScience UofK dataset is boresight calibration data for the RC20 camera and the POS AV 510 system. Since it is a calibration flight, the reference boresight is not available. Thus, QC is performed under a control-free environment on the whole 4x8 image block to determine the boresight value of the system. Table 4-8 presents the QC's boresight value and its corresponding residual.

**Table 4-8: Boresight Values and RMS Residuals of the PhotoScience UofK QC**

	Tx (deg)	Ty (deg)	Tz (deg)
Boresight Values	0.323	-0.004	0.168
RMS Boresight Residuals	0.004	0.004	0.006

The capability of boresight determination is correlated to the system's performance (section 2.3.3). Therefore, the RMS boresight residuals can provide some indication about the system's performance. In addition to the RMS boresight residuals, another parameter that can be used to monitor the performance of the data is the RMS of the Navigation Errors estimated by the Kalman Filter in GPS/IMU data post-processing. These values are very important as they are treated as the standard deviation for the initial EO parameters in the Integrated Sensor Orientation test which is discussed in Chapter 5. Table 4-9 lists the RMS navigation error for PhotoScience UofK Flight.

**Table 4-9: RMS of Navigation Error estimated by the Kalman Filter of the PhotoScience UofK Flight**

RMS Navigation Error					
Easting (m)	Northing (m)	Vertical (m)	Roll (deg)	Pitch (deg)	Heading (deg)
0.04	0.05	0.05	0.004	0.004	0.014

From Table 4-8 and Table 4-9 an interesting trend is observed. The RMS of boresight highly agrees with the POS AV 510 specification but the RMS of the navigation errors does not agree in with the Heading component. First, it is necessary to understand the determination of the reference boresight for this flight. Instead of using an external boresight from airborne calibration or other mission data, quality control is performed using the mission block. Such procedure will minimize some system residual errors from the data, as discussed in Chapters 2 and 3. Therefore, the Quality Controlled performance is

expected to be better than the *typical* Direct Georeferencing – RMS Navigation Errors estimated by the Kalman Filter. Also, the specification of the POS AV 510 is only a reference value for the overall system, and actual performance may vary slightly due to flight condition and dynamics. Therefore, it is not a surprise to see a slightly higher heading error in the data. This concept about *typical* and *quality controlled* Direct Georeferencing data is very important throughout this research and is discussed thoroughly.

While the PhotoScience UofK flight is collected with a POS AV 510 system, a degrading simulation (using 10 Monte Carlo trials) is performed targeting to achieve a POS AV 310 performance. Using the simulation algorithm developed (section 4.2.1), the RMS difference for each Monte Carlo Trial is presented in Table 4-10, and the corresponding Ensemble RMS and Root-Sum-Square are listed in Table 4-11.

**Table 4-10: Statistical report of Monte Carlo Trials on the PhotoScience UofK POS AV 310 Simulation**

Monte Carlo Trial #	RMS Difference					
	Easting (m)	Northing (m)	Vertical (m)	Roll (amin)	Pitch (amin)	Heading (amin)
1	0.01	0.01	0.01	0.63	0.65	3.52
2	0.01	0.01	0.00	0.83	0.50	1.50
3	0.03	0.02	0.00	0.53	0.88	1.69
4	0.02	0.02	0.02	0.73	0.77	1.92
5	0.04	0.04	0.03	0.70	0.98	1.94
6	0.04	0.03	0.01	0.69	0.55	2.25
7	0.03	0.03	0.02	0.55	0.67	1.60
8	0.03	0.02	0.01	1.12	0.61	1.74
9	0.01	0.01	0.02	0.64	0.71	2.35
10	0.04	0.03	0.02	0.78	0.68	1.46

**Table 4-11: Ensemble RMS difference and RSS of the PhotoScience UofK POS AV 310 Simulation**

Navigation Parameters	Theoretical RMS Difference	Ensemble RMS Difference	RSS / Simulated Data Accuracy
Northing (m)	0	0.03	0.06 – 0.3
Easting (m)	0	0.02	0.06 – 0.3
Vertical (m)	0	0.02	0.05 – 0.3
Roll (arc minute)	0.72	0.74	0.80
Pitch (arc minute)	0.72	0.71	0.77
Heading (arc minute)	2.04	2.08	2.13

From Table 4-11, the ensemble RMS difference is very close to the theoretical RMS difference ( $\pm 3$  cm in position and  $\pm 0.02$  arc-min in attitude). Although there is centimetre level of degradation in the position ensemble RMS difference, such magnitudes are insignificant to result any noticeable changes in the RRS value. On the other hand, in the attitude ensemble RMS difference, the randomness of the simulation leads the Monte Carlo Analysis to be unable to reach the exact value as the theoretical RMS difference. Based on the correlation between attitude error and absolute ground accuracy (section 2.3.4), the  $\pm 0.02$  arc-minute difference in ensemble RMS has negligible influence ( $< 5$  mm) on the simulated data. Therefore the simulation is a success.

#### **4.3.2. PASCO Toyonaka City Flight Using a POS AV 310**

This dataset is acquired in Japan to analyze the performance of the less accurate Direct Georeferencing system. The data is collected on three different scales: 1:4000, 1:8000 and

1:20000. While the POS AV 310 is considered as a less accurate GPS/IMU system, analysis of such a dataset in Integrated Sensor Orientation is very useful in addition to using simulated data only. Since it is a specially designed project, without proper airborne system calibration performed on the system, only valid camera calibration is available from the USGS and the reference boresight required to be resolved through quality control. While three scales of imagery are available, independent boresight calibration can always be processed through quality control on each photo scale to deliver maximum accuracy. However, in this research only one boresight value will be determined to preserve the definition of DG (section 2.3.3). From standard airborne calibration procedure, 1:8000 is the recommended scale to calibrate the boresight, to minimize the correlation of the GPS accuracy from large scale project, and the correlation of attitude error from the small scale project [Mostafa et al (2001b)] Evaluating this is an independent test performed using the PASCO 310 data. First, two 3x8 blocks are selected from the center of 1:8000 and 1:20000 imageries, then five 3x8 blocks are selected from the 1:4000 imageries from the four corners and the center of the image block. Furthermore, each corner of the 1:4000 QC block is inserted on a cross strip imagery to generate addition block combinations (see Appendix A-2 for block configurations of the three photo scales). Table 4-12 represents the QC block combination for each scale and Table 4-13 shows the statistics of the boresight value determined by the QC blocks and their corresponding RMS boresight residuals.

**Table 4-12: QC Block Combinations of the PASCO 310 Flight**

Scale	Location	Cross Strip Imagery	QC Block Name
1 : 20000	Center	No	20000
1 : 8000	Center	No	8000
1 : 4000	Bottom Left	No	4000S1
	Top Left	No	4000S2
	Top Right	No	4000S3
	Bottom Right	No	4000S4
Scale	Location	Cross Strip Imagery	QC Block Name
1 : 4000	Center	No	4000S1
	Top Left	Yes	4000S1A
	Top Right	Yes	4000S2A
	Bottom Left	Yes	4000S3A
	Bottom Right	Yes	4000S4A

**Table 4-13: Boresight Values and RMS Residuals of the PASCO 310 QC using different Block Combinations**

QC Block Name	Boresight Values (deg)			Boresight RMS (deg)		
	Tx	Ty	Tz	dTx	dTy	dTz
20000	-0.040	0.031	-0.157	0.003	0.002	0.005
8000	-0.037	0.026	-0.167	0.003	0.002	0.003
4000S1	-0.019	0.024	-0.167	0.002	0.002	0.003
4000S2	-0.020	0.025	-0.165	0.002	0.003	0.004
4000S3	-0.022	0.026	-0.163	0.003	0.004	0.004
4000S4	-0.020	0.027	-0.163	0.002	0.003	0.003
4000S5	-0.020	0.026	-0.165	0.003	0.003	0.003
4000S1A	-0.020	0.024	-0.170	0.002	0.002	0.006
4000S2A	-0.022	0.026	-0.167	0.002	0.003	0.005
4000S3A	-0.023	0.027	-0.165	0.003	0.003	0.005
4000S4A	-0.020	0.026	-0.165	0.002	0.003	0.005

From Table 4-13, the overall boresight values determined from different scale of imagery are very close to each other. The Tx determined from the 1:4000 QC blocks are slightly different from the 1:8000 and the 1:20000 scale, the  $<1$  arc minute difference will give insignificant effects on the EO parameters in such a low flying attitude (section 2.3.4). Furthermore, the QC blocks from the 1:4000 scale shows that cross strip images did not give significant improvement to the QC process. Therefore, the theory in section 3.2.2 that a **3x8** QC block can optimize the QC process is again evaluated. Without significant difference in boresight value, the value from the 1:8000 scale images is chosen as a reference value. In addition to the boresight RMS, the RMS navigation error estimated by the Kalman Filter is observed to understand the *typical* DG performance of the data; the statistical report is listed in Table 4-14.

**Table 4-14: RMS of Navigation Error estimated by the Kalman Filter of the PASCO 310 Flight**

RMS Navigation Error					
Easting (m)	Northing (m)	Vertical (m)	Roll (deg)	Pitch (deg)	Heading (deg)
0.02	0.02	0.03	0.010	0.010	0.032

From Table 4-14, the attitude accuracy of the data seems to be little better than the expected value (a RMS difference of  $\sim 0.008$  deg in roll/pitch and  $\sim 0.014$  deg in heading as compared to Table 4-3). This relates to the uncertainty of a less accurate system that cannot be controlled. There is no guarantee that the next data collected by the same system can achieve similar performance until it is statistically evaluated through a large number of test

data. Base on the magnitude of the RMS navigation errors, this data still falls into a less accurate GPS/IMU data category.

#### 4.4. Large Format Digital Camera Flights

The two large format digital camera datasets to be used in Chapter 5 are acquired over Alaska and Northern New Mexico, United States, respectively. The large format digital camera being used is Digital Mapping Camera (DMC) equipped with POS AV 510 DG System. In later sections, they are simply called the DMC Alaska and DMC F-Block. Table 4-15 and Table 4-16 list the properties of the two datasets, detailed information such as flight trajectory and block configuration are referenced in Appendix A-3 and A-4, respectively.

**Table 4-15: Configuration of the DMC Alaska Flight**

Dataset	DMC Alaska
Location	Alaska, United States
Camera	DMC
Scale	1 : 6000
# of Strips	3
# Photo / Strip	13
Flying Height, AGL (m)	720
Ground Sample Distance (m)	0.07
Forward / Side Overlap (%)	60 / 30
Mapping Projection	StatePlane Alaska Zone 04
Datum	WGS84
Height	Orthometric
# of Check Points	12
DGPS/IMU System	POS AV 510

**Table 4-16: Configuration of the DMC F-Block Flight**

Dataset	DMC F-Block
Location	Northern New Mexico, United States
Camera	RC 30
Scale	1 : 22000
# of Strips	4
# Photo / Strip	1*20 and 3*89
Flying Height, AGL (m)	2600
Ground Sample Distance (m)	0.26
Forward / Side Overlap (%)	60 / 25
Mapping Projection	UTM Zone 13
Datum	WGS84
Height	Orthometric
# of Check Points	10
DGPS/IMU System	POS AV 510

#### 4.4.1. DMC Alaska Flight

The DMC Alaska dataset is a high resolution DMC project. From the block configuration and the check point locations arrangement shown in Figure A-5, it is a calibration flight. Since there was no reference information available from ZI/Imaging, QC is carried out to determine the reference boresight value. Due to the ground feature availability in some part of the image block, instead of the recommended 3x8 QC block size, all images (3x13) are used in the control-free QC process. Table 4-17 presents the QC's boresight value and its corresponding RMS residuals. RMS navigation errors are listed in Table 4-18.

**Table 4-17: Boresight Values and RMS Residuals of the DMC Alaska QC**

	Tx (deg)	Ty (deg)	Tz (deg)
Boresight Value	0.038	-0.004	-0.532
RMS Boresight Residuals	0.003	0.002	0.004

**Table 4-18: RMS of Navigation Errors estimated by the Kalman Filter of the DMC Alaska Flight**

RMS Navigation Error					
Easting (m)	Northing (m)	Vertical (m)	Roll (deg)	Pitch (deg)	Heading (deg)
0.02	0.02	0.04	0.003	0.003	0.013

From the RMS navigation errors in the above table, the performance of the data is similar to the PhotoScience UofK Flight which also used a POS AV 510 System. In terms of QC, results from Table 4-17, they also have similar performance with other Quality Controlled data described earlier (PhotoScience UofK and PASCO 310). While the data has a Ground Sample Distance (GSD) less than 0.1m, this large scale mapping project should provide very useful result to understand the performance of high resolution data collected by digital camera. Therefore, using the same parameters as in the PhotoScience UofK simulation, a simulation test is performed and the RMS difference for each Monte Carlo trial is presented in Table 4-19, with the corresponding Ensemble RMS and Root-Sum-Square being shown in Table 4-20.

**Table 4-19: Statistical report of Monte Carlo Trials on the DMC Alaska POS AV 310 Simulation**

Monte Carlo Trial #	RMS Difference					
	Easting (m)	Northing (m)	Vertical (m)	Roll (amin)	Pitch (amin)	Heading (amin)
1	0.01	0.01	0.02	0.88	0.58	1.66
2	0.01	0.01	0.02	0.68	0.70	1.64
3	0.01	0.01	0.01	0.56	0.51	2.22
4	0.01	0.01	0.01	0.84	0.49	1.44
5	0.00	0.01	0.01	0.79	0.74	1.54
6	0.01	0.01	0.02	0.82	0.69	1.98
7	0.01	0.00	0.01	0.67	0.69	1.68
8	0.01	0.01	0.02	0.70	0.56	1.87
9	0.01	0.01	0.01	0.65	0.80	2.22
10	0.00	0.00	0.02	0.50	0.72	2.74

**Table 4-20: Ensemble RMS and RSS of the DMC Alaska POS AV 310 Simulation**

Navigation Parameters	Theoretical RMS Difference	Ensemble RMS Difference	RSS / Simulated Data Accuracy
Northing (m)	0	0.01	0.05 – 0.3
Easting (m)	0	0.01	0.05 – 0.3
Vertical (m)	0	0.02	0.05 – 0.3
Roll (arc minute)	0.72	0.72	0.78
Pitch (arc minute)	0.72	0.66	0.72
Heading (arc minute)	2.04	1.94	1.99

Similar to the PhotoScience UofK POS AV 310 simulation, the results in Table 4-20 show that a less accurate GPS/IMU data has been simulated, having similar performance as a POS AV 310 system as shown in Table 4-2. Again, the centimetre ensemble RMS difference in position results no changes on the corresponding RRS value Therefore, the

simulation is a success because it achieved the performance of a less accurate GPS/IMU system and is used in Chapter 5's Integrated Sensor Orientation Test.

#### 4.4.2. DMC F-Block New Mexico Flight

The DMC F-Block is a special dataset collected for internal research on the performance of DMC image georeferencing using GPS with the optional use of the IMU [Madani (2003)]. Madani's paper focused on the comparison of POS-assisted AT and GPS-assisted AT in a controlled environment (calibrated system parameters with well established GCPs and flight configuration), while this thesis research is focused on the operational point of view when using Direct Georeferencing and Integrated Sensor Orientation. Therefore, direct comparison is not made between the researches.

Similarly, quality control is performed to determine the boresight value when no reference information is available for the dataset. Having a larger image block with >80 images per strip, a **3x8** image block is selected from the residential area to ensure that the collected image tie points are within acceptable accuracy. Table 4-21 presents the QC's boresight values and its corresponding residual. Navigation RMS of the data is shown in Table 4-22.

**Table 4-21: Boresight Values and RMS Residuals of the DMC F-Block QC**

	Tx (deg)	Ty (deg)	Tz (deg)
Boresight Value	0.013	-0.020	-0.518
RMS Boresight Residuals	0.003	0.002	0.006

**Table 4-22: RMS of Navigation Error estimated by the Kalman Filter of the DMC F-Block Flight**

RMS Navigation Error					
Easting (m)	Northing (m)	Vertical (m)	Roll (deg)	Pitch (deg)	Heading (deg)
0.03	0.02	0.04	0.003	0.003	0.013

From both tables, the performance of the data are within expectation (POS AV 510 performance in Table 4-2) and therefore together with the DMC Alaska data, they provide excellent examples for both high and less accurate DG systems integrated with a large format digital camera for the Integrated Sensor Orientation test in the Chapter 5.

#### **4.5. Medium Format Digital Camera Flight**

Finally, one dataset is available to represent the Medium Format Digital Camera which uses Consumer Off-the-self (COTS) components. This is the Ajax flight acquired by the DSS equipped with a POS AV 410 DG system. Table 4-23 lists the properties of the Ajax datasets, detailed information such as flight trajectory and block configuration is referenced in Appendix A-5.

**Table 4-23: Configuration of the DSS Ajax Flight**

Dataset	DSS Ajax
Location	Ajax, Canada
Camera	DSS
Scale	1 : 20000
# of Strips	9
# Photo / Strip	8
Flying Height, AGL (m)	1100
Ground Sample Distance (m)	0.18
Forward / Side Overlap (%)	60 / 20
Mapping Projection	UTM Zone 17
Datum	WGS84
Height	Ellipsoid
# of Check Points	41
DGPS/IMU System	POS AV 410

#### 4.5.1. DSS Ajax Flight

The DSS Ajax flight is a specially designed mapping project to evaluate the performance of fast orthophoto production under an actual mapping environment [Ip et al (2004a)]. Therefore, as listed in Table 4-23, the side overlap is only 20% while other evaluated datasets have at least 25%. This coverage gives maximum ground coverage while providing enough overlapping area for stereo viewing, tie point collection or DTM discussion. Discussion for further applications using this dataset – fast orthophoto production is presented in Chapter 6. For mapping missions, quality control is always recommended to mapping companies as the first step. Therefore, the data was collected in a way that the boresight value is assumed to be determined using the dataset itself through QC, and therefore no reference information is available from airborne calibration or other mission

data. Thus, a 3x8 image block is chosen to perform QC under a control-free environment, Table 4-24 presents the QC's boresight value and its corresponding residual, with navigation RMS listed in Table 4-25.

**Table 4-24: Boresight Values and RMS Residuals of the DSS Ajax QC**

	Tx (deg)	Ty (deg)	Tz (deg)
Boresight Value	-0.121	-0.854	0.168
RMS Boresight Residuals	0.008	0.006	0.008

**Table 4-25: RMS of Navigation Error estimated by the Kalman Filter of the DSS Ajax Flight**

RMS Navigation Error					
Easting (m)	Northing (m)	Vertical (m)	Roll (deg)	Pitch (deg)	Heading (deg)
0.02	0.02	0.04	0.003	0.003	0.009

From Table 4-25, the result shows that the Kalman Filter reports a better navigation performance than the POS AV 410 specification. This result might be related to the mission trajectory as shown in Figure A-9. In this flight, images are collected in multiple areas of Southern Ontario. When heading accuracy continues to improve throughout heading changes [Mostafa and Hutton (2001)], for the data that is being taken over one hour after take off, it is not surprising to observe an accurate heading error estimation by the Kalman Filter. But, when comparing the boresight RMS listed in Table 4-24, the residual is higher than the previous POS AV 510 data results. This is the result of the true performance of a POS AV 410, that the capability of attitude determination is still weaker than a POS AV 510 system, especially in heading accuracy. Based on the above observation, the true

performance of a GPS/IMU system is very important. Thus, proper standard deviation for the exterior orientation parameters should be always used [Cramer et al, (2001a)]. More discussion is given in Chapter 5 during the Integrated Sensor Orientation test.

To understand the performance of less accurate GPS/IMU systems in all types of *frame* cameras described in this thesis (section 2.3.1), simulation is carried out on the DSS Ajax flight. instead of building a new degraded model, the same model used on POS AV 510 data is used again. The RMS difference for each Monte Carlo Trial is presented in Table 4-26, and the corresponding Ensemble RMS and Root-Sum-Square are listed in Table 4-27.

**Table 4-26: Statistical report of Monte Carlo Trials on the DSS Ajax POS AV 310 Simulation**

Monte Carlo Trial #	RMS Difference					
	Easting (m)	Northing (m)	Vertical (m)	Roll (amin)	Pitch (amin)	Heading (amin)
1	0.03	0.05	0.03	0.64	0.81	2.03
2	0.10	0.11	0.06	0.73	0.66	2.43
3	0.03	0.03	0.03	0.61	0.68	2.25
4	0.03	0.03	0.02	0.62	0.59	1.75
5	0.03	0.03	0.03	0.70	0.80	1.93
6	0.03	0.04	0.02	0.73	0.68	1.97
7	0.03	0.04	0.03	0.79	0.85	2.15
8	0.04	0.04	0.02	0.72	0.63	1.98
9	0.02	0.03	0.03	0.74	0.74	2.35
10	0.03	0.04	0.03	0.71	0.66	2.29

**Table 4-27: Ensemble RMS and RSS of the DSS Ajax POS AV 310 Simulation**

Navigation Parameters	Theoretical RMS Difference	Ensemble RMS Difference	RSS / Simulated Data Accuracy
Northing (m)	0	0.04	0.07 – 0.3
Easting (m)	0	0.05	0.07 – 0.3
Vertical (m)	0	0.03	0.06 – 0.3
Roll (arc minute)	0.61	0.70	0.85
Pitch (arc minute)	0.61	0.72	0.86
Heading (arc minute)	1.90	2.12	2.31

From Table 4-27, it can be seen that similar ensemble RMS difference is achieved when performing degradation on the two POS AV 510 data (Table 4-11 for PhotoScience UofK and Table 4-20 for DMC Alaska). Based on the results of the three simulations in this research, it can be deduced that the corresponding ensemble RMS difference could be similar, regardless of the original GPS/IMU data accuracy when a degrading model is applied to any GPS/IMU data; which would be.. Although the ensemble RMS difference is slightly higher than any other simulation done for the film and DMC data, the RSS of the simulation behaves similarly to a POS AV 310 performance (Table 4-2). Therefore, the DSS Ajax flight is expected to have similar navigation performance as other simulations. This will be evaluated in Chapter 5 through the Integrated Sensor Orientation tests.

In this Chapter, the datasets from three types of imaging sensor have been reviewed: Film Camera, Digital Mapping Camera (DMC) and Digital Sensor System (DSS). High accuracy GPS/IMU data has been collected using the POS AV Direct Georeferencing systems and simulations have been performed to degrade their accuracy in order to obtain a lower grade GPS/IMU system data under the same condition.

## CHAPTER FIVE: DATA RESULTS AND ANALYSIS

Through the OEEPE test, the use of both Direct Georeferencing and Integrated Sensor Orientation have been deeply discussed in multiple papers [Heipke et al (2001b), Cramer et al (2001a,b) and Jacobsen et al (2001)]. Also, independent tests were performed to further discuss the performance of Integrated Sensor Orientation [Casella et al (2004), Honkavarra et al (2002), Hinsken et al (2002)]. Recommendations have been given to improve both processes and throughout the years they have been instigated into the operational workflow. One example is the QC procedure. This is a step in which camera self-calibration (camera focal length and principal point offsets only), boresight mis-alignment refinement and local datum shift determination (with the use of one or more GCPs) takes place. This becomes a necessary step in DG to minimize the system error residuals and to ensure data integrity. Having the high accuracy GPS/IMU data quality controlled, the difference between *Typical* DG and *Quality Controlled* DG must be differentiated. *Typical* DG refers to the use of direct georeferencing data when reference system parameters (boresight mis-alignment and IMU/imaging sensor lever arm) are available from the airborne/terrestrial calibration report or from previous flight missions. This approach is typically used by companies who do not have access to aerial triangulation packages to improve accuracy through Quality Control or Integrated Sensor Orientation. Another use of this approach is for applications that need fast orthophoto which means they must be delivered as soon as possible or the absolute accuracy is not the main concern, such as emergence response and remote sensing

applications. On the other hand, the Quality controlled DG data has some system and mission specific residual error minimized and therefore performance is expected to be better than the typical DG data in certain levels, depending on the imaging sensor used and the corresponding project scale [Casella et al (2004), Ip et al (2004c) and Honkavaara et al (2002)].

## **5.1. Typical DG Performance**

This section looks into the expected and actual *typical* DG performance. Comparison is made between an error model and the simulated POS AV 310 data.

### **5.1.1. DG System Error Budget Analysis**

An error budget analysis is carried out to understand the expected performance of a less accurate GPS/IMU system, using a POS AV 310 system as an example. Such results provide an understanding of why a high accuracy GPS/IMU system is more accurate in handling Direct Georeferencing applications than less accurate ones. To build the error budget model, a stereopair of imagery is assumed to be horizontally located in the air with 60% forward overlap. Then, using the specification of the POS AV 310 system, the corresponding y-parallax of a point located around the center of the overlapping area is calculated. The deriving of the equation is given in Appendix C-1. Such analysis is carried out on three imaging sensors: film camera (153mm focal length), the DMC and the DSS,

under different mapping scale. The results are shown in Figure 5-1, Figure 5-2 and Figure 5-3, respectively. Notice that the theoretical y-parallax is pessimistic and has a larger value than the real data.

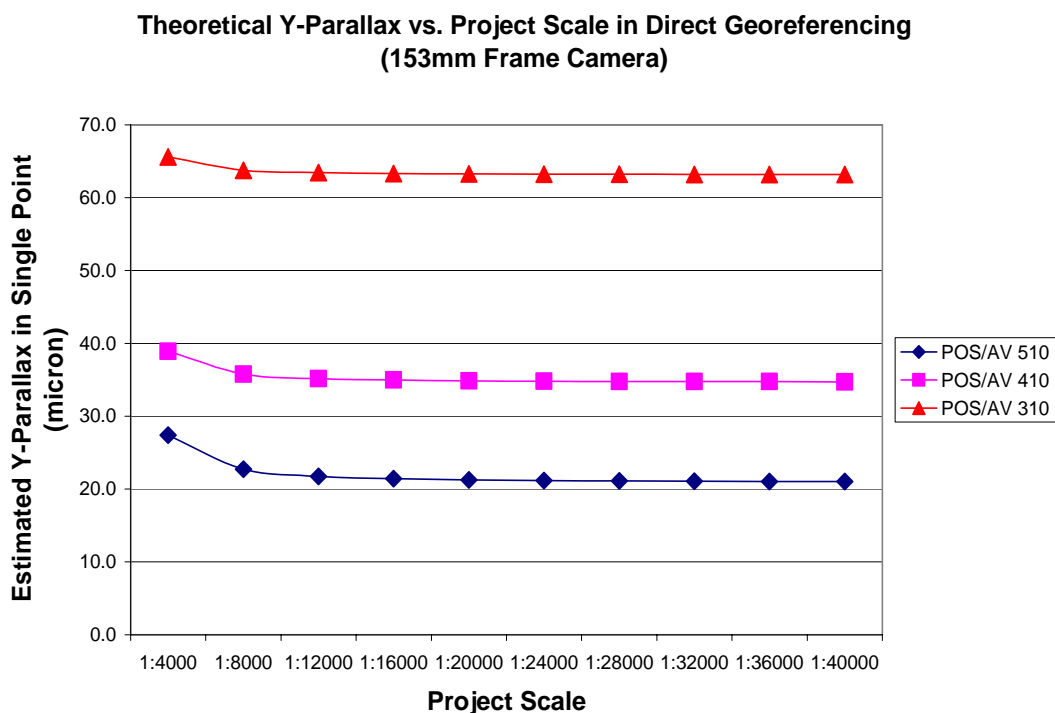


**Figure 5-1: Error Budget Analysis of 153mm Film Camera System**  
(see Appendix C-1)

From Figure 5-1, it can be seen directly the benefits of high accuracy DG system. For small scale mapping projects using a POS AV 510 system, pixel accuracy can be easily achieved if image scan resolution is ~20 micron. Between a photo scale of 1:12000 and 1:40000, attitude error dominates the y-parallax and therefore the level is very stable until the scale increases to 1:8000 or more. At this point, residual error from DGPS starts to dominate and

y-parallax increases rapidly in large scale photography. Thus, centimetre accuracy cannot be achieved from the corresponding y-parallax level when scanning resolution is between 15-20 microns. This is the reason why the DG system becomes marginal for very large scale mapping with the limitation of DGPS position accuracy. Using a POS AV 410 system, the 1.5 to 2.0 pixel accuracy for 15-20 microns scanning resolution is very marginal for direct use of the EO parameter, except for some projects with less accuracy requirements (0.5 to 1.0 m). Furthermore, when a POS AV 310 is used, the >60 microns in y-parallax becomes unacceptable for any stereo or mapping operation. This explains why direct use of less accurate GPS/IMU data is impossible unless some refinement of the EO parameters through Quality Control or Integrated Sensor Orientation is implemented.

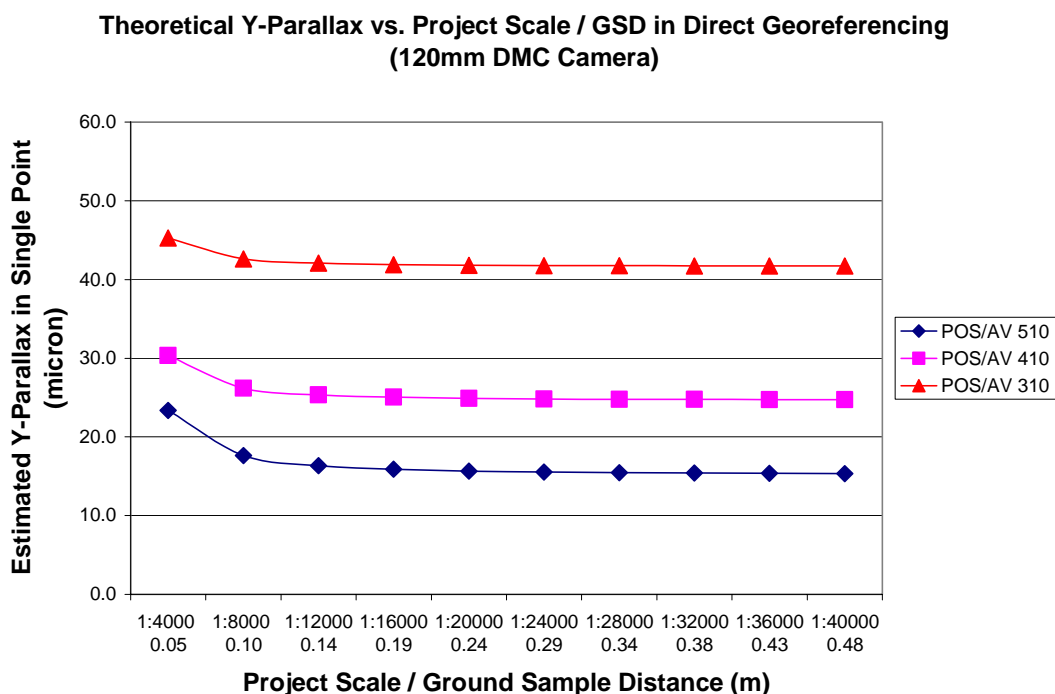


**Figure 5-2: Error Budget Analysis of Digital Mapping Camera (DMC)**  
(see Appendix C-1)

For the DMC camera, a similar trend can be observed when comparing its results with the Film Camera analysis. Data from a POS AV 510 is very impressive to provide pixel accuracy (with 12 micron pixel size for the DMC) until GSD < 0.15m. Data from a POS AV 410 is marginal for direct EO usage (~2 pixels) and for POS AV 310 it is unacceptable with its ~3.5 pixels y-parallax. Notice that Ground Sample Distance (GSD) is introduced in addition to the project scale. When digital cameras have different focal length, direct comparison between project scales is no longer valid. Therefore, GSD – the geometric resolution on the ground is used as a common scale because the pixel size for digital cameras is constant, unlike the film imagery that have a wide range of scanning resolution.

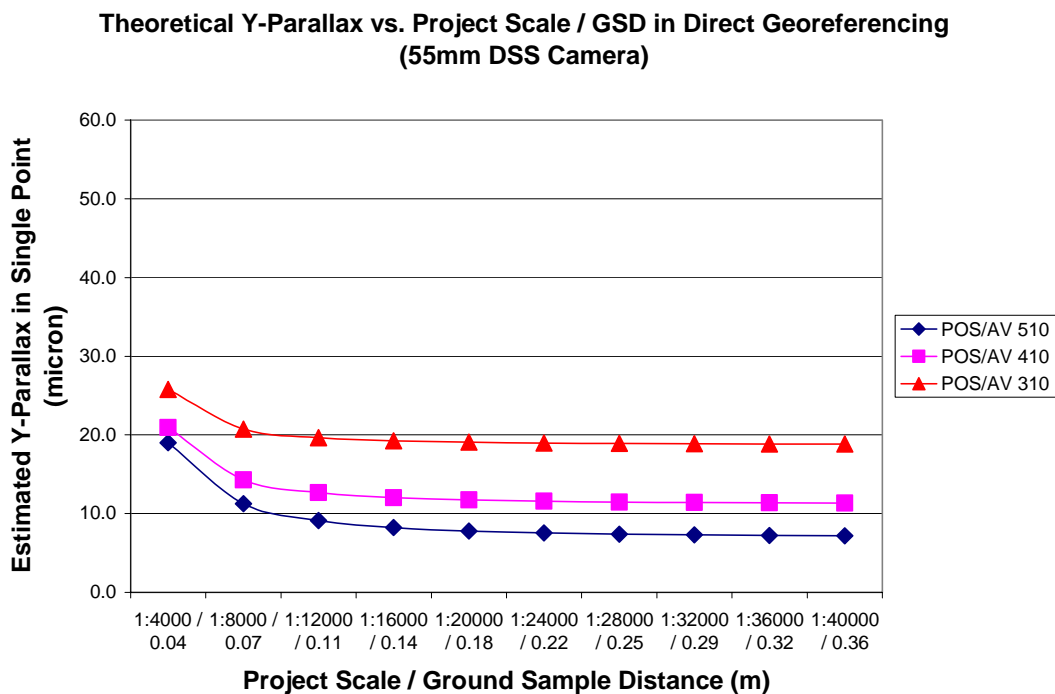


**Figure 5-3: Error Budget Analysis of Digital Sensor System (DSS)**  
(see Appendix C-1)

From Figure 5-3, the shorter focal length (55mm) of the DSS has shown some benefit when the flying height is ~50% over the other two cameras under the same GSD. The relative performance between different DG systems on the same camera data is very similar, especially between POSAV 510 and 410, as the flying height dominates most of the y-parallax. Here, a POS AV 410 can deliver pixel accuracy with the 9 micron pixel size for the DSS. If a POS AV 510 is used instead, the benefit can only be observed when image measurement accuracy is <1 pixel all the time. Based on an economical point of view, using a POS AV 410 on a DSS can lower the overall system cost while maintaining a similar level of performance as when a POS AV 510 system is used.

### 5.1.2. DG Performance of Simulated POS AV 310 Data

This section investigates the expected performance of the simulated POS AV 310 data using the EO analysis function in ISAT as used in Section 4.2.1. By comparing the surveyed coordinates with the space intersected coordinates from image models, the RMS check point residuals are recorded. While all the simulated data is created from the Monte Carlo Analysis, the RMS value of each trial is presented and the ensemble RMS is calculated as the final value for the data. Notice in this test, the boresight value being used to determine the EO parameters of the simulated data are determined using a corresponding high end system, which is referred as the *reference* boresight of the GPS/IMU system. Realistically this is impossible to be achieved using actual flight data because when a system with two qualities of IMUs are installed at the same time, even if they are mounted on the imaging sensor with one on top of another, their boresight value will not be the same. However, in this thesis, the less accurate GPS/IMU data is simulated from the corresponding high end system data, therefore, in theory, their boresight values will be the same because both GPS/IMU data come from the same system configuration. Therefore, the following result is only to represent the ideal scenario when the boresight can be independent determined accurately, and the corresponding result evaluates the expected check point RMS when a POS AV 310 system is used for *typical* Direct Georeferencing application. First, the results from all three simulation tests are presented, followed with discussion. Figure 5-4, Figure 5-5 and Figure 5-6 present the EO analysis results for

PhotoScience UofK, DMC Alaska and DSS Ajax and the corresponding statistical reports for each Monte Carlo trial are shown in Table 5-1, Table 5-2 and Table 5-3, respectively.

PhotoScience UofK (1:6000 / 0.09m GSD)

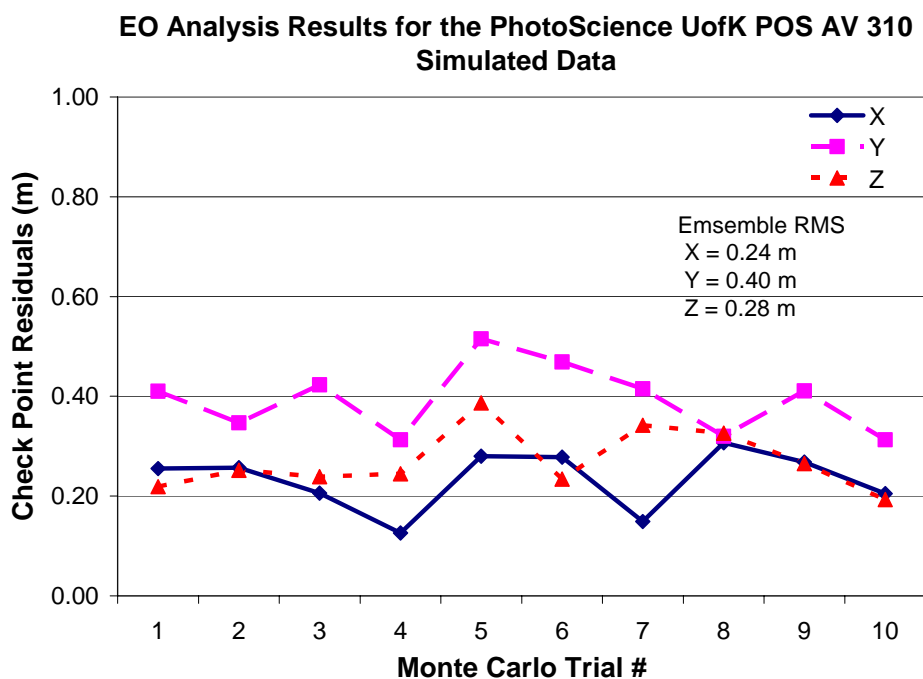


**Figure 5-4: EO Analysis on PhotoScience UofK POS AV 310 Simulated Data**

**Table 5-1: Statistical Report of EO Analysis on the PhotoScience UofK POS AV 310 Simulation**

Monte Carlo Trial #	Check Point RMS		
	X (m)	Y (m)	Z (m)
1	0.26	0.41	0.22
2	0.26	0.35	0.25
3	0.21	0.42	0.24
4	0.13	0.31	0.25
5	0.28	0.52	0.39
6	0.28	0.47	0.23
7	0.15	0.42	0.34
8	0.31	0.32	0.33
9	0.27	0.41	0.27
10	0.21	0.31	0.19
Ensemble	0.24	0.40	0.28

*DMC Alaska (1:6000 / 0.15m GSD)*

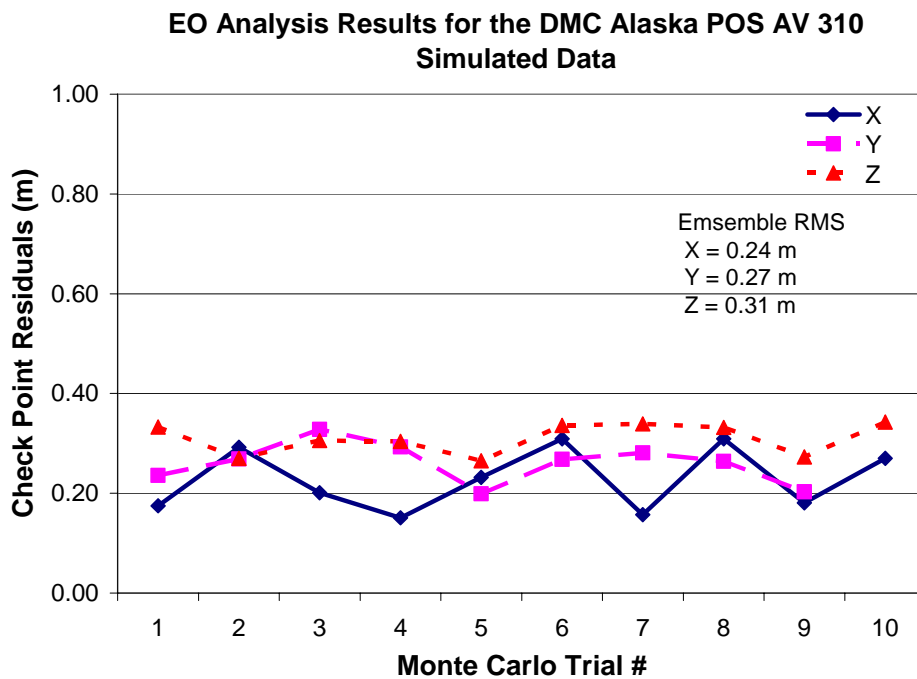


**Figure 5-5: EO Analysis of DMC Alaska POS AV 310 Simulation**

**Table 5-2: Statistical report of EO Analysis on the DMC Alaska POS AV 310 Simulation**

Monte Carlo Trial #	Check Point RMS		
	X (m)	Y (m)	Z (m)
1	0.18	0.36	0.33
2	0.29	0.24	0.27
3	0.20	0.27	0.31
4	0.15	0.33	0.30
5	0.23	0.29	0.27
6	0.31	0.20	0.34
7	0.16	0.27	0.34
8	0.31	0.28	0.33
9	0.18	0.26	0.27
10	0.27	0.20	0.34
Ensemble	0.24	0.27	0.31

*DSS Ajax (1:20000 / 0.18 GSD)*

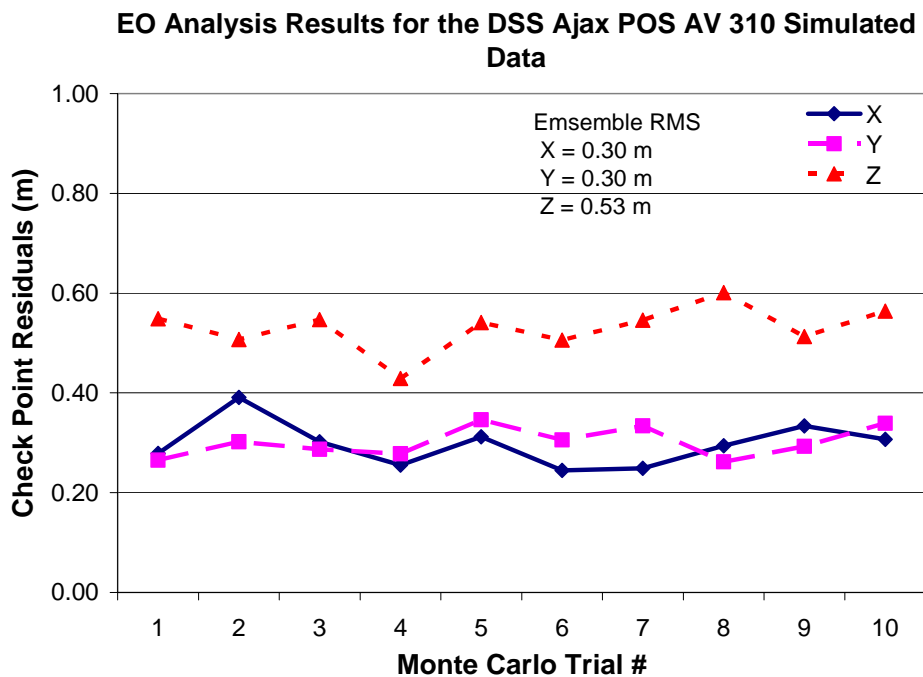


**Figure 5-6: EO Analysis on DSS Ajax POS AV 310 Simulated Data**

**Table 5-3: Statistical report of EO Analysis on DSS Ajax POS AV 310 Simulated Data**

Monte Carlo Trial #	Check Point RMS		
	X (m)	Y (m)	Z (m)
1	0.28	0.27	0.55
2	0.39	0.30	0.51
3	0.30	0.29	0.55
4	0.26	0.28	0.43
5	0.31	0.35	0.54
6	0.25	0.31	0.51
7	0.25	0.33	0.55
8	0.29	0.26	0.60
9	0.33	0.29	0.51
10	0.31	0.34	0.56
Ensemble	0.30	0.30	0.53

The above results demonstrate the performance of less accurate GPS/IMU data under *typical* direct georeferencing application. When comparing the check point RMS with the GSD, about 1.5 to 3.0 pixels 3D ground accuracy is experienced. This explains why less accurate GPS/IMU is not designed for direct georeferencing applications (typically <1.5 pixels), and required to be improved through Integrated Sensor Orientation. This theory will be evaluated in section 5.2.

## **5.2. Quality Controlled DG vs. ISO**

Understanding the limitations of less accurate GPS/IMU data through the *typical* Direct Georeferencing EO analysis, the next step is to evaluate if Integrated Sensor Orientation can be used to improve the accuracy. In Chapter 4, the high accuracy GPS/IMU data has been quality controlled (control free) to determine the reference boresight, the QC results (using EO Analysis function) is compared with the ISO result from less accurate GPS/IMU data. Since most mapping projects consist of image blocks some GCPs are available, the comparison is divided into two categories: control-free and the use of one ground control point around the center of the test block. The standard deviations being used in the ISO process for the EO parameters come from the RMS navigation errors estimated by the Kalman Filter. As described in OEEPE test [Cramer (2001b)], the use of accurate standard deviation is very important and therefore the navigation errors estimated by the Kalman Filter should provide a very good estimate of the actual performance of the system.

While performing the ISO test, analysis on the relationship between accuracy improvement and the number of tie point requirement is performed. Therefore, different PPVG values for automatic tie point collections are used throughout the ISO test.

Some information about the EO Analysis has been discussed (section 2.3.3). However, in the following results, not only the absolute accuracy (check point RMS) but also the relative accuracy (y-parallax RMS) will be presented. The EO Analysis evaluates the quality or condition of exterior orientation parameters by comparing the given coordinates of control points and check points with the intersection of the rays of these points as projected on overlapping photo pairs by the EO data [Madani and Mostafa (2001)]. The absolute accuracy presented by the check point RMS measures how close the stereoplotted coordinates are to their true values. On the other hand, the y-parallax ( $P_y$ ) RMS (based on  $(y_p = y_2 - y_1)$ ) measures how well the homologous rays intersect in the overlapping area [Casella et al (2004)].

The following results are focused on the performance comparison between QC and ISO. While a large quantity of data has been processed, especially in the simulated data, results for each Monte Carlo trial is not presented, Instead the presentation of ensemble values can statistically represent the performance of the simulated data.

### 5.2.1. Film Camera Flights

#### *PhotoScience UofK Flight*

Since the data contains a total of 4 strips, the results from different number of strip combinations are presented. This is very useful to analyze the optimal operating condition for ISO. Similar presentations of results are used throughout the rest of the section for other datasets. Table 5-4 presents the results of the quality controlled POS AV 510 data and the ISO result of the simulated POS AV 310 data. For the simulated POS AV 310 data, Figure 5-7 presents the results graphically to analyze the correlation with different PPVG values.

**Table 5-4: PhotoScience UofK Flight – POS AV 510 (after QC) vs. Simulated POS AV 310 (after ISO), Control Free**

# of Strip	Control Free							
	POS AV 510 (after QC)				Simulated POS AV 310 (after ISO)			
	Check Point RMS			Py RMS	Check Point RMS			Py RMS
	X (m)	Y (m)	Z (m)	( $\mu\text{m}$ )	X (m)	Y (m)	Z (m)	( $\mu\text{m}$ )
1	0.11	0.06	0.16	7.0	0.14	0.15	0.21	4.7
2	0.09	0.10	0.14	16.1	0.08	0.12	0.15	4.0
3	0.09	0.12	0.15	15.4	0.09	0.13	0.17	4.3
4	0.10	0.13	0.15	14.8	0.08	0.14	0.15	4.0

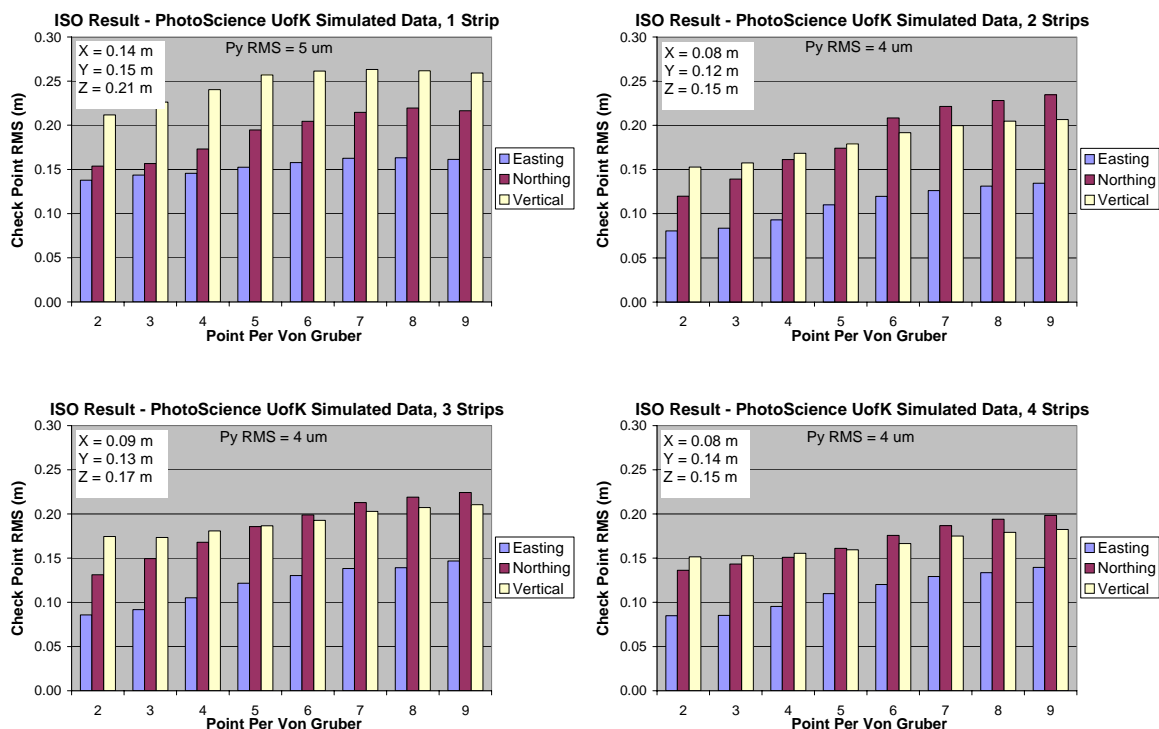


**Figure 5-7: ISO Results of the PhotoScience UofK Simulated POS AV 310 Data (Control Free)**

(see Appendix A-1 - GSD = 0.09 m)

From Table 5-4, the benefit of high accuracy DG data is observed. Pixel accuracy can be obtained with high level of 3-D position accuracy. Such accuracy can be used to perform any mapping application: stereo mapping, DTM extraction and orthophoto. On the other hand, after running ISO on the simulated PSO AV 310 data the ground accuracies have been improved in all cases. However when only one strip of data is used, the overall improvement is only ~10%, which is insignificant in comparison with the other combinations that have ~50% improvement in the horizontal component and ~30% improvement in the vertical component. This means running ISO on strip/corridor images

is not very cost effective. However for all cases, the parallax of models can be brought to about 4  $\mu\text{m}$ . This is a significant improvement as it allows this less accurate GPS/IMU data to be used for any stereo mapping application. Except for the strip/corridor case, similar ground accuracy as the POS AV 510 data is achieved after ISO is performed. This gives a strong potential for less accurate GPS/IMU system to be used in an image block in conjunction with the ISO approach in order to reach similar level of accuracy as a high accuracy system. Further analysis of the data and results when 1 center GCP is used is shown in Table 5-5.

**Table 5-5: PhotoScience UofK Flight – POS AV 510 (after QC) vs. Simulated POS AV 310 (after ISO), 1 Center GCP**

# of Strip	1 Center GCP Used							
	POS AV 510 (after QC)				Simulated POS AV 310 (after ISO)			
	Check Point RMS			Py RMS	Check Point RMS			Py RMS
	X (m)	Y (m)	Z (m)	( $\mu\text{m}$ )	X (m)	Y (m)	Z (m)	( $\mu\text{m}$ )
1	0.07	0.08	0.12	7.9	0.12	0.13	0.18	4.6
2	0.08	0.09	0.11	13.9	0.08	0.12	0.15	4.0
3	0.07	0.12	0.12	13.9	0.09	0.13	0.18	4.3
4	0.08	0.12	0.11	12.9	0.09	0.13	0.15	4.0

When quality controlling using one GCP, absolute accuracy is improved especially in the vertical component, this shows that 2 – 3 cm of vertical datum shift exists in the data. But, the determination of such datum shift is depended on the accuracy of the GCP being used and such correlation will be observed further when processing other datasets in this chapter. On the other hand, when using one GCP in the center of the block, only the strip/corridor

case improves in vertical accuracy, bringing similar accuracy as other strip combinations. This shows that GCP is not mandatory to perform ISO for an image block, except the centimetre level local datum shift is required to be resolved. However, when observing the POS AV 310 ISO results, using a single GCP, one cannot achieve similar vertical accuracy as the quality controlled POS AV 510 data. Since the GCP being used in the QC is different from the ones being used in the different strip combinations, therefore the accuracy of the GCP is beyond the magnitude of the local datum shift and more GCPs are then required to determine the local datum shift properly. Figure 5-8 and Table 5-6 presents further analysis of the data using the ISO for the POS AV 510 data.

**Table 5-6: ISO Results of the PhotoScience UofK POS AV 510 data, Control Free vs. 1 Center GCP**

# of Strip	Control Free				1 Center GCP Used			
	Check Point RMS			Py RMS ( $\mu\text{m}$ )	Check Point RMS			Py RMS ( $\mu\text{m}$ )
	X (m)	Y (m)	Z (m)		X (m)	Y (m)	Z (m)	
1	0.12	0.10	0.15	4.3	0.15	0.17	0.16	4.5
2	0.08	0.11	0.12	3.2	0.08	0.10	0.12	4.2
3	0.08	0.12	0.16	3.5	0.08	0.12	0.16	4.7
4	0.08	0.13	0.13	4.4	0.08	0.14	0.13	4.4

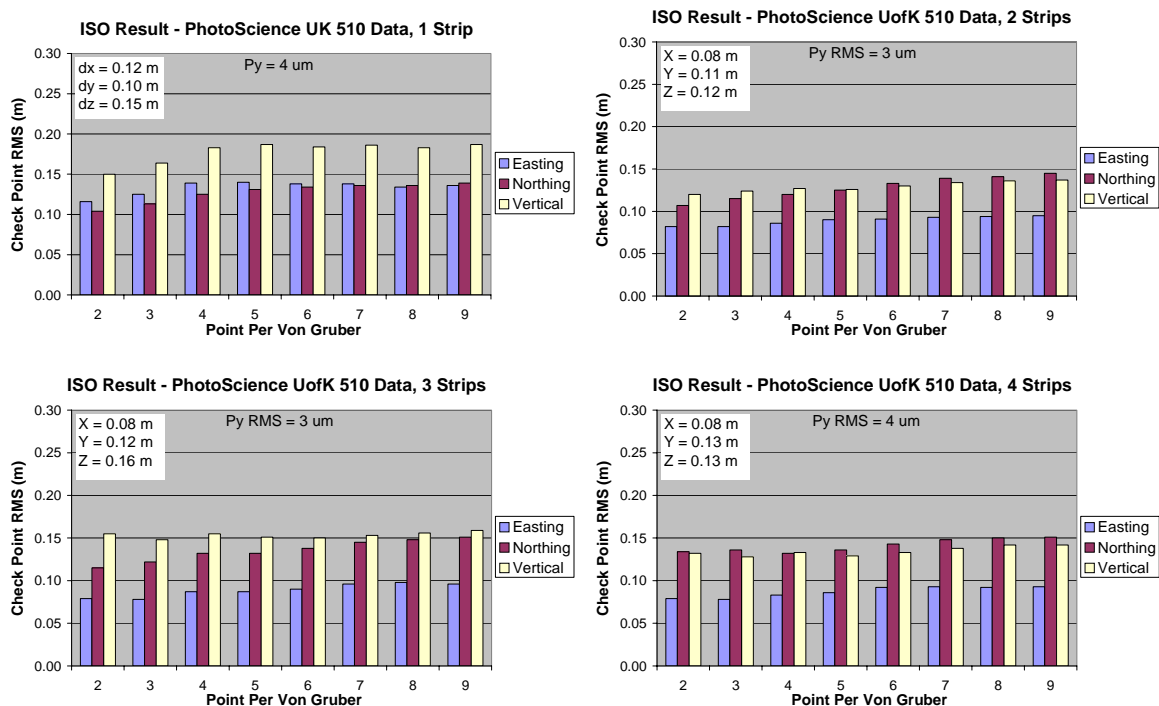


**Figure 5-8: ISO Result of PhotoScience UofK POS AV 510 Flight (Control Free)**

(see Appendix A-1- GSD = 0.09 m)

The results in Figure 5-8, clearly indicate that when running ISO on one strip of high accuracy GPS/IMU data, no improvement in ground accuracy can be achieved, except the y-parallax is reduced to  $\frac{1}{4}$  of a pixel. Moreover, the improvement when 2 or more strips are used makes no more than 20% improvement in ground accuracy. Similarly, when one GCP in the center is used in the ISO, there is insignificant difference from the control-free solutions case. Therefore, the use of GCP is only needed for local shift detection if necessary. While a large scale mapping project requires centimetre accuracy, based on both results at a y-parallax level of  $\sim 4$  microns, project scale of 1:6000 and scanning resolution of 20 $\mu\text{m}$ , relative accuracy can reach a maximum level of 3 cm, which fulfills the accuracy

requirement. On the other hand, the one pixel accuracy delivered by quality controlled GPS/IMU data from the POS AV 510 system is sufficient for most mapping applications, and therefore ISO is not a necessary procedure.

From both results (POS AV 310 and simulated POS AV 310), there exists a correlation between the number of tie points (PPVG value) and the accuracy improvement, and such correlation decreases when more number of strips are used. However, further analysis is, required to understand change in correlation.

### *PASCO Toyonaka City Flight*

Since these datasets contain 3 blocks of images in different scales, the test will take the advantage of multiple scale and cross strip availability. Different block combinations are used to test the performance of ISO under this less accurate GPS/IMU data. Table 5-7 summarizes the different block combinations being used, and the corresponding EO analysis results using quality controlled data are shown in Table 5-8.

**Table 5-7: Block Combinations for the PASCO 310 ISO Test**

	Block 1	Block 2	Block 3	Block 4	Block 5	Block 6
Scale	1:4000	1:8000	1:20000	1:4000	1:4000 & 1:8000	1:4000 & 1:8000
Cross Strip	No	No	No	Yes	No	Yes
# of Strips	10	5	4	12	15	17
# of Images	170	45	29	208	215	253
GSD	0.08 m	0.16 m	0.40 m	0.08 m	Combined	Combined

**Table 5-8: EO Analysis Results of the PASCO 310 Flight (after QC), Control Free vs. 1 Center GCP**

Block	Control Free				1 Center GCP Used			
	Check Point RMS			Py RMS ( $\mu\text{m}$ )	Check Point RMS			Py RMS ( $\mu\text{m}$ )
	X (m)	Y (m)	Z (m)		X (m)	Y (m)	Z (m)	
1	0.17	0.07	0.16	14.9	0.19	0.06	0.08	14.9
2	0.13	0.08	0.18	12.3	0.08	0.07	0.14	12.3
3	0.42	0.24	0.29	15.6	0.38	0.25	0.42	18.5
4	0.15	0.11	0.16	14.9	0.18	0.10	0.08	14.9
5	0.15	0.07	0.17	14.5	0.15	0.06	0.11	14.3
6	0.14	0.10	0.17	14.4	0.15	0.09	0.11	14.4

Comparing the above results with simulated data, this real data performs much better than expected after quality control. Unfortunately, there is no reference boresight available for the data; otherwise it could be used to analyze the *typical* DG performance. A possible explanation is discussed later, after observing the test result of other less accurate GPS/IMU data. The quality control procedure using one GCP is only based on the local datum shift determined by the 1:8000 QC block . Such results improve vertical accuracy in both 1:4000 and 1:8000 image blocks. However, such improvement cannot be observed in the 1:20000 image block. This implies that separate QC procedure might be required when processing small scale imagery. However, the performance of such a procedure still correlates with the achievable measurement accuracy when the GCP is measured on the image. Further analysis the data, Figure 5-9 and Table 5-9 shows the ISO result for different block combinations.

**Table 5-9: ISO Results of the PASCO 310 Flight, Control Free vs. 1 Center GCP**

Block	Control Free				1 Center GCP Used			
	Check Point RMS			Py RMS ( $\mu\text{m}$ )	Check Point RMS			Py RMS ( $\mu\text{m}$ )
	X (m)	Y (m)	Z (m)		X (m)	Y (m)	Z (m)	
1	0.09	0.10	0.18	5.7	0.08	0.10	0.19	5.7
2	0.12	0.12	0.20	5.5	0.12	0.12	0.20	5.5
3	0.35	0.23	0.45	6.6	0.35	0.22	0.42	6.7
4	0.07	0.10	0.18	5.9	0.07	0.10	0.18	5.9
5	0.09	0.09	0.18	5.6	0.09	0.09	0.18	5.6
6	0.07	0.09	0.18	5.7	0.07	0.09	0.18	5.7

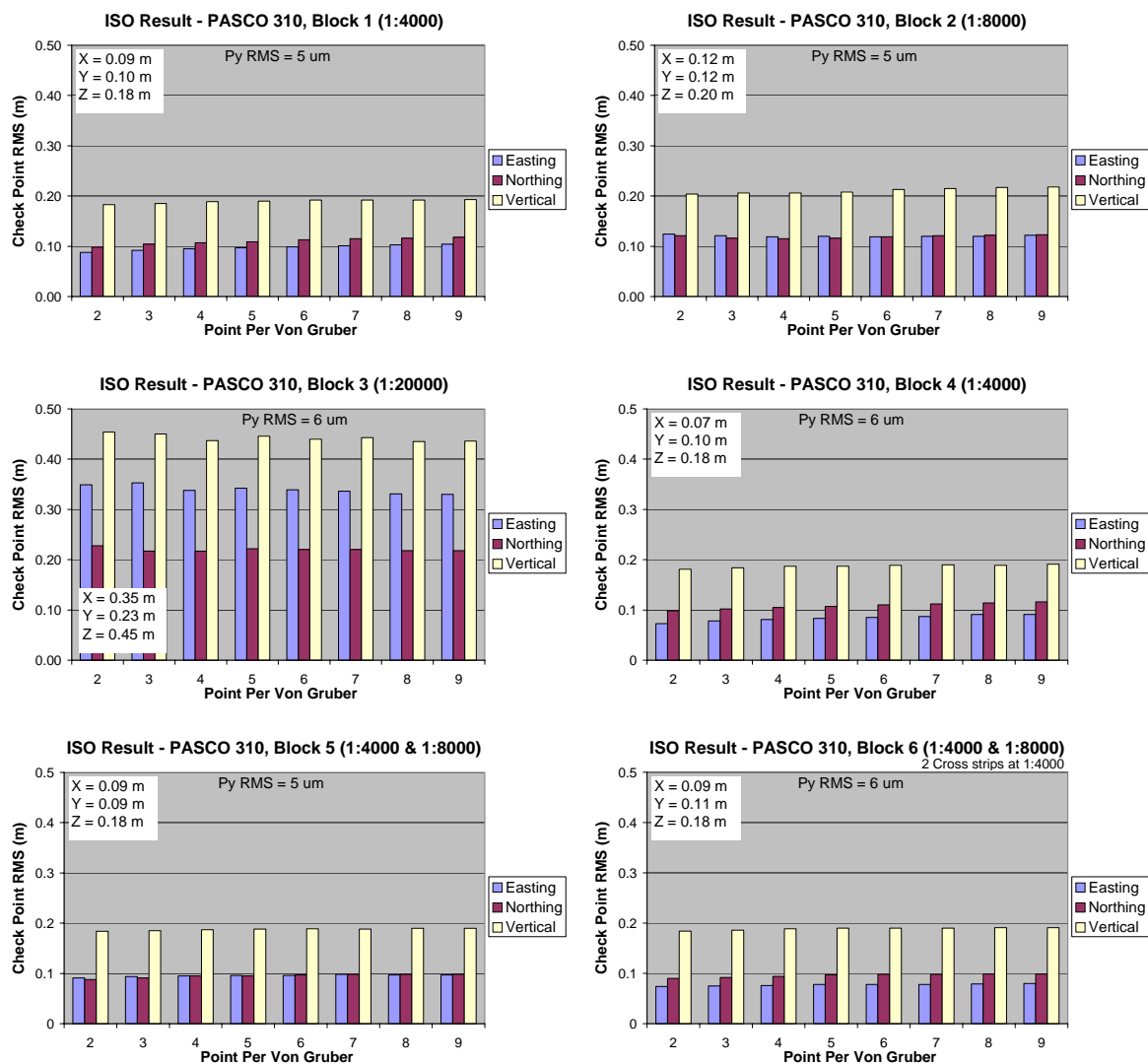


**Figure 5-9: ISO Results of the PASCOCO 310 Flight (Control Free)**

(See Appendix A-2)

From Figure 5-9, the benefit of ISO is again observed – the improvement of y-parallax to a level of 1/3 of a pixel. Such improvement is consistent for different block combinations and therefore cross strip and/or multiple scale imagery are *not* required in ISO. When the quality controlled PASCOCO 310 data already has a relatively high level of ground accuracy,

the ISO process in 1:4000 (Block 1), 1:8000 (Block 2), or their combined scale block (Block 4, 5 and 6) can only achieve a centimetre level of horizontal improvement in this control-free environment. Without any specific local datum shift, the use of the single GCP makes no difference between the two solutions. An important result is from Block 3 (1:20000 block), after running ISO. The vertical accuracy is degraded by nearly 15 cm, and a similar result is found for both the control free and the single GCP solutions. It shows that the EO parameters provided by the GPS/IMU system are more accurate than the solution from ISO. Due to the correlation between attitude errors and flying height, small scale mapping project with unstable geometry makes it difficult to benefit from the ISO process, regardless of the number of tie points being used (insignificant improvement when PPVG = 9).

### **5.2.2. Large Format Digital Camera Flights**

#### ***DMC Alaska Flight***

Similar test procedures are performed as the film camera dataset (section 5.2.1). Table 5-10 presents the results of the quality controlled POS AV 510 data and the ISO results of the simulated POS AV 310 data, followed by graphical representation in Figure 5-10.

**Table 5-10: DMC Alaska Flight – POS AV 510 (after QC) vs. Simulated POS AV 310 (after ISO), Control Free**

# of Strip	Control Free							
	POS AV 510 (after QC)				Simulated POS AV 310 (after ISO)			
	Check Point RMS			Py RMS	Check Point RMS			Py RMS
	X (m)	Y (m)	Z (m)	( $\mu\text{m}$ )	X (m)	Y (m)	Z (m)	( $\mu\text{m}$ )
1	0.22	0.14	0.30	14.3	0.17	0.13	0.20	1.7
2	0.19	0.24	0.26	10.8	0.13	0.25	0.24	1.9
3	0.17	0.22	0.24	11.3	0.13	0.21	0.20	1.8

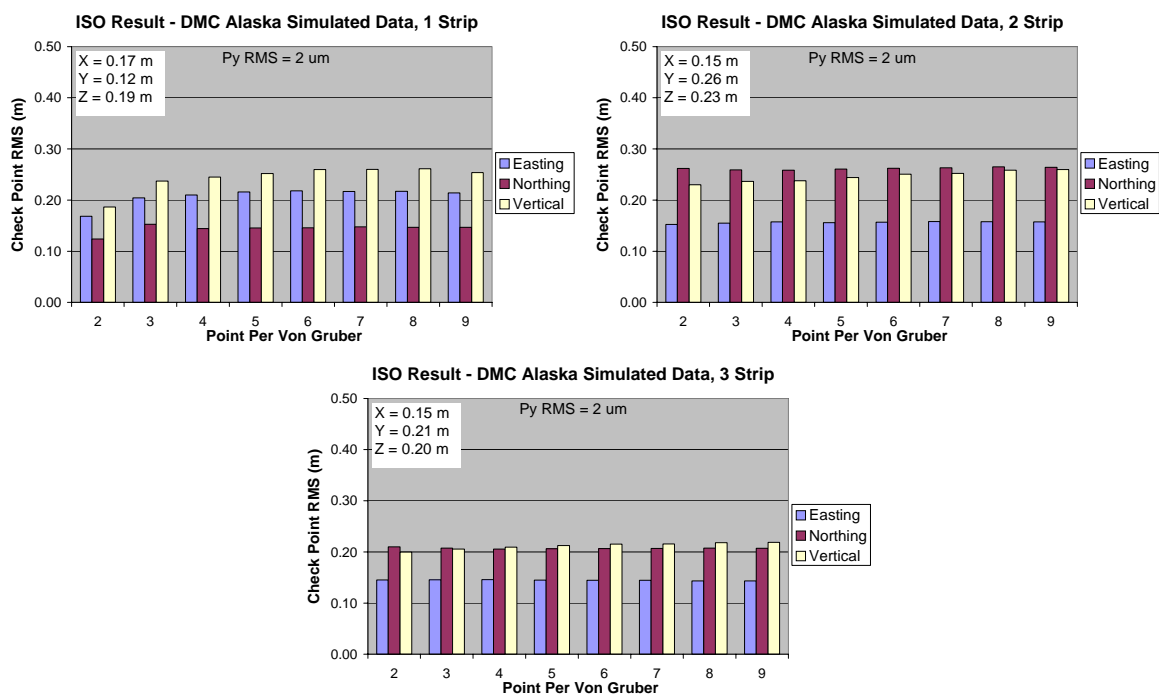


**Figure 5-10: ISO Results of the DMC Alaska Simulated POS AV 310 Data (Control Free)**

(see Appendix A-3)

Table 5-10 clearly indicates that the quality controlled POS AV 510 data achieves very good ground accuracy, with y-parallax about 1 pixel. With a relative accuracy of 7 cm, direct usage of such EO parameters is sufficient for nearly any mapping application. On the other hand, after running ISO on the simulated POS AV 310 data, the accuracy improvement is impressive. When the film camera requires at least 2 strips of data in order to receive benefit from the ISO process (section 5.2.1), the DMC Alaska data does not have any limitations, and the single strip data also shows absolute accuracy improvement, especially in vertical component for ~ 10 cm. A possible explanation might be the high resolution imagery acquired in the project. With 7 cm ground sample distance, the image measurement is extremely accurate. Combining this with the low flying height, the little effect from attitude error created a very stable geometry, even in a strip/corridor case. Further analysis of a center GCP is used and the results are shown in Table 5-11.

**Table 5-11: DMC Alaska Flight – POS AV 510 (after QC) vs. Simulated POS AV 310 (after ISO), 1 Center GCP**

# of Strip	1 Center GCP Used							
	POS AV 510 (after QC)				Simulated POS AV 310 (after ISO)			
	Check Point RMS			Py RMS	Check Point RMS			Py RMS
	X (m)	Y (m)	Z (m)	( $\mu$ m)	X (m)	Y (m)	Z (m)	( $\mu$ m)
1	0.19	0.21	0.27	14.3	0.10	0.13	0.12	1.8
2	0.16	0.17	0.22	10.8	0.14	0.26	0.19	1.8
3	0.14	0.14	0.21	11.3	0.13	0.21	0.18	1.7

Observing the results in Table 5-11, using a GCP in the QC procedure achieves insignificant position accuracy improvement because the magnitude of local datum shift is minimal. But, when the GCP is used in ISO for the simulated POS AV 310 data, it greatly improves the single strip data, especially in the vertical component. Both results shows a very high level of accuracy and the sub-pixel accuracy delivered can be used for nearly any mapping applications. Further investigating the performance of ISO, , the POS AV 510 data is processed and the results are shown in Figure 5-11 and Table 5-12.

**Table 5-12: ISO Results of the DMC Alaska POS AV 510 data, Control Free vs. 1 Center GCP**

# of Strip	Control Free				1 Center GCP Used			
	Check Point RMS			Py RMS ( $\mu\text{m}$ )	Check Point RMS			Py RMS ( $\mu\text{m}$ )
	X (m)	Y (m)	Z (m)		X (m)	Y (m)	Z (m)	
1	0.21	0.09	0.19	1.6	0.13	0.05	0.21	1.8
2	0.18	0.27	0.18	1.7	0.17	0.28	0.16	1.7
3	0.16	0.22	0.18	1.8	0.15	0.22	0.17	1.8

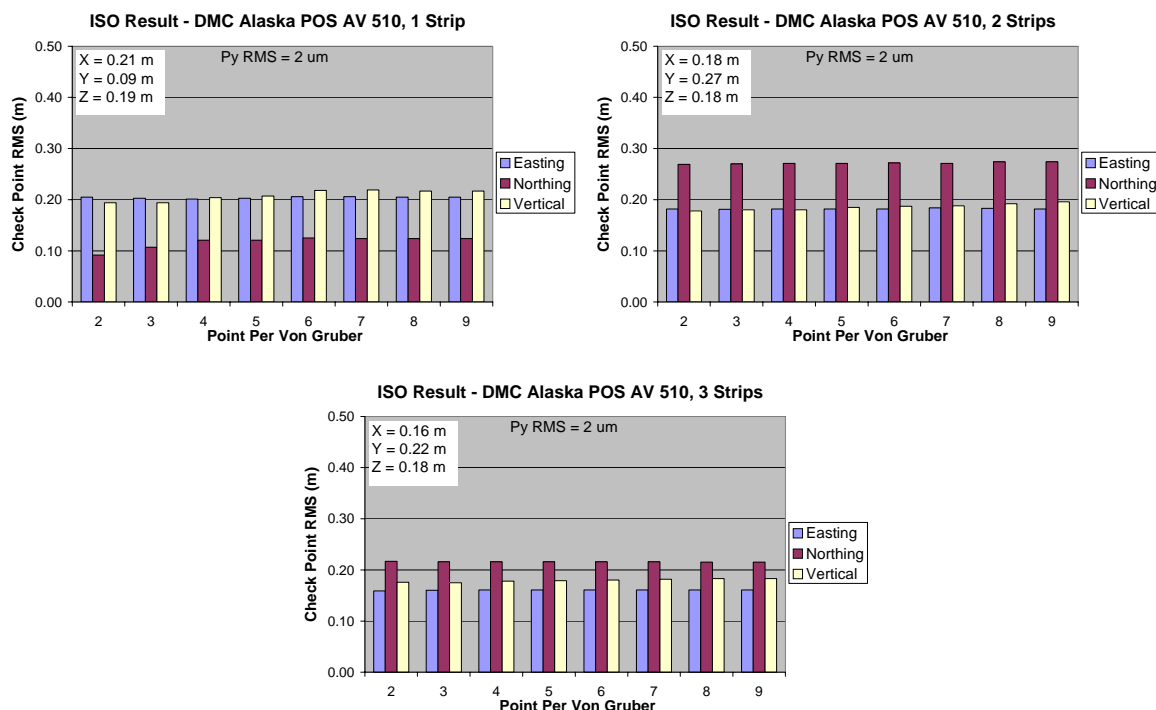


**Figure 5-11: ISO Results of the DMC Alaska POS AV 510 Data (Control Free)**

(see Appendix A-3)

This high accuracy GPS/IMU data behaves similarly as was the case with other film camera data. After quality control, the ground accuracy is already at a very high level (quantify). Therefore, performing ISO can only provide ~10-20% improvement in both environments; because the result will not go beyond the accuracy of the check point to be used. But, ISO improves parallax to 1/6 of a pixel, making it useful for projects requiring sub-centimetre accuracy. Analyzing Figure 5-11 thoroughly, it clearly indicates that the correlation between the number of tie points (PPVG value) and the ground accuracy is smaller when compared to the case of film camera. This probably relates to the high accuracy image measurement with little noise level. Such benefit enhances the efficiency of

ISO and therefore only a minimum number of tie points are required. Notice that with the single GCP solution, the result from simulated data performs better than the POS AV 510 data. This might relate to the standard deviation used in the simulated data. When attitude accuracy is poorer, the corresponding standard deviation on EO parameter is more relaxed to fit with the ground control, especially in one strip of data consisting of 8 images only. In comparison, the POS AV 510 EO parameter has tighter standard deviation which limits the change of EO parameters.

### ***DMC F-Block Flight***

Another high accuracy GPS/IMU dataset using the DMC is the F-Block data. Quality controlled EO analysis results are listed in Table 5-13.

**Table 5-13: EO Analysis Results of the DMC F-Block Flight (after QC), Control Free**

# of Strip	Control Free			
	Check Point RMS			Py RMS ( $\mu\text{m}$ )
	X (m)	Y (m)	Z (m)	
1	0.13	0.09	0.47	8.9
2	0.13	0.17	0.44	8.5
3	0.20	0.21	0.52	7.5
4	0.20	0.21	0.58	7.2

In Table 5-13, the quality control procedure using one GCP is not performed because there is insignificant GCP available in the QC block. The accuracy level of the GCPs is very poor

(~50 cm in vertical) and no additional check point is available in the QC block to verify if the local datum shift has been correctly determined. Therefore, limitation arises when trying to determine local datum shift if GCP is poor in both accuracy and distribution. But, with a smaller scale than the DMC Alaska flight, the quality control results in a better y-parallax. It is expected when observing the relationship between y-parallax and project scale/GSD in Figure 5-2, in which the level of y-parallax starts to become stable when the scale is <1:12000 or 0.15m GSD. Therefore under a control-free environment, the y-parallax is a better representation of the system performance, instead of observing the check point residual only. After running ISO on the data, the corresponding results are shown in Table 5-14 and Figure 5-12.

**Table 5-14: ISO Results of the DMC F-Block Flight, Control Free vs. 1 Center GCP**

# of Strip	Control Free				1 Center GCP Used			
	Check Point RMS			Py RMS ( $\mu\text{m}$ )	Check Point RMS			Py RMS ( $\mu\text{m}$ )
	X (m)	Y (m)	Z (m)		X (m)	Y (m)	Z (m)	
1	0.15	0.07	0.46	2.7	0.11	0.08	0.46	2.7
2	0.06	0.23	0.46	2.6	0.04	0.24	0.46	2.6
3	0.19	0.30	0.56	2.7	0.19	0.31	0.58	2.7
4	0.19	0.18	0.59	2.7	0.19	0.18	0.61	2.6

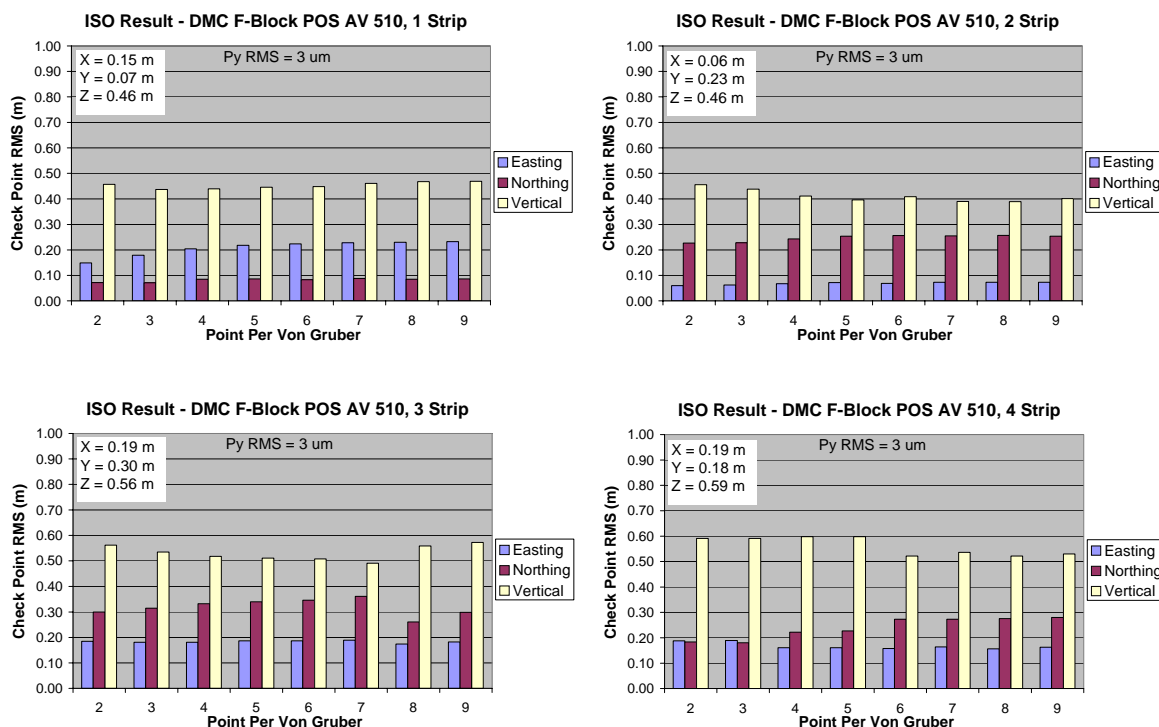


**Figure 5-12: ISO Results of the DMC F-Block Flight (Control Free)**

(see Appendix A-4)

Up to this point, all datasets collected by POS AV 510 system have similar ISO performance in terms of y-parallax under a control-free environment. Such relative accuracy improves at least 50% but ground accuracy does not improve significantly. Thus, it can be concluded that ISO is not necessary on high accuracy GPS/IMU data except when centimetre level accuracy is required (which requires  $<1$  pixel accuracy). Specifically for this dataset, the same correlation between PPVG value and ground accuracy is observed but the pattern is somehow random. This probably relates to the image measurement noise from the collected tie points. For this DMC mission, the block has large ground coverage but at least 60% is under vegetation or mountain areas. Tie point measurement over such an

area is less accurate even though digital camera imagery has a higher radiometric resolution than the film camera imagery. Thus, the unstable geometry influences the ISO solution. From this result, the availability of terrain features should always be considered for the use of ISO. The ISO solution might degrade ground accuracy or diverge it if large amounts of tie point measurement noises exists. Such patterns are more easily observed when only a few strips of data are used. As the number of strips increases, the geometry strengthens and the image measurement noise influence starts to be minimized through the bundle adjustment process.

### **5.2.3. Medium Format Digital Camera Flights**

#### ***DSS Ajax Flight***

This dataset is the second type of digital camera discussed in this research. A direct comparison between the DSS and DMC will not be made, as they are designed for different applications. But, the ISO test is carried out to understand the potential of using less accurate GPS/IMU data on such an imaging sensor. First, the comparison between the quality controlled POS AV410 data and ISO results from the simulated POS AV 310 is presented. Having a large block with 11 strips, all strip combinations cannot be presented with such huge amounts of data. instead, results from strip combinations of 1, 2, 3, and 4 strips are presented, followed by the results of the full image block. Table 5-15 presents the

results of control free solutions, followed by the graphical results of the simulated POS AV 310 ISO shown in Figure 5-13.

**Table 5-15: DSS Ajax Flight – POS AV 510 (after QC) vs. Simulated POS AV 310 (after ISO), Control Free**

# of Strip	Control Free							
	POS AV 510 (after QC)				Simulated POS AV 310 (after ISO)			
	Check Point RMS			Py RMS	Check Point RMS			Py RMS
	X (m)	Y (m)	Z (m)	( $\mu\text{m}$ )	X (m)	Y (m)	Z (m)	( $\mu\text{m}$ )
1	0.26	0.23	0.14	4.4	0.37	0.21	0.27	3.3
2	0.20	0.21	0.23	9.4	0.36	0.20	0.39	4.6
3	0.23	0.23	0.30	7.7	0.21	0.34	0.43	4.8
4	0.19	0.23	0.35	6.8	0.21	0.34	0.43	4.8
Full	0.26	0.22	0.46	7.1	0.21	0.26	0.54	4.8

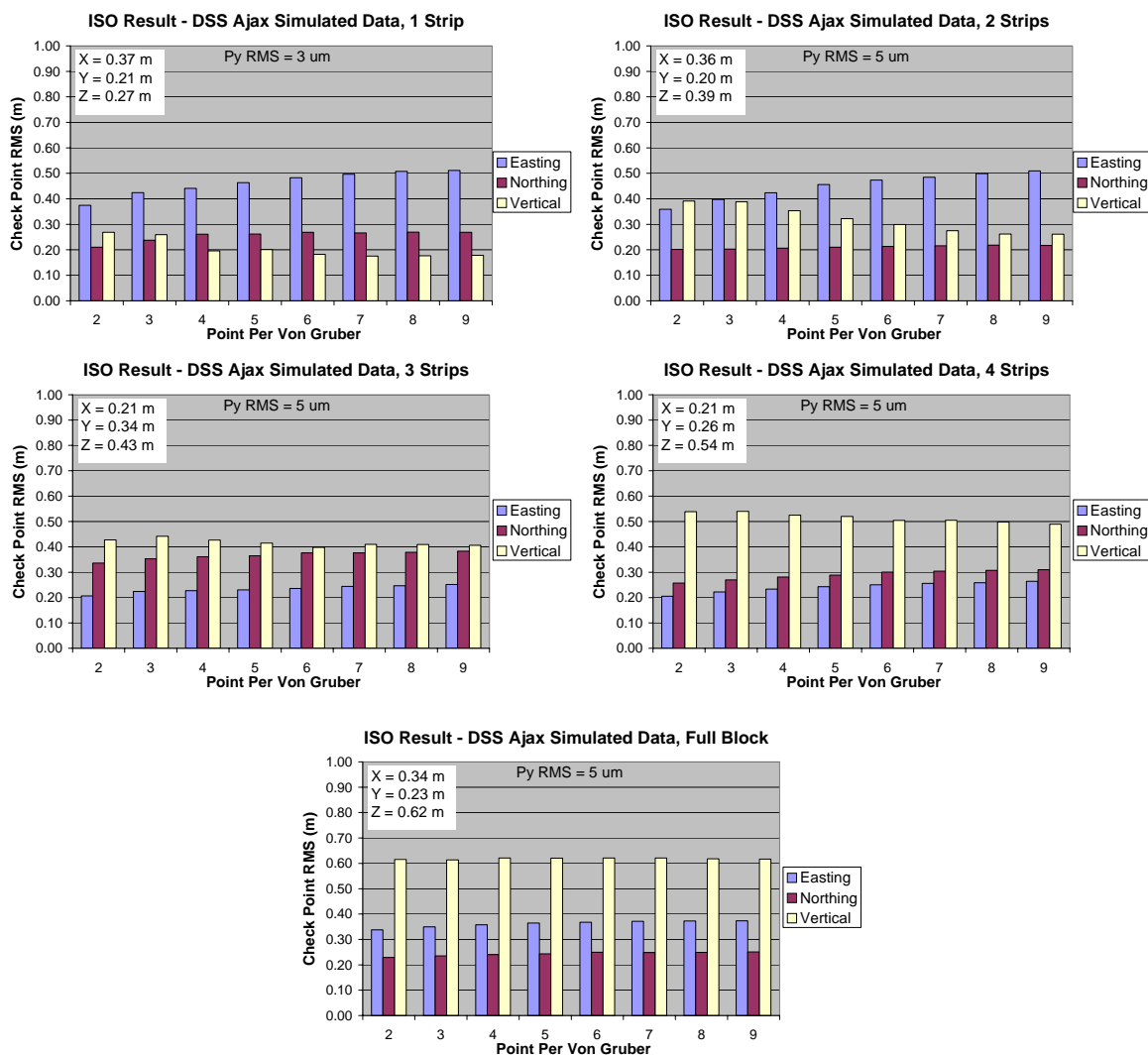


**Figure 5-13: ISO Results of the DSS Ajax Simulated POS AV 310 Data**  
(see Appendix A-5)

From the above results, it is clear that the high accuracy GPS/IMU data continues to provide a very good relative and ground accuracy, even though they are acquired with a POS AV 410 system. When running EO analysis in the full image block, the check point

RMS is very close to the expected accuracy, which is collected by DGPS technique and being measured on the DSS image with 20cm GSD. On the other hand, after running ISO on the simulated POS AV 310 data, the unstable solution for 1 strip of data is expected because of the lacking of side overlap (Figure 5-13). But, unlike other simulated data, ISO result continues to be unstable when an addition strip (2 strips) is included. This might be explained by the percentage of side overlap for this mapping project. While other data has at least 25% of overlap, the DSS Ajax is designed to have 20% to maximize the ground coverage. Also, without an azimuth mount on the system, the aircraft heading generates some side overlapping area with a reduced percentage of ~15% only. Such condition makes a great influence towards the geometry of these 2 strips. Therefore, when >3 strips of data are used, the solution becomes stable. This concludes an important point that side overlap is also needed to be considered in the use of ISO. But, the major improvement through ISO over the simulated POS AV 310 data can be observed through the y-parallax, which achieves ½ of a pixel. Further analysis of the data and results when 1 center GCP is used is shown in Table 5-16.

**Table 5-16: DSS Ajax Flight – POS AV 510 (after QC) vs. Simulated POS AV 310 (after ISO), 1 Center GCP**

# of Strip	1 Center GCP Used							
	POS AV 510 (after QC)				Simulated POS AV 310 (after ISO)			
	Check Point RMS			Py RMS ( $\mu\text{m}$ )	Check Point RMS			Py RMS ( $\mu\text{m}$ )
X (m)	Y (m)	Z (m)	X (m)		Y (m)	Z (m)		
1	0.25	0.23	0.14	4.4	0.18	0.06	0.08	3.4
2	0.20	0.20	0.22	9.4	0.31	0.22	0.37	4.6
3	0.22	0.22	0.30	7.7	0.20	0.35	0.43	4.8
4	0.20	0.23	0.34	6.8	0.19	0.28	0.53	4.8
Full	0.26	0.22	0.46	7.1	0.32	0.23	0.58	4.9

Similar to the DMC F-Block, the use of one GCP does not improve the position accuracy because it is limited by the GCP accuracy. Similar performance can be achieved after running ISO on the simulated POS AV 310 data, this evaluates that the use of a less accurate GPS/IMU system in conjunction with ISO is a cost efficient alternative other than the high end systems . Continuing the test, the results of the ISO test over the POS AV 410 data is shown in Figure 5-14 and Table 5-17.

**Table 5-17: ISO Results of the DSS Ajax POS AV 410 data, Control Free vs. 1 Center GCP Solution**

# of Strip	Control Free				1 Center GCP Used			
	Check Point RMS			Py RMS ( $\mu\text{m}$ )	Check Point RMS			Py RMS ( $\mu\text{m}$ )
	X (m)	Y (m)	Z (m)		X (m)	Y (m)	Z (m)	
1	0.23	0.23	0.14	3.7	0.18	0.15	0.03	3.7
2	0.20	0.14	0.42	5.1	0.18	0.15	0.40	5.1
3	0.13	0.20	0.41	5.1	0.14	0.21	0.41	5.2
4	0.12	0.14	0.54	5.1	0.12	0.14	0.53	5.1
Full	0.24	0.15	0.54	5.1	0.24	0.15	0.54	5.1

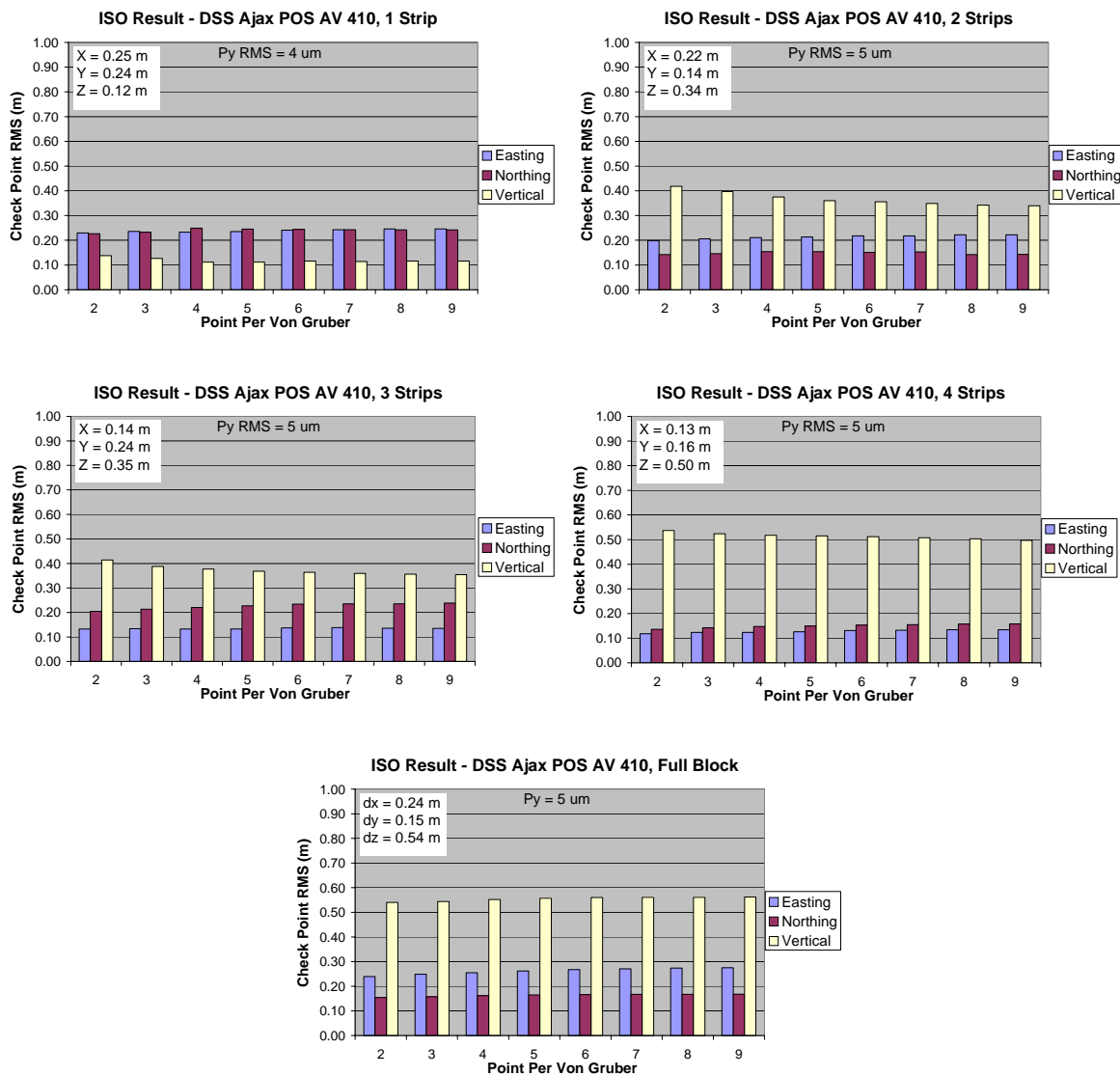


**Figure 5-14: ISO Results of the DSS Ajax POS AV 410 Data (Control Free)**  
 (see Appendix A-5)

Although the ISO solution is very stable in all cases, a slight degrade in position accuracy happens. With the high performance data delivered by quality control, the geometry given by Direct Georeferencing is accurate enough. From the 1:20000 photo scale result of PASCO 310, a small scale image block does not receive any benefit from running ISO in addition to QC; and a similar case is observed here. Also, when one center GCP is used to perform ISO on a single strip of data, position accuracy is improved significantly. This is similar to the case when running ISO on the DMC F-block with single GCP. The geometry of the single strip data allows a better fit with the ground when GCP is used, resulting in an overestimated accuracy when comparing with only one check point available in the strip. If more check points can be used, the RMS check point residual is more realistic.

### **5.3. Performance of Less Accurate GPS/IMU Data, Simulation vs. Real Data**

From the PASCO 310 data, a significant improvement has been achieved after QC. But, the same improvement cannot be achieved in the simulated data. Understanding this requires the observation of the IMU data from both the simulated and real data. Recall that IMU error consists of deterministic and stochastic parts, and the deterministic type of error can be minimized by the Kalman Filter through proper error modelling. Since the stochastic error can only be minimized, it becomes the major interest of the less accurate GPS/IMU data simulation. Therefore, the simulation is focused on the addition of stochastic errors

onto the IMU raw data, to achieve poorer attitude accuracy as compared to a high accuracy IMU system. This is evaluated through the ensemble result with Monte Carlo Analysis. But, the PASCO 310 data is only a single mission on a less accurate GPS/IMU system. Statistically, such a result can not represent the actual performance of the system unless multiple missions are collected and analysis is done thoroughly. It is highly possible that the data is accidentally at the lower boundary of the uncertainty/randomness in the stochastic error of the IMU. During DGPS/IMU data post-processing a relaxed solution is determined because a POS AV 310 error model is used. But, when the data is quality controlled, the remaining deterministic errors are minimized, leaving the stochastic part which has a close performance to a high accuracy IMU. Proving this will require the observation of the RMS boresight residual of all the less accurate GPS/IMU data, as listed in Table 5-18.

**Table 5-18: Boresight RMS Residual of Less Accurate GPS/IMU Data**

	Boresight RMS Residual		
	Tx (deg)	Ty (deg)	Tz (deg)
PASCO 310	0.003	0.002	0.003
PhotoScience UofK POS AV 310 Simulation	0.007	0.007	0.028
DMC Alaska POS AV 310 Simulation	0.005	0.004	0.016
DSS Ajax POS AV 310 Simulation	0.009	0.006	0.021

The boresight residual has some correlation with the attitude accuracy of the system (section 4.3.1). From Table 5-18, it can be seen that the boresight RMS residual of the

PASCO 310 data is very close to the case of a POS AV 510 system, such as the PhotoScience UofK and the two DMC flights. On the other hand, the simulated data has a higher boresight residual, especially in the Tz component. This indicates that the simulated data has poorer attitude accuracy in the data. This is mainly due to the stochastic error introduced to the raw IMU data. While only the PASCO 310 data has been collected by the real POS AV 310 system, the single flight cannot truly present a less accurate GPS/IMU data because of the randomness in the stochastic error. Instead, the simulation results shows the worst case scenario and provides an important measure on what will happen when a less accurate IMU is used in practice. But, the PASCO 310 results should not be ignored because it is a real dataset, this leaves an important factor that the uncertainty in a less accurate GPS/IMU system should be studied thoroughly. To understand if there is any correlation with the efficiency of ISO, thorough analysis should be carried out repeatedly on a single system, using the same project area, to observe the possibility of performance change from mission to mission.

#### **5.4. Calibration Error and ISO**

This section is dedicated to investigate the efficiency of ISO under calibration errors. By inserting some calibration errors into the EO parameters, ISO is performed to analyze whether the process can minimize the errors in a control-free environment or not. The errors that are tested include: the IMU/imaging sensor lever arm, the boresight errors and

the synchronization errors. These error sources are chosen because they are the major parameters in the transformation of post-processed GPS/IMU data to EO parameters. If these errors exist and quality control cannot be performed to detect and remove them, because post-processed GPS/IMU data is not available, the user can only rely on ISO to compensate for these errors by refining the EO parameter directly. Therefore, the following test can be used to understand the limitations of ISO.

Unlike other datasets which only have 1 flying height, the selected dataset is the PASCO 310 which has 3 project scales to provide more detailed comparisons. In addition, a film camera has poorer geometric and radiometric resolutions and therefore the results can be considered as a worst case scenario. Based on the block combinations from Table 5-19, calibration errors are applied to the EO parameters on the three photo scales (Block 1-3). Multiple scale combinations (Block 4-6) are not considered in this test because it usually happen in airborne calibration only but not in actual mapping project. And, if multiple scale or cross strip is available in the project, QC should able to identify the problem beforehand (section 2.3.4).

**Table 5-19: Combinations of Calibration Error applied to the PASCO 310 EO Parameters**

Error Type	Description
1	0.1m Lever Arm on X-axis
2	0.1m Lever Arm on Y-axis
3	0.1m Lever Arm on Z-axis
4	0.1m Lever Arm on all axes
5	10amin Boresight Error on Tx
6	10amin Boresight Error on Ty
7	10amin Boresight Error on Tz
8	10amin Boresight Error all axes
9	1ms Synchronization Error

Table 5-20, Table 5-21 and Table 5-22 present the EO analysis results after calibration errors are applied in Block 1, Block 2 and Block 3, respectively. The quality controlled EO analysis result is placed on the top of the table, named as *QC'd* for accuracy comparison.

**Table 5-20: PASCO 310 Block 1 EO Analysis result after Calibration Error applied**

Error Type	Check Point RMS (Block 1)			Py RMS ( $\mu\text{m}$ )
	X (m)	Y (m)	Z (m)	
QC'd	0.17	0.07	0.16	14.9
1	0.17	0.10	0.16	15.0
2	0.08	0.07	0.16	14.9
3	0.17	0.07	0.09	14.8
4	0.08	0.10	0.09	14.9
5	1.83	0.08	0.65	18.4
6	0.24	1.74	0.85	96.5
7	0.46	0.61	0.17	270.1
8	1.91	1.89	1.04	276.8
9	0.17	0.07	0.16	22.7

**Table 5-21: PASCO 310 Block 2 EO Analysis result after Calibration Error applied**

Error Type	Check Point RMS (Block 2)			Py RMS ( $\mu\text{m}$ )
	X (m)	Y (m)	Z (m)	
QC'd	0.13	0.08	0.18	12.3
1	0.13	0.10	0.18	12.4
2	0.16	0.08	0.18	12.3
3	0.13	0.08	0.14	12.3
4	0.16	0.10	0.14	12.3
5	3.37	0.13	1.31	16.1
6	0.36	3.47	1.70	97.3
7	0.87	1.26	0.20	265.1
8	3.44	3.46	2.15	303.6
9	0.13	0.08	0.18	12.6

**Table 5-22: PASCO 310 Block 3 EO Analysis result after Calibration Error applied**

Error Type	Check Point RMS (Block 3)			Py RMS ( $\mu\text{m}$ )
	X (m)	Y (m)	Z (m)	
QC'd	0.42	0.24	0.29	15.6
1	0.42	0.28	0.49	21.7
2	0.47	0.26	0.55	20.0
3	0.42	0.25	0.43	18.5
4	0.47	0.29	0.52	23.2
5	8.60	0.39	2.69	16.8
6	0.92	8.92	3.93	69.2
7	1.98	2.84	0.40	275.2
8	9.14	9.01	4.93	286.7
9	0.41	0.27	0.50	20.6

From the above tables, it is clear that the lever arm and synchronization error has the least influence on the ground accuracy. First, for the lever arm error, the magnitude of error projected on each axis depends on the flight dynamics. Since aircraft motion is fairly stable during image acquisition, the corresponding position error can be observed directly, with a

slight degradation in y-parallax ( $\pm 0.1 \mu\text{m}$  on 1:4000 and 1:8000,  $\pm 6.0 \mu\text{m}$  on 1:20000). Secondly, while synchronization error behaves similarly to the x-lever arm error (section 2.3.4), at an aircraft speed of 60-65 m/s, the 1 ms synchronization error introduces about 6 cm navigation errors along the flight direction. The corresponding position error has similar magnitude as the one generated by lever arm error. However, boresight error has a significant influence on ground accuracy and y-parallax. While attitude is amplified by flying height, at 1:20000, check point residuals are increased by 20 times, with a parallax level of at least 10 pixels. Through the above results, boresight mis-alignment is the most important system calibration parameter to be considered, as the correlation with position accuracy is significant.

The results of running ISO with calibration errors in the EO parameters are shown in Table 5-23, Table 5-24 and Table 5-25 for Block 1, 2 and 3, respectively. In the first column of the test result, an error type of *ISO* represents the statistics shown in Figure 5-9, which is the ISO result when no error is introduced. In addition, the results of two PPVG values, 2 and 9 are presented to analyze the performance when a different number of tie points are used.

**Table 5-23: ISO result of PASCO 310 Block 1 (Calibration Error Inserted)**

Error Type	Block 1							
	PPVG = 2				PPVG = 9			
	X (m)	Y (m)	Z (m)	Py RMS ( $\mu\text{m}$ )	X (m)	Y (m)	Z (m)	Py RMS ( $\mu\text{m}$ )
ISO	0.09	0.10	0.18	5.7	0.10	0.12	0.19	5.1
1	0.09	0.10	0.18	7.6	0.11	0.11	0.19	7.1
2	0.08	0.10	0.18	7.0	0.10	0.12	0.19	6.7
3	0.08	0.10	0.10	7.1	0.10	0.12	0.11	6.8
4	0.08	0.10	0.10	7.3	0.11	0.11	0.10	7.0
5	0.12	0.10	0.17	18.3	0.12	0.11	0.18	12.0
6	0.08	0.10	0.19	17.4	0.10	0.12	0.20	11.3
7	0.08	0.10	0.18	9.0	0.11	0.12	0.19	7.5
8	0.12	0.10	0.17	24.9	0.12	0.11	0.18	15.3
9	0.08	0.10	0.19	7.2	0.11	0.11	0.19	6.8

**Table 5-24: ISO result of PASCO 310 Block 2 (Calibration Error Inserted)**

Error Type	Block 2							
	PPVG = 2				PPVG = 9			
	X (m)	Y (m)	Z (m)	Py RMS ( $\mu\text{m}$ )	X (m)	Y (m)	Z (m)	Py RMS ( $\mu\text{m}$ )
ISO	0.12	0.12	0.20	5.5	0.12	0.12	0.22	5.2
1	0.14	0.13	0.21	5.1	0.13	0.13	0.22	5.1
2	0.13	0.12	0.21	4.7	0.12	0.12	0.22	4.8
3	0.12	0.12	0.12	4.7	0.12	0.12	0.14	4.8
4	0.14	0.13	0.13	5.1	0.13	0.13	0.14	5.1
5	0.13	0.13	0.23	15.0	0.11	0.13	0.22	10.4
6	0.13	0.11	0.20	15.2	0.12	0.11	0.22	10.5
7	0.13	0.12	0.20	6.7	0.12	0.12	0.22	5.7
8	0.13	0.11	0.22	21.4	0.11	0.12	0.22	14.3
9	0.13	0.12	0.21	4.9	0.13	0.13	0.22	5.0

**Table 5-25: ISO result of PASCO 310 Block 3 (Calibration Error Inserted)**

Error Type	Block 3							
	PPVG = 2				PPVG = 9			
	X (m)	Y (m)	Z (m)	Py RMS ( $\mu\text{m}$ )	X (m)	Y (m)	Z (m)	Py RMS ( $\mu\text{m}$ )
ISO	0.35	0.23	0.45	6.6	0.33	0.22	0.44	6.2
1	0.35	0.22	0.44	5.8	0.33	0.20	0.41	5.8
2	0.35	0.23	0.46	5.8	0.33	0.22	0.44	5.8
3	0.35	0.23	0.36	5.8	0.33	0.22	0.35	5.8
4	0.36	0.22	0.35	5.8	0.34	0.23	0.47	5.8
5	0.39	0.26	0.57	17.3	0.34	0.23	0.47	10.7
6	0.35	0.32	0.69	17.0	0.33	0.26	0.56	10.5
7	0.34	0.23	0.45	8.0	0.33	0.22	0.44	6.5
8	0.37	0.34	0.78	24.2	0.34	0.27	0.60	14.1
9	0.35	0.22	0.45	5.8	0.33	0.21	0.42	5.8

From the above tables, it can be seen that lever arm error on x and y axis can be compensated by ISO using imagery taken from the opposite flight line, with only a minimum number of tie points. But, the offset on z-axis cannot be fixed and remained as a constant bias to the solution. When the error magnitude is within the accuracy of the ground control, at least several well distributed GCP might be needed to compensate for the position error. On the other hand, synchronization error can be compensated by ISO because it has similar behaviour as x lever arm error, which mostly only influences the horizontal component because of the fairly stable aircraft motion during image acquisition. Again, only a minimum number of tie points are required to resolve the synchronization error. For boresight error, the condition is different. In 1:4000 and 1:8000 image block, ISO can compensate the position error and bring down the y-parallax level significantly. But, to

reach the same level of y-parallax as in other cases, a significant number of tie points are required. The 1:20000 image block has difficulty resolving the position error introduced by boresight error from both  $T_x$  and  $T_y$ , especially in the vertical component. Since attitude error and position accuracy are highly correlated in small scale mapping, this limits the ISO to improve the vertical accuracy, even if large numbers of tie points are used. Similar cases have happened in the DSS Ajax for a scale of 1:20000 / 0.18 GSD. From the above results, the importance of correct system parameters is addressed, as some errors can not be compensated easily through the use of ISO.

## CHAPTER SIX: IMPACT OF DIRECT GEOREFERENCING ON MAPPING PRODUCT

This chapter investigates the influence of Direct Georeferencing over the mapping procedure. Figure 6-1 illustrates the difference of workflow between tradition aerial mapping using film camera and the latest digital sensor with Direct Georeferencing System.

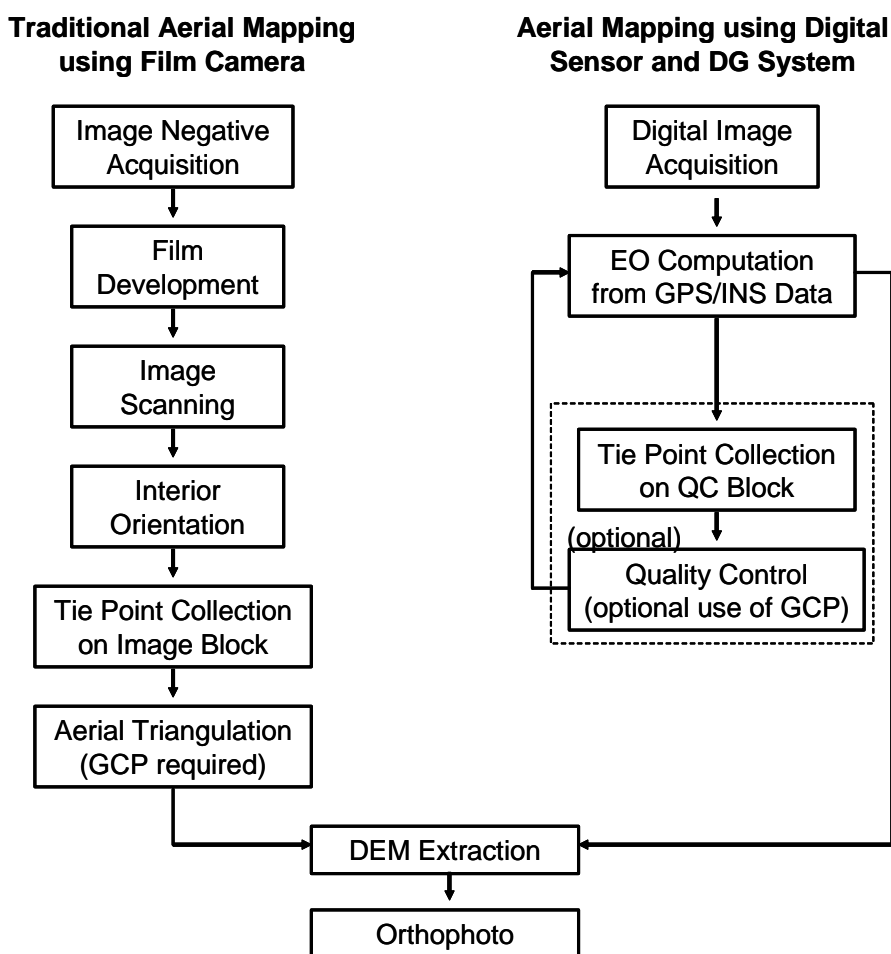


**Figure 6-1: Illustration of Aerial Mapping Workflow using Traditional Technique and Latest Technology**

Clearly, the benefit of digital sensor and DG system combination can be observed through the simplified procedure. The time consuming and costly steps of image scanning, GCP availability, and tie point collection / aerial triangulation are not required. Such improvements in mapping workflow allow users to perform *Fast DEM Generation and Orthophoto Production* and to have *Near Real-time Data for Rapid Response applications*.

### 6.1. Fast DEM Generation and Orthophoto Production

To be considered as *Fast DEM Generation and Orthophoto Production*, the expected time of delivery is in hours after data acquisition. To illustrate the fast product delivery, the DSS Ajax flight is used to perform the *fast* procedure as shown in right side of Figure 6-1 [Ip et al (2004a)]. Table 6-1 shows the approximate processing time of each task. The information about hardware and software used in the orthophoto production is listed in Table 6-2. The extracted DEM and the orthophoto product are shown in Figure 6-2.

**Table 6-1: Approximate Processing Time for Fast DEM Generation and Orthophoto Production**

Task	Approximate Processing Time
Image Processing	15 minutes
GPS/IMU Data Processing	30 minutes
Quality Control (including automatic tie point collection)	15 minutes
DEM extraction at 5m resolution	15 minutes
Orthophoto Production with Color Balancing at 0.2m GSD	60 minutes
Total Time	195 min / 3.3 hour

**Table 6-2: Hardware and Software Specification**

Software/Hardware	Processing Time
Processor	Intel Pentium 4 @ 2.8GHz
RAM	2 Gigabytes
Storage	250 Gigabytes
Video Adapter	PNY NVIDIA FX-1000 with Stereo
DGPS/IMU Post Processing	Applanix POSPac™ 4.2
Automatic Tie Point Collection	ZI/Imaging ISAT
Quality Control	Applanix POSCal™
DEM Extraction	Leica Photogrammetry Suite (LPS)
Orthophoto Production	Leica Photogrammetry Suite (LPS)



● Checkpoint Location

**Figure 6-2: Extracted DEM and Fast Orthophoto from the DSS Ajax Flight**

(Ip et al, 2004a)

Table 6-1 shows that within 3.5 hour, an orthophoto using 72 images covering a 2.7 km x 5.1 km area can be produced using self-extracted DEM. While the whole South Ontario mission (total of 2 hour) is processed, the DGPS/IMU data post-processing time takes little longer. If only the Ajax flight is concerned, expected processing time can be reduced to ~15 minutes. Notice that the orthophoto production takes 4 times the processing time than the DEM self-extraction. This is related to the color balancing algorithm used to create the final mosaic. Processing time can be reduced with simpler algorithm but it might influence the image quality, especially on the overlapping areas. Using the self-extracted DEM, no extra cost is needed to collect elevation points through LIDAR or to purchase from a mapping firm/agency. In addition, the self-extracted DEM provides consistency with the ground feature. In the project area, some parts are newly developed residential areas. When using a 1:50000 DEM (dated 2001) purchased from National Resource in May 2004, a mis-match happened and the resulting orthophoto created large position offset in the new residential area. Therefore, DEM self-extraction is the cost efficient choice to acquire the elevation model for the project area when existing DEM is not available or out of date. After the orthophoto production, the next step is to analyze the accuracy. To do so, the available check points in the area are measured on the orthophoto and the statistical report is shown in Table 6-3.

**Table 6-3. Orthophoto Check Point Residuals**

	dX		dY	
	(m)	GSD	(m)	GSD
Min	-0.09	-0.5	-0.28	-1.4
Max	0.67	3.4	0.59	3.0
Mean	0.02	0.1	0.06	0.3
RMS	0.29	1.5	0.30	1.5
# GCP	40			

From the results in Table 6-3, it can be seen that the orthophoto created through the *fast* algorithm still maintained relatively high horizontal accuracy. Having a pixel size of 0.2m, the RMS error of check point residuals is not more than 1.5 pixels (i.e.0.3m in the ground). Such accuracy meets orthophoto mapping standards such as the USGS standard as shown in Table 6-4.

**Table 6-4. USGS. Orthophoto Horizontal Accuracy Requirement**

Map Scale	Horizontal Accuracy Requirement
1 : 24,000	+/- 12 m
1: 12,000	+/- 10 m
1 : 1,200	+/- 1 m
1 : 600	+/- 0.5 m

## **6.2. Near Real-time Data for Rapid Response**

While fast orthophoto takes at least an hour or two to create, another application requires a much faster delivery time – Rapid Response Application. This is another type of application which requires Near Real-Time Data for emergency purposes such as forest fire fighting, flooding and earthquake mapping, etc. The main objective is to collect imagery data right after the emergency event happens and to be able to deliver orthophotos (individual or mosaic) as soon as possible after the aircraft lands. Traditional aerial mapping procedures are not suitable, even with a digital camera because there is no time available to spend in collecting tie points and performing aerial triangulation. In addition, for the case of emergency, most likely ground control points will not be available on site. So, the only solution is to use DG on a digital camera which is light weight with great mobility and therefore can be installed on a helicopter or small single engine aircraft for quick access to remote areas. Delivering orthophoto in near real-time, real time GPS/IMU measurement is used to determine the corresponding EO parameter for the acquired imagery. In addition, a special orthophoto engine is required to orthorectify the imagery “on the fly”. The challenge is the real-time navigation accuracy, especially in attitude determination, which correlates with the use of aerial platform. In addition to navigation accuracy, data processing is another factor. Although the algorithm behind orthophoto creation is very simply, the handling of large amounts of data is an issue because the image

acquisition cycle is faster than the development of the image file. Therefore, research in handling such a large amount of data is in development to avoid data latency.

Currently, some additional engines are in development to fit certain applications. For example, in the case of forest fire mapping, in addition to delivering orthophotos of the fire site to the ground command centre for mission planning, potential hot-spots also need to be detected. Using a hot-spot detection engine, the potential spot is first located on the image, then the georeferenced location is determined using the real-time EO parameters and reported to ground crews. Such a system using Infrared Camera with real-time GPS/IMU technology is in development at The University of Calgary [Wright and El-Sheimy (2001)].

## CHAPTER SEVEN: CONCLUSIONS AND RECOMMENDATIONS

### 7.1. Conclusions

In the first part of the research, two types of Image Georeferencing approaches were discussed: Direct Georeferencing (DG), and Indirect Georeferencing. Through the OEEPE test in 2001 and other independent researches, the concept of Integrated Sensor Orientation (ISO) has been introduced which combines the benefits from both Direct and In-Direct Georeferencing. Using only collected tie points, ISO allows the DG system error discussed in Chapter 2 to be minimized by refining the EO parameters and calibration parameters directly. But, the cost efficiency of ISO is in question because of the time consuming part – tie point collection over the whole image block. In projects having large number of imagery and ground coverage, such as large area mapping using film camera, the whole process can become inconvenient. Furthermore, ISO is fundamentally limited to stereo collects only, while an existing DEM, Direct Georeferencing can be used to generate orthomosaic products without the need to fly significant overlap. This can save both time and cost.

A simplified version of ISO is ideal for performing Quality Control for Direct Georeferencing. In this case only a small image block is used to *refine* the system calibration parameters, which are then applied when generating the EO from the IMU/GPS solution for the rest of the mission. This method also applies to strip/corridor projects or

monoscopic collects (i.e. mapping using an existing DEM without the need to fly stereo imagery) since the QC block can be acquired before or after the mission. The following summarizes the findings on the use of ISO for Quality Control.

- Quality Control can be used to improve both relative and absolute accuracy in a ground control-free environment when using a *high* accuracy GPS/IMU (similar performance as the POS AV 410 and 510 systems) that meets specifications for Direct Georeferencing. A Minimum QC block size should be **3x8** to provide strong enough geometry, especially on side overlap. When local datum shift needs to be determined, one or more GCPs must be used.
- Only a minimum number of tie points are required for Quality Control; when an advanced automatic tie point collection module is used, the average requirement is between 15 – 20 tie points per image.
- Quality Control on a *high* accuracy GPS/IMU data delivers ~1 pixel relative accuracy in all imaging sensors tested, including the film camera, the DMC and the DSS, which is accurate enough for most stereo and mapping application. On the other hand, absolute accuracy is close to the expected value when considering both GCP accuracy and ground sample distance of the image.

Assuming the QC concept is applied when using Direct Georeferencing, the question then becomes what additional benefits can ISO bring when stereo imagery is available? The following summarizes the findings in this research.

- Integrated Sensor Orientation is not necessary for quality controlled high accuracy GPS/IMU data except for large scale mapping projects requiring centimetre level of ground accuracy, which need a y-parallax level better than 1 pixel.
- Using quality controlled less accurate GPS/IMU data (similar performance as the POS AV 310 system), performing ISO under the ground control-free environment has the most benefit on film camera data, in which both relative and absolute accuracy can be improved. In the case of digital cameras, only relative accuracy improvements can be observed.
- The use of ground control points in Integrated Sensor Orientation gives the most benefit on strip/corridor data, which improves the weak geometry due to the lack of side overlap. For block imagery, it is not necessary unless local datum shift needs to be resolved.
- In Lever arms, boresight and synchronization errors can be compensated through Integrated Sensor Orientation directly. Difficulty is observed when correcting error in the vertical/height component, leaving some parallax but in acceptable levels. Some difficulty encounters when compensating boresight error in small scale image blocks due to correlation with attitude accuracy from GPS/IMU system

- If uncertainty exists in collecting tie points on areas with little ground features, the Integrated Sensor Orientation approach might result in a divergent solution.

## **7.2. Recommendations**

Based on the discussion and result of the research, the following recommendations are made for the use of Direct Georeferencing, Quality Control and Integrated Sensor Orientation.

### **7.2.1. Direct Georeferencing**

- Proper Mission planning is very important for the use of Direct Georeferencing. This includes the collection of basestation data, minimum flight dynamics (banking angle) and periodical manoeuvre. These enhance data integrity over the whole mission to avoid data gap or poor measurements due to heading drift.
- System parameters must be well calibrated, this includes:: system initialization, approximate GPS/IMU lever arm, proper IMU/Imaging Sensor lever arm, boresight value, camera parameters and sensor synchronization. Any error from above can degrade the system performance. Proper calibration reports should be available at all times, even though Quality Control and Integrated Sensor Orientation can be used to minimize the residual errors.

- The use of a high quality GPS/IMU system is highly recommended from an operational point of view, especially with the benefits for strip/corridor projects and the compatibility with all imaging sensor tested. Pixel accuracy delivered by quality control data is efficient for most mapping and stereo applications.

### **7.2.2. Quality Control and Integrated Sensor Orientation**

- Quality Control should be performed whenever it is possible, to confirm the stability of system parameters and data integrity.
- Under the strong correlation between boresight and camera parameter, camera self-calibration should be avoided when multiple scale imagery is not available, unless camera instability is confirmed.
- Ground features are very important to deliver high quality image measurements for Quality Control. Therefore, QC block selection should avoid areas with lots of vegetation; residential areas are preferred.
- Integration with photogrammetry software is greatly recommended, advanced tie point collection strategies are required to deliver only the best quality image measurements using the least amount of processing time with the help of the seed EO parameters from the DG system.

- For projects with existing DEM, ground coverage can only be maximized by reducing overlapping areas to sufficient levels. Data integrity can be confirmed through QC block being flown before or after the mission.
- While the Integrated Sensor Orientation approach is based on GPS/IMU assisted bundle adjustment, several parameters must be considered: standard deviation of EO parameters, quality of tie point measurements and percentage of image overlapping. These parameters are highly correlated with the performance of ISO
- Performing ISO on strip/corridor project is not recommended. Under a ground control-free environment, the stability (especially along flight direction) is poor. Large numbers of tie points are required in forward overlapping areas to strengthen the geometry and therefore the cost efficiency of ISO is greatly reduced.
- There is a strong potential for a less accurate GPS/IMU system in conjunction with the use of Integrated Sensor Orientation, providing a less expensive alternative for users always acquiring images in a block.

### **7.3. Recommendation on Future Research**

- It will be very useful to analyze flight data from the ADS40 system, as 3-line scanner technique is used in image acquisition.
- More tests on *real* data from commercial less accurate GPS/IMU data integrated with different sensor types are necessary. The uncertainty in attitude accuracy is

needed to be analyzed thoroughly to understand if the PASCO 310 results is an exceptional case or not.

- The price difference between Tactical grade and MEMS IMU has a strong potential to deliver a very low cost GPS/IMU system. However, the uncertainty in IMU performance also needs to be analyzed thoroughly.

## REFERENCES

- Abdel-Hamid, W., A. Noureldin A., N. El-Sheimy and G. Lachapelle (2002), Performance Analysis of MEMS-based Inertial Sensors for Positioning Applications, Proceedings of the International Workshop on System-on-Chip for Real Time Applications, Banff, Canada, July 6-7, 2002.
- Abdel-Hamid, W., A. Osman, A. Noureldin and N. El-Sheimy (2004), Improving the Performance of MEMS-based Inertial Sensors by Removing Short-Term Errors Utilizing Wavelet Multi-Resolution Analysis, Proceedings of the US institute of Navigation (ION), National Technical Meeting (NTM), ION NTM 2004, 26-28 Jan. 2004, San Diego, CA, pp 260-266.
- Abdullah, Q. (1997), Evaluation of GPS-inertial navigation system for airborne photogrammetry, Proceedings of the ASPRS/MAPPS Softcopy Conference, Arlington, Virginia, July 27-30, pp. 237, 1997.
- Ackermann, F. (1992). Kinematic GPSControl for Photogrammetry. Photogrammetric Record. 14(80):pp. 261-276.
- Bossler, J.D. and Ch. Toth (1996), Feature Positioning Accuracy in Mobile Mapping: Results Obtained by the GPSVan<sup>TM</sup>, International Archives of Photogrammetry and Remote Sensing, ISPRS Comm. IV, Vol. XXXI, part B4, pp. 139-142.
- Braun, J. (2003), Aspects on True-Orthophoto Production. Proceedings of the 49th Photogrammetric Week, Stuttgart, Germany, Sept 1-5, 2003.

- Britting, K.R. (1997), *Inertial Navigation Systems Analysis*, Willey-Intersciences, New York.
- Bruton, A.M, M.M.R. Mostafa and B. Scherzinger (2001), *Airborne DGPS Without Dedicated Base Stations for Mapping Applications*, Proceedings of ION-GPS 2001, Salt Lake City, Utah, USA, Sept. 11-14, 2001.
- Cannon, M.E., S. Skone, Y. Gao, Y. Moon, K. Chen, S. Crawford and G. Lachapelle (2002), *Performance Evaluation of Several Wide-Area GPS Services*, Proceedings of ION-GPS 2002, Portland, Oregon, USA, Sept. 24-27, 2002.
- Casella V., M. Franzini, G. Forlani, R. Galetto, A. Manzano, F. Radicioni, G. Sona and B. Villa (2004), *Initial Results of The Italian Projects on Direct Georeferencing in Aerial Photogrammetry*, International Archives of Photogrammetry and Remote Sensing, XX<sup>th</sup> ISPRS Congress, Comm. III, Vol. XXXV, Part B3, pp. 881-886, Istanbul, Turkey, July 12-23, 2004.
- Casella, V. (2004), *Methodologies for reducing residual parallaxes in directly oriented images*, Proceedings of XX<sup>th</sup> ISPRS Congress Comm. III, Istanbul, Turkey, July 12-23, 2004.
- Chian, K.W. and N. El-Sheimy (2004), *The Performance Analysis of Neural Network Based IMU/GPS Integration Method for Land Vehicle Navigation*, The 4<sup>th</sup> International Symposium on Mobile Mapping Technology (MMT 2004), Kunming, China, Mar. 29-31, 2004.

- Colomina, I. (1999), GPS, IMU and Aerial Triangulation: what is the best way for the operational determination of photogrammetric image orientation?, International Archives of Photogrammetry and Remote Sensing, ISPRS Conference “Automatic Extraction of GIS Objects from Digital Imagery”, Vol. 32, Munchen, pp. 121-130, 1999.
- Colomina, I. (1993), A note on the analytics of aerial triangulation with GPS aerial control, PE&RS 59(11): 1619-1624, 1993.
- Congalton, R.G., M. Balogh, C. Bell, K. Green, J.A. Milliken, and R. Ottman, (1998), Mapping and Monitoring Agricultural Crops and other LandCover in the Lower Colorado River Basin, PE&RS, 64 (11):1107-1113, 1998.
- Cramer, M., (2004), Performance of Medium Format Digital Aerial Sensor Systems, International Archives of Photogrammetry and Remote Sensing, ISPRS Comm. V, Vol. XXXV, Part B5, pp. 769-774, Istanbul, Turkey, July 12-23, 2004.
- Cramer, M. and D. Stallmann (2001a), OEEPE Test on “Integrated Sensor Orientation” – IFP Results and Experience, OEEPE Workshop, Integrated Sensor Orientation, Hannover, Germany, Sept 17-18, 2001.
- Cramer, M. and D. Stallmann (2001b), On the use of GPS/Inertial Exterior Orientation Parameters in Airborne Photogrammetry, OEEPE Workshop, Integrated Sensor Orientation, Hannover, Germany, Sept 17-18, 2001.

- Cramer, M. and D. Stallmann, and N. Halla (1997), High Precision Georeferencing Using GPS/IMU and Image Matching, Proceedings of the International Symposium on Kinematic Systems in Geodesy, Geomatics and Navigation, Banff, Canada, pp. 453-462, 1997.
- Dardanelli, G., D. Emmolo, V. Franco, M. Lo-Brutto, P. Orlando and B. Villa (2004), GPS/IMU Systems for Compilation of Digital Large-Scale Orthophotos, International Archives of Photogrammetry and Remote Sensing, ISPRS Comm. 2, Vol. XXXV, Part B2, pp. 575-580, Istanbul, Turkey, July 12-23, 2004.
- Doerstel, C. W., Zeitler and K. Jacobsen (2002), Geometric Calibration of the DMC: Method and Results, International Archives of Photogrammetry and Remote Sensing, ISPRS Comm. I, Vol. XXXIV, Part 1, pp. 324-333, Denver, USA, Nov 10-14, 2002.
- Efron, B. (1982). The Jackknife, the Bootstrap, and other Resampling Plans, Regional Conference Series in Applied Mathematics, SLAM, Philadelphia, PA
- Ellum, C.M. and N. El-Sheimy (2003), The Calibration of Image-Based Mobile Mapping Systems, 6<sup>th</sup> Conference on Optical 3D Measurement Techniques, Switzerland, Sept. 22-25, 2003.
- Ellum, C.M. and N. El-Sheimy (2002), Land-Based Integrated Systems for Mapping and GIS application, Survey Review Journal, January 2002 issue, vol. 36, no. 283, pp. 323-339.

- El-Sheimy, N. (2000), *Inertial Techniques and IMU/DGPS Integration*, Department of Geomatics Engineering, The University of Calgary
- El-Sheimy, N. and M. Lavigne (1998), "3-D GIS Data Acquisition Using GPS/IMU/Video Mobile Mapping System", *The International Symposium on Kinematic Systems In Geodesy, Geomatics and Navigation*, Eisenstadt, Vienna, Austria, April 20 to April 23, 1998, pp. 375-380.
- El-Sheimy, N. (1996a), *A Mobile Multi-Sensor System For GIS Applications In Urban Centers*, *International Archives of Photogrammetry and Remote Sensing*, Comm. II, Working Group 1, Vol. XXXI, Part B2, pp. 95-100, Vienna, Austria, July 9-19, 1996.
- El-Sheimy, N. (1996b), *The Development of VISAT-A Mobile Survey System for GIS Applications*, Ph.D Thesis, UCGE Report #20101, Department of Geomatics Engineering, The University of Calgary, Canada, 1996.
- Eun-Hwan, S. and N. El-Sheimy (2004), *An Unscented Kalman Filter for In-Motion Alignment of Low-Cost IMUs*, *Proceeding of the IEEE PLANS*, Monterey, CA, pp. 273-279, April 2004.
- Galetto, R., V. Casella, M. Franzini and A. Spalla (2004), *An Italian Research Project on Direct Photogrammetry*, *International Archives of Photogrammetry and Remote Sensing*, XXth ISPRS Congress, Comm. III, Vol. XXXV, Part B3, pp. 891-896, Istanbul, Turkey, July 12-23, 2004.

- Greening, T., W. Schickler and A. Thorpe (2000), The Proper Use of Directly Observed Orientation Data: Aerial Triangulation is not Obsolete, Proceeding of the ASPRS Annual Conference, Washington, DC, USA, May 22-26, 2000.
- Grejner-Brezezinska, D.A. (2001), Direct Sensor Orientation in Airborne and Land-based Mapping Application, Report No. 461, Geodetic GeoInformation Science, Department of Civil and Environmental Engineering and Geodetic Science, The Ohio State University, Ohio, United States, 2001.
- Grejner-Brezezinska, D.A. (2000), Direct Exterior Orientation of Airborne Imagery with GPS/IMU Systems: Performance Analysis, *Navigation*, 46(4): 261-270, 2000.
- Grejner-Brezezinska, D.A. (1998), Direct Platform Orientation with Tightly Integrated GPS/IMU in Airborne Applications, ION-GPS 98, Nashville, Tennessee, USA, Sept. 15-18, pp. 85-894, 1998.
- Habib, A. and T. Schenk (2001), Accuracy Analysis of Reconstructed Points in Object Space from Direct and Indirect Orientation Methods. In: Heipke, C., Jacobsen, K., Wegmann H. (Eds), *Integrated Sensor Orientation*, OEEPE Official Publication No 43.
- Habib F.A., A. M. Pullivelli and M. Morgan (2004), Quantitative Measures for The Evaluation of Camera Stability, *International Archives of Photogrammetry and Remote Sensing*, XXth ISPRS Congress, Comm. I, Vol. XXXV, Part B1, pp. 63-69, Istanbul, Turkey, July 12-23, 2004.

- Heipke, C., K. Jacobsen and H. Wegmann (2001a), Test Goals and Test Set Up for the OEEPE Test “Integrated Sensor Orientation” OEEPE Workshop, Integrated Sensor Orientation, Hannover, Germany, Sept 17-18, 2001.
- Heipke, C., K. Jacobsen and H. Wegmann (2001b), Analysis of the Results of the OEEPE test “Integrated Sensor Orientation”, OEEPE Workshop, Integrated Sensor Orientation, Hannover, Germany, Sept 17-18, 2001.
- Hinsken, L., S. Miller, U. Tempelmann, R. Uebbing, S. Walker (2002) Triangulation of LH Systems ADS40 Imagery Using Orima GPS/IMU, International Archives of the Photogrammetry, Remote Sensing and Spatial Information Science, Photogrammetric Computer Vision, ISPRS Comm. III Symposium 2002, Sept. 9-13, Graz, Austria, Part A, pp. 156-162.
- Honkavaara, E., E. Ahokas, J. Jaakkola., J. Hyypä, R. LIVES and J. Vihomaa (2002), Investigation of system calibration of GPS/IMU and camera for direct georeferencing, International Archives of the Photogrammetry, Remote Sensing and Spatial Information Science, Photogrammetric Computer Vision, ISPRS Comm. III Symposium 2002, Sept. 9-13, Graz, Austria, Part B, pp. 85-89.
- Ip, A.W.L., M.M.R. Mostafa and N. El-Sheimy (2004a), Fast Orthophoto Production using the Digital Sensor System, Map India 2004, New Delhi, India, Jan 28-30, 2004.

- Ip, A.W.L., N. El-Sheimy and M.M.R. Mostafa (2004b), System Performance Analysis of IMU/DGPS Integrated System for Mobile Mapping System (MMS), The 4<sup>th</sup> International Symposium on Mobile Mapping Technology (MMT 2004), Kunming, China, Mar 29-31, 2004.
- Ip, A.W.L., N. El-Sheimy and J. Hutton (2004c), Performance Analysis of Integrated Sensor Orientation, International Archives of Photogrammetry and Remote Sensing, XX<sup>th</sup> ISPRS Congress, Comm. V, Vol. XXXV, Part B5, pp. 797-802, Istanbul, Turkey, July 12-23, 2004.
- Jacobsen, K. and H. Wegmann, Dependencies and Problems of Direct Sensor Orientation, OEEPE Workshop, Integrated Sensor Orientation, Hannover, Germany, Sept 17-18, 2001.
- Kersten T., O'Sullivan, W., 1996. Digital aerial triangulation with the helava automated triangulation system. OEEPE Workshop on Application of Digital Photogrammetric Workstations, Lausanne, OEEPE Official Publication, 33, 139-148.
- King, D., P. Walsh and F. Ciuffreda (1994), Airborne Digital Frame Camera for Elevation Determination, PE&RS 60(11): 1321-1326, 1994.
- Koopman, S. J. (2002). Testing the Assumptions Behind the Use of Importance Sampling, Economics Papers, 2002-W17 / Economics Group, Nuffield College, University of Oxford.

- Lithopoulos, E. D.B., Reid, B. Scherzinger (1996), The Position and Orientation System (POS) for Survey Applications, International Archives of Photogrammetry and Remote Sensing, ISPRS Comm. III, Vol. XXXI, Part B3, pp. 467-471, Vienna, Austria, July 9-19, 1996.
- Madani, M., C. Dorstel, C. Heipke and K. Jacobsen (2004), DMC Practical Experience and Accuracy Assessment, ISPRS Comm. II, Vol. XXXV, Part B2, pp. 396-401, Istanbul, Turkey, July 12-23, 2004.
- Madani, M. (2003), Accuracy Comparison of Using IMU Data for DMC Projects, Z/I Imaging Corporation, Huntsville, AL, United States, Sept 26, 2003.
- Madani, M. and M.M.R, Mostafa, (2001), ISAT Direct Exterior Orientation QA/QC Strategy using POS Data, OEEPE Workshop, Integrated Sensor Orientation, Hannover, Germany, Sept 17-18, 2001.
- Mills, J.P., I. Newton, and R.W. Graham (1996), Aerial Photography for Survey Purposes with a High Resolution, Small Format, Digital Camera, Photogrammetric Record 15 (88): 575-587, October, 1996.
- Mostafa, M.M.R. (2003), Design and Performance of the DSS, Proceedings, 49th Photogrammetric Week, Stuttgart, Germany, September 1-5, 2003.
- Mostafa, M.M.R., (2002), Camera/IMU Boresight Calibration: New Advances and Performance Analysis, Proceedings of the ASPRS Annual Meeting, Washington, DC, USA, April 21-26, 2002.

- Mostafa, M.M.R. (2001), Digital Multi-Sensor Systems – Calibration and Performance Analysis, OEEPE Workshop, Integrated Sensor Orientation, Hannover, Germany, Sept 17-18, 2001.
- Mostafa, M.M.R. and J. Hutton (2001), Direct Positioning and Orientation Systems – How Do They Work? What is The Attainable Accuracy? Proceeding, ASPRS Annual Meeting, St. Louis, Mo, USA, April 22-27, 2001.
- Mostafa, M.M.R., J. Hutton and B. Reid (2001a), GPS/IMU Products – The Applanix Approach, Proceedings of the 48<sup>th</sup> Photogrammetric Week, Stuttgart, Germany, Sept. 24-28, 2001.
- Mostafa, M.M.R., J., Hutton and E., Lithopoulos (2001b), Airborne Direct Georeferencing of Frame Imagery: An Error Budget, The 3<sup>rd</sup> International Symposium on Mobile Mapping Technology, Cairo, Egypt, Jan 3-5, 2001.
- Mostafa, M.M.R. and K.P., Schwarz (2001), Digital Image Georeferencing from a Multiple Camera System by GPS/IMU, IPSRS Journal of Photogrammetry & Remote Sensing, Elsevier Science, B.V., PE&RS(56), No. 1, pp. 1-12, 2001.
- Mostafa, M.M.R., K.P. Schwarz, and P. Gong (1997), A Fully Digital System for Airborne Mapping, Proceedings of the International Symposium on Kinematic Systems in Geodesy, Geomatics and Navigation, Banff, Canada, pp. 463-471.
- Olynik, M., M.G. Petobello, M.E. Cannon and G. Lachapelle (2002), Temporal Impact of Selected GPS Errors on Relative Point Positioning, GPS Solutions, 6, 1-2, pp. 47-57.

- Reda Taha, M. M., A. Noureldin and N. El-Sheimy (2003), Improving IMU/GPS Positioning Accuracy During GPS Outages Using Fuzzy Logic, Proceedings of the 16<sup>th</sup> annual conference of the institute of Navigation, ION-GPS/GNSS 2003, Portland, Oregon, USA, Sept 2003
- Reid, D.B., E. Lithopoulos and J. Hutton (1998), Position and Orientation System for Direct Georeferencing (POS/DG), ION 54th Annual Meeting, Denver, Colorado, June 1-3, pp. 445-449.
- Ressl, C. (2001), The OEEPE-Test 'Integrated Sensor Orientation' and its handling with the Hybrid Block-Adjustment Program Orient, OEEPE Workshop, Integrated Sensor Orientation, Hannover, Germany, Sept 17-18, 2001.
- Scherzinger, B. (1997), A Position and Orientation Post-Processing Software Package for Inertial/GPS Integration (POSProc), Proceedings of the International Symposium on Kinematic Systems in Geodesy, Geomatics and Navigation (KIS 97), Banff, Canada, June 1997.
- Schwarz, K.P. and N. El-Sheimy (2004), Mobile Mapping Systems – State of the Art and Future Trends, ISPRS Comm. V, Vol. XXXV, Part B5, pp. 759 - 769, Istanbul, Turkey, July 12-23, 2004.
- Schwarz, K.P. (1995), Integrated airborne navigation systems for photogrammetry, In: Fritsch, D., Hobbie, D. (Eds.), Photogrammetric Week'95, Wichmann Verlag, Heidelberg, Germany, pp. 193-153, 1995.

- Schwarz, K.P., N. El-Sheimy and Z. Liu (1994), Fixing GPS Cycle Slips by IMU/GPS: Methods and Experience, Proceedings of the International Symposium on Kinematic Systems in Geodesy, Geomatics and Navigation, KIS94, Banff, Canada Aug 30 – Sept 2, 1994, pp. 265-275, 1994.
- Schwarz, K.P., M.A. Chapman, M.E. Cannon, and P. Gong (1993), An Integrated IMU/GPS Approach to The Georeferencing of Remotely Sensed Data, PE&RS, 59(11): 1167-1674, 1993.
- Schwarz, K.P., C.S. Fraser and P.C. Gustafon (1984), Aerotriangulation Without Ground Control, Int. Arch. Of Photogrammetry and Remote Sensing, 25 (Part A1), Tio de Janeiro, Brazil, 1984.
- Skaloud, J. (1999), Problems in Direct-Georeferencing by IMU/DGPS in the Airborne Environment, ISPRS Commission III, WG III/1 Barcelona, Spain, Nov 25-26, 1999
- Skaloud, J., M. Cramer and K.P. Schwarz (1996), Exterior Orientation by Direct Measurement of Camera Position and Attitude, International Archives of Photogrammetry and Remote Sensing, Vol. XXXI, Part B3, pp. 125-130, 1996.
- Skaloud, J. (1995), Strapdown IMU Orientation Accuracy with GPS Aiding, M.Sc. Thesis, UCGE Report #20079, Department of Geomatics Engineering, The University, Calgary, Canada, 1995.
- Skaloud, J., D. Cosandier, K.P. Schwarz and M.A. Chapman (1994), GPS/IMU Orientation Accuracy Derived From A Medium Scale Photogrammetry Test, International

- Symposium on Kinematic Systems in Geodesy, Geomatics and Navigation – KIS94, Banff, Alberta, Canada, Aug 30-Sept 2, pp. 341-348, 1984.
- Snay, R., G. Adams, M. Chin, S. Frakes, T. Soler & N. Weston (2002). The synergistic CORS program continues to evolve, Proc. ION-GPS 2002, Portland, OR, September 24-27, 2630-2639.
- Soler, T., R.A. Snay, R.H. Foote & M.W. Cline (2003). Maintaining accurate coordinates for the National CORS network, Proc. FIG Working Week, Paris, France, April 13-17.
- Titterton, D.H., and J.L., Weston (1997), Strapdown Inertial Navigation Technology, Peter Peregrinus Ltd., The institution of Electrical Engineers, Stevenage, Herts, United Kingdom.
- Toth, C. and D.A. Grejner-Brzezinska (1998), Performance Analysis of The Airborne Integrated Mapping System (AIMSTM), International Archives of Photogrammetry and Remote Sensing, 32 (2):320-326, 1998.
- Toth, C. (1997), Direct Sensor Platform Orientation: Airborne Integrated Mapping System (AIMS), ISPRS Comm. III, Vol. XXXII, part 3-2W3, pp. 148-155.
- Wegmann, H. (2002), Image Orientation by Combined (A)AT with GPS and IMU, Integrated Remote Sensing at the Global, Regional and Local Scale, IAPRS, Comm. I, Vol. XXXIV, Part 1, Denver, Colorado, USA, Nov. 10-15, 2002.
- Wei, M. and K.P. Schwarz (1990), Testing a Decentralized Filter for GPS/IMU Integration, Proceeding of IEEE PLANS 1990, Las Vegas, USA Mar 20-23, 1990, pp. 429-435.

- Wright, B. and El-Sheimy, N. (2001), Real Time Identification and Location of Forest Fire Hotspots through the Integrated Video, GPS and IMU Systems, 5<sup>th</sup> Conference on Optical 3D Measurement Techniques, Vienna, Austria, Oct. 1-4, 2001.
- Yastikli, N. (2004), The Effect of System Calibration on Direct Sensor Orientation, International Archives of Photogrammetry and Remote Sensing, ISPRS Comm. I, Vol. XXXV, Part B1, pp. 205-209, Istanbul, Turkey, July 12-23, 2004.

## APPENDIX A: DATASET INFORMATION

### A-1. PhotoScience UofK Flight

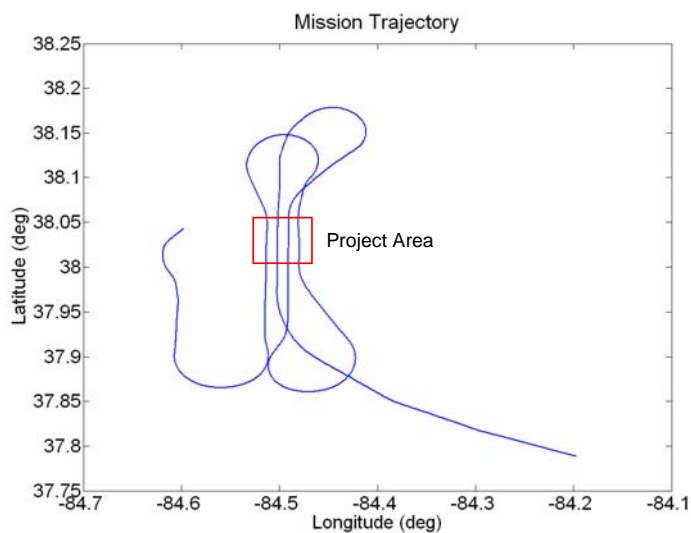


Figure A-1: Flight Trajectory of PhotoScience UofK Data

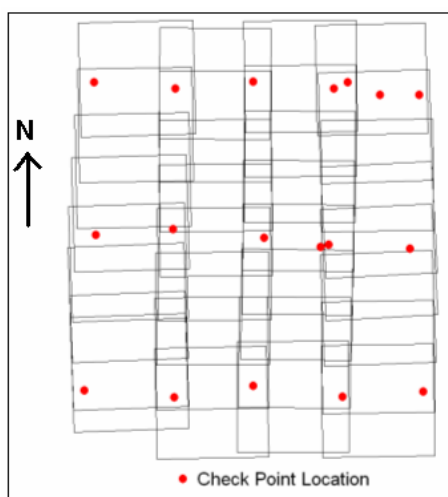
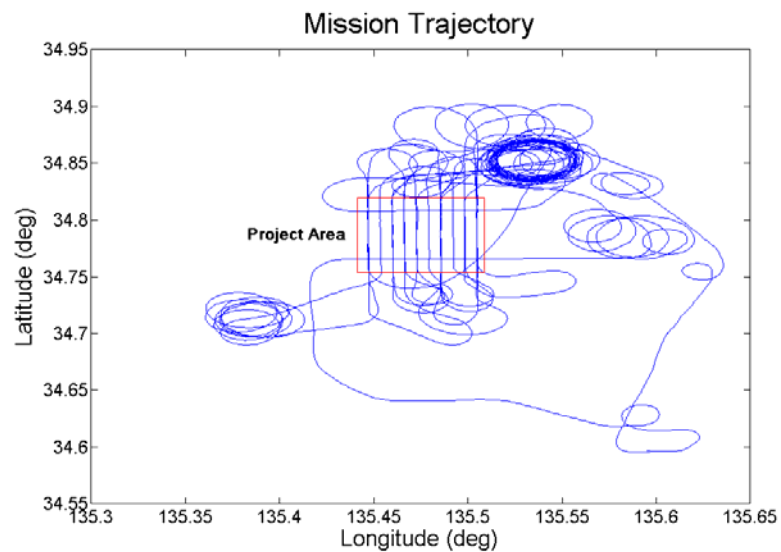
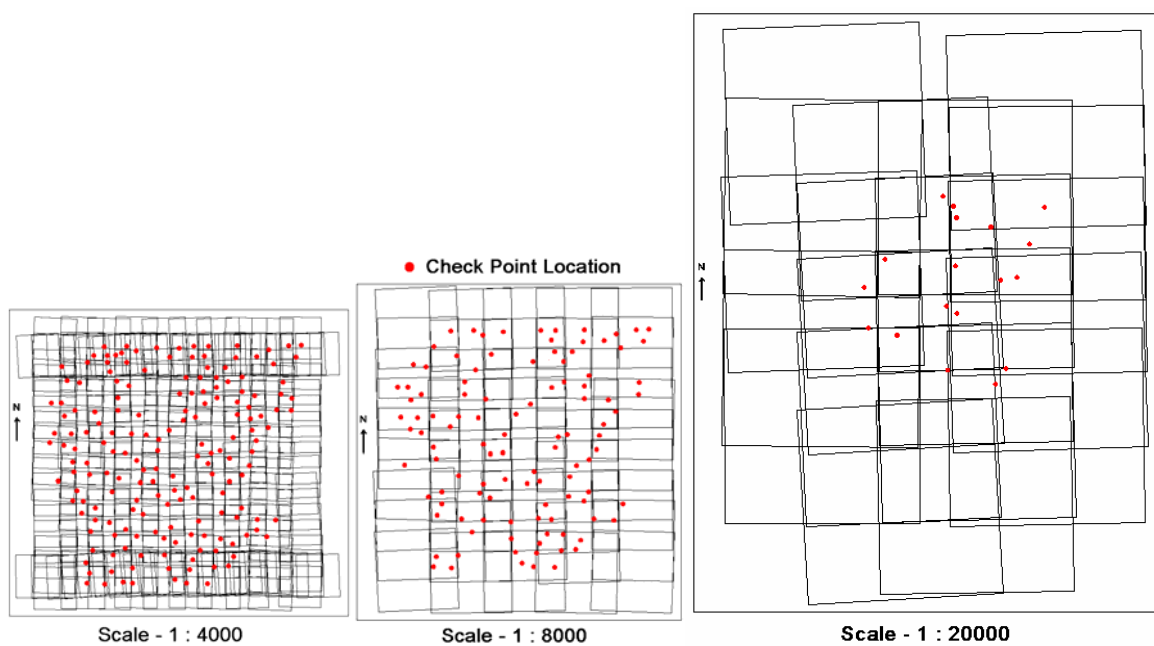


Figure A-2: Block Configuration of PhotoScience UofK Flight

## A-2. PASCO Toyonaka City Flight



**Figure A-3: Flight Trajectory of PASCO 310 Data**



**Figure A-4: Block Configuration of PASCO 310 Flight**  
 (Figure shown is based on relative size between each image block)

### A-3. DMC Alaska Flight

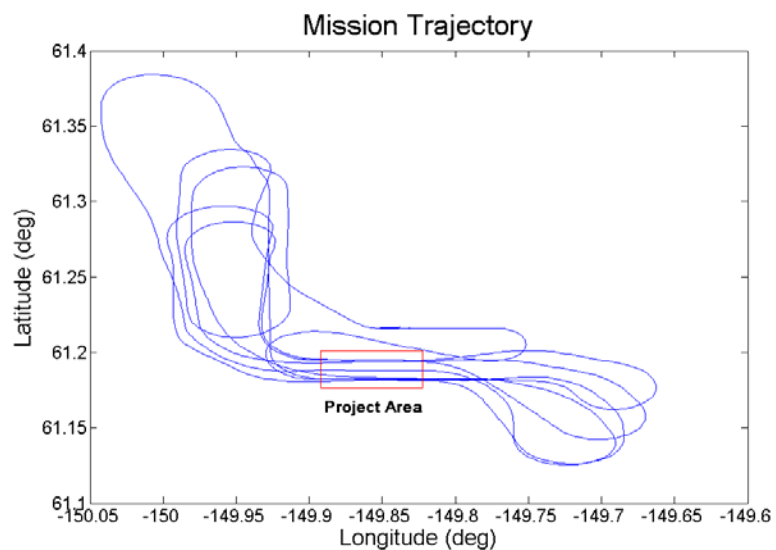


Figure A-5: Flight Trajectory of DMC Alaska Data

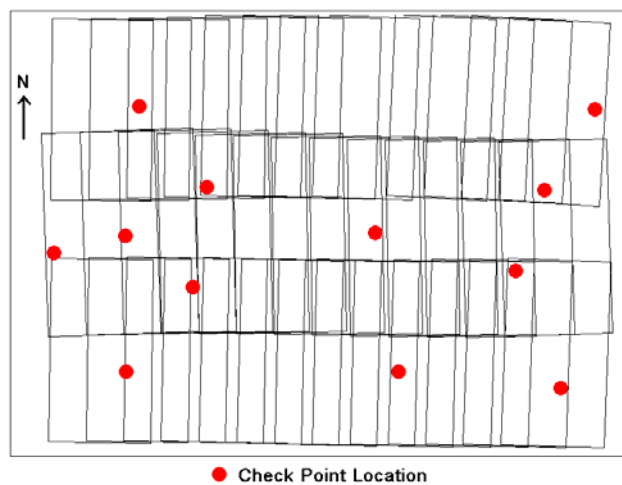


Figure A-6: Block Configuration of DMC Alaska Flight

#### A-4. DMC F-Block Flight

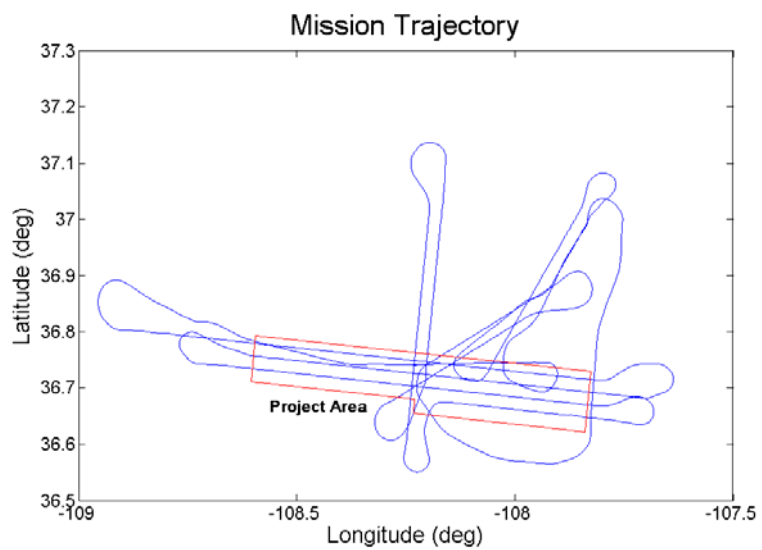


Figure A-7: Flight Trajectory of DMC Alaska Data

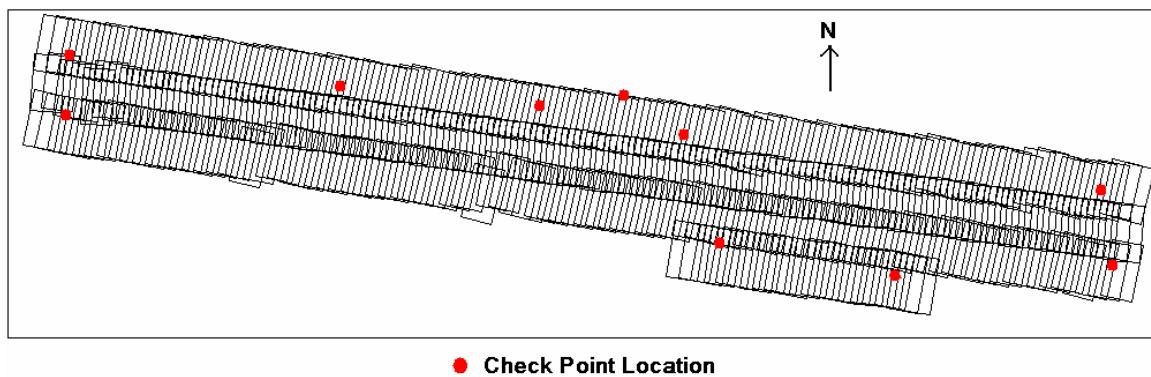


Figure A-8: Block Configuration of DMC Alaska Flight

### A-5. DSS Ajax Flight

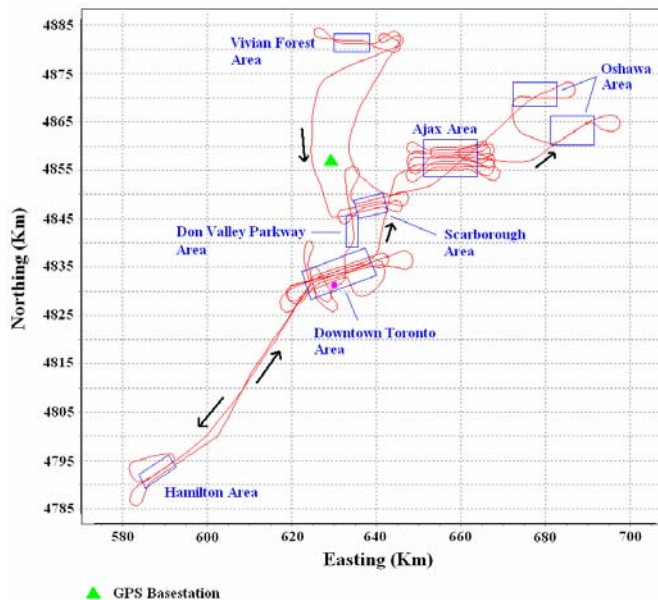


Figure A-9: Flight Trajectory of DSS Ajax Data

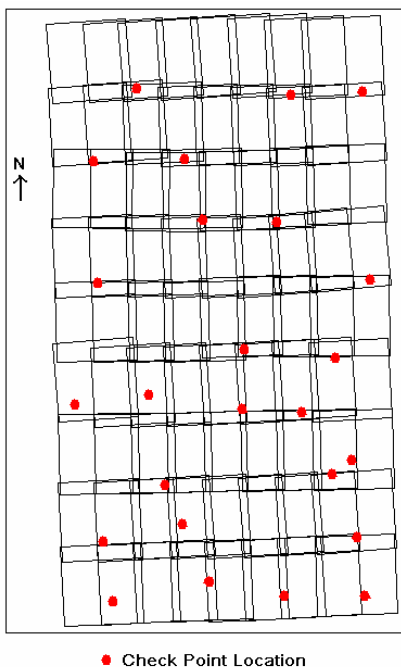


Figure A-10: Block Configuration of DSS Ajax Flight

## A-6. DSS Japan Data

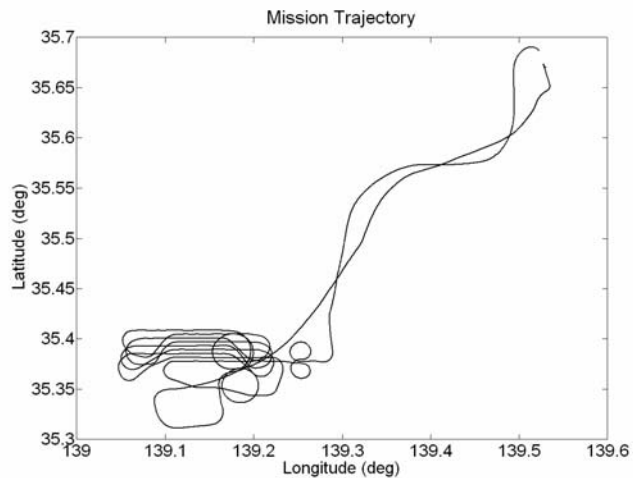


Figure A-11: Flight Trajectory of DSS Japan Data

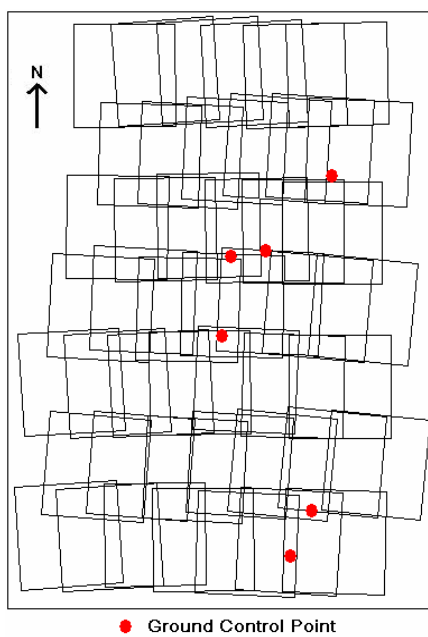
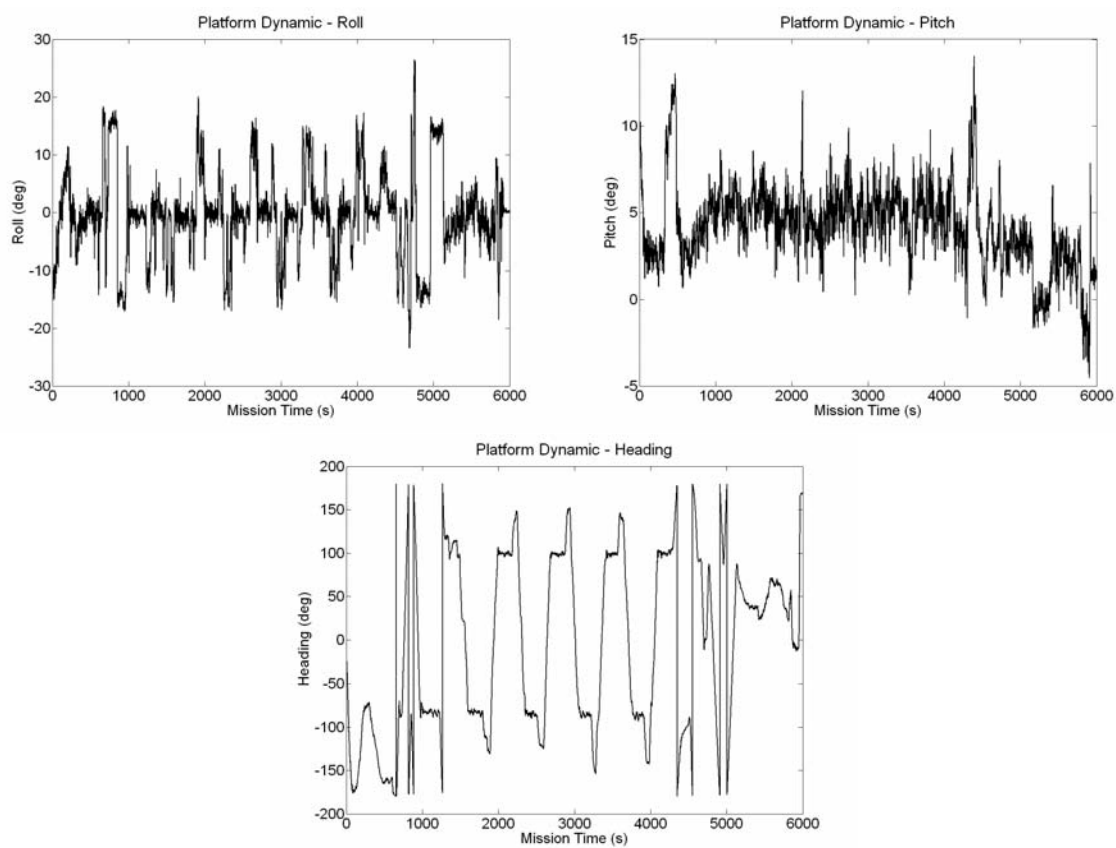


Figure A-12: Block Configuration of DSS Japan Flight



**Figure A-13: Flight Dynamics of DSS Japan Data**

## APPENDIX B: SYSTEM SPECIFICATIONS

### B-1. Applanix POS AV Specification

**Table B-1: Detail Specification of the POS AV Systems**

(Courtesy of Applanix Corporation)

	POS AV 510	POS AV410	POS AV 310
Noise (deg/sqrt(hr))	0.02	0.07	0.15
Drift (deg/hr) <sup>2</sup>	0.1	0.5	0.5
Post-Processed Accuracy			
Position (m)	0.05 – 0.3	0.05 – 0.3	0.05 – 0.3
Roll and Pitch (deg)	0.005	0.008	0.013
True Heading (deg)	0.008	0.015	0.035
Velocity (m/s)	0.005	0.005	0.075
RTK			
Position (m)	0.1 – 0.3	0.1 – 0.3	0.1 – 0.3
Roll and Pitch (deg)	0.008	0.015	0.03
True Heading (deg)	0.04	0.04	0.07
Velocity (m/s)	0.01	0.01	0.01
DGPS			
Position (m)	0.5 – 2.0	0.5 – 2.0	0.5 – 2.0
Roll and Pitch (deg)	0.008	0.015	0.03
True Heading (deg)	0.05	0.05	0.08
Velocity (m/s)	0.05	0.05	0.05
C/A			
Position (m)	4.0 – 6.0	4.0 – 6.0	4.0 – 6.0
Roll and Pitch (deg)	0.008	0.015	0.03
True Heading (deg)	0.07	0.08	0.10
Velocity (m/s)	0.05	0.05	0.05

## B-2. Leica Geosystems ADS40 Specification

**Table B-2: Detail Specification of the ADS 40**

(Courtesy of Leica Geosystems)

Camera Heads	2 * 12 k Panchromatic 4 * 12 k Multispectral
Focal Length	100 mm
Pixel Size	3.25 $\mu$ m
Radiometric Resolution	8 bits
DG System	Applanix's POS AV 510
Storage	Up to 1 Terabytes

## B-3. ZI/Imaging DMC Specification

**Table B-3: Detail Specification of the DMC**

(Courtesy of ZI/Imaging)

Camera Heads	4 * 7 k x 4 k Panchromatic 4 * 3 k x 2 k Multispectral
Focal Length	120 mm
Pixel Size	12 $\mu$ m
Radiometric Resolution	12 bits
DG System	Applanix's POS AV
Camera Mount	Gyro Stabilized with Suspension
Motion Compensation	Forward, Electronic
Storage	280 Gigabytes per Drive

#### B-4. Vexcel UltraCam Specification

**Table B-4: Detail Specification of the UltraCAM**

(Courtesy of Vexcel)

Camera Heads	11.5 k x 7.5 k Panchromatic 3.7 k x 2.4 k Multispectral
Focal Length	100 mm for Panchromatic 28 mm for Multispectral
Pixel Size	9 $\mu\text{m}$
Radiometric Resolution	12 bits
DG System	IGI's Aerial Control or Applanix's POS AV
Motion Compensation	Forward, TDI-controlled
Storage	1.5 Terabytes

#### B-5. Applanix DSS Specification

**Table B-5: Detail Specification of the DSS**

(Courtesy of Applanix Corporation)

Camera Heads	4k x 4k Color (VIS) or ColorIR (CIR)
Focal Length	55 mm for VIS/CIR Optional 35mm for VIS
Pixel Size	9 $\mu\text{m}$
Radiometric Resolution	12 bits
DG System	Applanix's POS AV 410
Camera Mount	Azimuth Mount, Single Axis with Shock/Vibration Isolation
Storage	80 Gigabytes per Drive

## APPENDIX C: DERIVATION OF EQUATIONS

### C-1. Equations for DG System Error Budget Analysis

Determination of y-parallax through Collinearity Equation

$$\begin{aligned}
 Py &= y_2 - y_1 \\
 &= \left( y_p - c \frac{m_{21_2}(X_A - X_{0_2}) + m_{22_2}(Y_A - Y_{0_2}) + m_{23_2}(Z_A - Z_{0_2})}{m_{31_2}(X_A - X_{0_2}) + m_{32_2}(Y_A - Y_{0_2}) + m_{33_2}(Z_A - Z_{0_2})} \right) - \left( y_p - c \frac{m_{21_1}(X_A - X_{0_1}) + m_{22_1}(Y_A - Y_{0_1}) + m_{23_1}(Z_A - Z_{0_1})}{m_{31_1}(X_A - X_{0_1}) + m_{32_1}(Y_A - Y_{0_1}) + m_{33_1}(Z_A - Z_{0_1})} \right) \\
 &= c \left( \frac{m_{21_1}(X_A - X_{0_1}) + m_{22_1}(Y_A - Y_{0_1}) + m_{23_1}(Z_A - Z_{0_1})}{m_{31_1}(X_A - X_{0_1}) + m_{32_1}(Y_A - Y_{0_1}) + m_{33_1}(Z_A - Z_{0_1})} - \frac{m_{21_2}(X_A - X_{0_2}) + m_{22_2}(Y_A - Y_{0_2}) + m_{23_2}(Z_A - Z_{0_2})}{m_{31_2}(X_A - X_{0_2}) + m_{32_2}(Y_A - Y_{0_2}) + m_{33_2}(Z_A - Z_{0_2})} \right)
 \end{aligned} \tag{C.1}$$

where

$$m = \begin{pmatrix} \cos \phi \cos \kappa & \cos \omega \sin \kappa + \sin \omega \sin \phi \cos \kappa & \sin \omega \sin \kappa - \cos \omega \sin \phi \cos \kappa \\ -\cos \phi \sin \kappa & \cos \omega \cos \kappa - \sin \omega \sin \phi \sin \kappa & \sin \omega \cos \kappa + \cos \omega \sin \phi \sin \kappa \\ \sin \phi & -\sin \omega \cos \phi & \cos \omega \cos \phi \end{pmatrix} \tag{C.2}$$

and

$m$	Rotation in Space
$(X_A, Y_A, Z_A)$	Ground Coordinates
$(X_{0_1}, Y_{0_1}, Z_{0_1}, \omega_1, \phi_1, \kappa_1)$	Exterior Orientation Parameters of Left Image
$(X_{0_2}, Y_{0_2}, Z_{0_2}, \omega_2, \phi_2, \kappa_2)$	Exterior Orientation Parameters of Right Image
$(x_p, y_p, c)$	Interior Orientation Parameters

let

$$\begin{aligned}
 A &= m_{21_1}(X_A - X_{0_1}) + m_{22_1}(Y_A - Y_{0_1}) + m_{23_1}(Z_A - Z_{0_1}) \\
 B &= m_{31_1}(X_A - X_{0_1}) + m_{32_1}(Y_A - Y_{0_1}) + m_{33_1}(Z_A - Z_{0_1}) \\
 C &= m_{21_2}(X_A - X_{0_2}) + m_{22_2}(Y_A - Y_{0_2}) + m_{23_2}(Z_A - Z_{0_2}) \\
 D &= m_{31_2}(X_A - X_{0_2}) + m_{32_2}(Y_A - Y_{0_2}) + m_{33_2}(Z_A - Z_{0_2})
 \end{aligned}$$

and perform partial derivative on each component with respect to  $Py$

$$\frac{\partial Py}{\partial X_{0_1}} = c \left( \frac{-Bm_{21_1} + Am_{31_1}}{B^2} \right)$$

$$\frac{\partial Py}{\partial Y_{0_1}} = c \left( \frac{-Bm_{22_1} + Am_{31_1}}{B^2} \right)$$

$$\frac{\partial Py}{\partial Z_{0_1}} = c \left( \frac{-Bm_{23_1} + Am_{33_1}}{B^2} \right)$$

$$\frac{\partial Py}{\partial \omega_1} = c \left( \frac{B \left( \frac{\delta m_{22_1}}{\delta \omega_1} (Y_A - Y_{0_1}) + \frac{\delta m_{23_1}}{\delta \omega_1} (Z_A - Z_{0_1}) \right) - A \left( \frac{\delta m_{32_1}}{\delta \omega_1} (Y_A - Y_{0_1}) + \frac{\delta m_{33_1}}{\delta \omega_1} (Z_A - Z_{0_1}) \right)}{B^2} \right)$$

$$\frac{\partial Py}{\partial \phi_1} = c \left( \frac{B \left( \frac{\partial m_{21_1}}{\partial \phi_1} (X_A - X_{0_1}) + \frac{\partial m_{22_1}}{\partial \phi_1} (Y_A - Y_{0_1}) + \frac{\partial m_{23_1}}{\partial \phi_1} (Z_A - Z_{0_1}) \right) - A \left( \frac{\partial m_{31_1}}{\partial \phi_1} (X_A - X_{0_1}) + \frac{\partial m_{32_1}}{\partial \phi_1} (Y_A - Y_{0_1}) + \frac{\partial m_{33_1}}{\partial \phi_1} (Z_A - Z_{0_1}) \right)}{B^2} \right)$$

$$\frac{\partial Py}{\partial \kappa_1} = c \left( \frac{B \left( \frac{\partial m_{21_1}}{\partial \kappa_1} (X_A - X_{0_1}) + \frac{\partial m_{22_1}}{\partial \kappa_1} (Y_A - Y_{0_1}) + \frac{\partial m_{23_1}}{\partial \kappa_1} (Z_A - Z_{0_1}) \right)}{B} \right)$$

and

$$\begin{aligned}
\frac{\partial Py}{\partial X_{0_2}} &= c \left( \frac{-Dm_{21_2} + Cm_{31_2}}{D^2} \right) \\
\frac{\partial Py}{\partial Y_{0_2}} &= c \left( \frac{-Dm_{22_2} + Cm_{31_2}}{D^2} \right) \\
\frac{\partial Py}{\partial Z_{0_2}} &= c \left( \frac{-Dm_{23_2} + Cm_{33_2}}{D^2} \right) \\
\frac{\partial Py}{\partial \omega_2} &= c \left( \frac{D \left( \frac{\partial m_{22_2}}{\partial \omega_2} (Y_A - Y_{0_2}) + \frac{\partial m_{23_2}}{\partial \omega_2} (Z_A - Z_{0_2}) \right) - C \left( \frac{\partial m_{32_2}}{\partial \omega_2} (Y_A - Y_{0_2}) + \frac{\partial m_{33_2}}{\partial \omega_2} (Z_A - Z_{0_2}) \right)}{D^2} \right) \\
\frac{\partial Py}{\partial \phi_2} &= c \left( \frac{D \left( \frac{\partial m_{21_2}}{\partial \phi_2} (X_A - X_{0_2}) + \frac{\partial m_{22_2}}{\partial \phi_2} (Y_A - Y_{0_2}) + \frac{\partial m_{23_2}}{\partial \phi_2} (Z_A - Z_{0_2}) \right) - C \left( \frac{\partial m_{31_2}}{\partial \phi_2} (X_A - X_{0_2}) + \frac{\partial m_{32_2}}{\partial \phi_2} (Y_A - Y_{0_2}) + \frac{\partial m_{33_2}}{\partial \phi_2} (Z_A - Z_{0_2}) \right)}{D^2} \right) \\
\frac{\partial Py}{\partial \kappa_2} &= c \left( \frac{B \left( \frac{\partial m_{21_2}}{\partial \kappa_2} (X_A - X_{0_2}) + \frac{\partial m_{22_2}}{\partial \kappa_2} (Y_A - Y_{0_2}) + \frac{\partial m_{23_2}}{\partial \kappa_2} (Z_A - Z_{0_2}) \right)}{D} \right)
\end{aligned}$$

The following are partial derivative of rotation matrix (m) with respect to the EO parameters

$$\begin{aligned}
\frac{\partial m_{22}}{\partial \omega} &= -\sin \omega \cos \kappa - \cos \omega \sin \phi \sin \kappa \\
\frac{\partial m_{23}}{\partial \omega} &= \cos \omega \cos \kappa - \sin \omega \sin \phi \sin \kappa \\
\frac{\partial m_{32}}{\partial \omega} &= -\cos \omega \cos \phi \\
\frac{\partial m_{33}}{\partial \omega} &= -\sin \omega \cos \phi \\
\frac{\partial m_{21}}{\partial \phi} &= \sin \phi \sin \kappa \\
\frac{\partial m_{22}}{\partial \phi} &= -\sin \omega \cos \phi \sin \kappa \\
\frac{\partial m_{23}}{\partial \phi} &= \cos \omega \cos \phi \sin \kappa
\end{aligned}$$

$$\begin{aligned}\frac{\partial m_{31}}{\partial \phi} &= \cos \phi \\ \frac{\partial m_{32}}{\partial \phi} &= \sin \omega \sin \phi \\ \frac{\partial m_{33}}{\partial \phi} &= -\cos \omega \sin \phi \\ \frac{\partial m_{21}}{\partial \kappa} &= -\cos \phi \cos \kappa \\ \frac{\partial m_{22}}{\partial \kappa} &= -\cos \omega \sin \kappa - \sin \omega \sin \phi \cos \kappa \\ \frac{\partial m_{23}}{\partial \kappa} &= -\sin \omega \sin \kappa + \cos \omega \sin \phi \cos \kappa\end{aligned}$$

Finally, the error model  $\sigma_{Py}$  of Direct Georeferencing can be formulated as following,

$\sigma$  represent the stand standard of the EO parameters

$$\begin{aligned}\sigma_{Py} &= \left(\frac{Py}{dX_{0_1}}\right)^2 \sigma_{X_{0_1}}^2 + \left(\frac{Py}{dY_{0_1}}\right)^2 \sigma_{Y_{0_1}}^2 + \left(\frac{Py}{dZ_{0_1}}\right)^2 \sigma_{Z_{0_1}}^2 + \left(\frac{Py}{d\omega_1}\right)^2 \sigma_{\omega_1}^2 + \left(\frac{Py}{d\phi_1}\right)^2 \sigma_{\phi_1}^2 + \left(\frac{Py}{d\kappa_1}\right)^2 \sigma_{\kappa_1}^2 \\ &+ \left(\frac{Py}{dX_{0_2}}\right)^2 \sigma_{X_{0_2}}^2 + \left(\frac{Py}{dY_{0_2}}\right)^2 \sigma_{Y_{0_2}}^2 + \left(\frac{Py}{dZ_{0_2}}\right)^2 \sigma_{Z_{0_2}}^2 + \left(\frac{Py}{d\omega_2}\right)^2 \sigma_{\omega_2}^2 + \left(\frac{Py}{d\phi_2}\right)^2 \sigma_{\phi_2}^2 + \left(\frac{Py}{d\kappa_2}\right)^2 \sigma_{\kappa_2}^2\end{aligned}\tag{C.3}$$